

# Monitoring Past, Present, and Future Water Quality Using Remote Sensing

## Final Project Report

### Southern Nevada Public Lands Management Act Lake Tahoe Environmental Improvement Program

Prepared by:

Todd Steissberg, Ph.D. <sup>1</sup>  
Geoffrey Schladow, Ph.D. <sup>1</sup>  
Simon J. Hook, Ph.D. <sup>2</sup>

<sup>1</sup> Tahoe Environmental Research Center  
John Muir Institute of the Environment  
University of California, Davis  
One Shields Avenue  
Davis, California 95616

<sup>2</sup> Jet Propulsion Laboratory (NASA/JPL)  
4800 Oak Grove Drive, M/S 183-501  
Pasadena, California 91109

December 6, 2010

## Abstract

A system was developed to semi-automatically acquire, store, and process satellite imagery to measure nearshore and offshore water quality at Lake Tahoe. An automated atmospheric correction procedure and processing code were developed to produce high quality maps and time series of water quality at Lake Tahoe. Algorithms were developed to predict nearshore and offshore Secchi Depths and chlorophyll *a* from MODIS data. One set of algorithms allows measurement of these parameters in the nearshore region at 250 m and 500 m resolution. The second set of algorithms allows higher-confidence measurements of these parameters at 1 km resolution. A web-accessible repository was created to store and distribute these and other satellite data products acquired or developed at Lake Tahoe on a near-real-time basis. The methodology developed for this study can be used to study historical or future changes in nearshore and offshore water clarity for any region of concern around Lake Tahoe, which can be used in water quality management decision-making and design.

MODIS-derived maps of water quality (Secchi Depth and chlorophyll *a*) and nearshore/offshore time series extracted from these maps were analyzed to identify spatial and temporal patterns of Secchi Depth and chlorophyll *a* and their variability over the 2002 – 2010 study period. *In situ* streamflow, nutrient, Secchi Depth, and chlorophyll *a* data were paired with the satellite data to determine the effects of streamflow, upwelling, currents, circulation (gyres and smaller-scale eddies), and other factors on the seasonal and spatial changes in lake clarity and chlorophyll *a*.

The time series of stream inflows, sediment and nutrient loadings, and MODIS-derived Secchi Depths and chlorophyll *a* indicate that streamflow, and therefore sediment input, is the major contributor to short-term decreases in clarity. The lowest mean Secchi Depths were obtained nearest the streamflow locations around the lake coincident with peak spring inflows. However, autochthonous inputs due to sediment resuspension and vertical transport of nutrients appear to play a significant role in water quality distribution and variability.

Comparison of the nearshore, coastal, and offshore time series indicated that water clarity was significantly lower and chlorophyll *a* was significantly higher in the nearshore regions than the offshore regions, on average. The variability of these parameters was also much higher nearshore than offshore. In fact nearshore water quality was periodically better than offshore water quality, typically following upwelling.

The MODIS-derived water quality maps show that Secchi Depth and chlorophyll *a* often covary spatially and temporally, even though Secchi Depth itself is much more dependent on light scattering due to fine particles. The time series extracted from these maps show that chlorophyll *a* and particles generally covary during peak spring runoff, as suspended sediment and nutrients flow into the lake. While there is an immediate reduction in Secchi Depths, there is a delay of days or weeks between peak inflows and peaks in chlorophyll *a*, since chlorophyll *a* levels are dependent on phytoplankton growth. Since other environmental factors influence phytoplankton growth, chlorophyll *a* levels are not as closely linked to inflows as are Secchi Depths. Nevertheless, chlorophyll *a* and opacity (low Secchi Depth) levels are significantly increased during high flow years. Similar effects could be seen in moderate flow years that followed low flow years, releasing sediment that had accumulated over the previous two years.

Surface chlorophyll *a* and particle levels are typically inversely correlated during the fall, as upwelling transports clear, nutrient-rich water to the surface. Strong upwelling can transport high clarity water to the surface, which contains low levels of particles but high levels of nutrients. If this water is transported from around the depth of the deep chlorophyll *a* maximum (DCM), chlorophyll *a* concentrations in the surface layer can increase immediately. Otherwise, chlorophyll *a* concentrations will increase over time, following upwelling-induced transport of nutrients to the surface layer. Both of these scenarios were observed in the satellite and field data.

The chlorophyll *a* maps and the nearshore/offshore chlorophyll *a* cycle derived from them reveal a significant seasonal pattern. Coincident with spring runoff, chlorophyll *a* begins to increase along the southern shore, concentrated near Stateline, and along the eastern shore, extending just north of Glenbrook Bay. The elevated chlorophyll *a* concentrations observed in the satellite-derived maps were found along the southern and eastern shores in all but two years of this study, 2002 and 2008, which were low flow years. Patches of elevated chlorophyll *a* concentrations appeared during spring runoff and appear to be concentrated along the

southern shore adjacent to the Upper Truckee River, Trout Creek, and Edgewood Creek inflows. Elevated concentrations were also observed near Incline Village and Glenbrook. The elevated concentrations appear to spread around the lake via large-scale circulation (gyres), with flow reversals and shore-to-shore (south-to-south or south-to-west) transport via smaller-scale (“spiral”) eddies 3 – 5 km in diameter. Chlorophyll *a* was observed to spread offshore in plumes or jets following upwelling events. The plumes and eddies may contribute to offshore diffusion.

The satellite data showed that a chlorophyll *a* plume often emanated from the southern shore, near the Upper Truckee River inflow, increasing chlorophyll *a* levels along the western and eastern shores. For the western shore, this chlorophyll *a* plume increased chlorophyll *a* levels along the western shore, just as chlorophyll *a* levels from spring runoff were decreasing. The difference in chlorophyll *a* between the western and southern shores prior to transport was larger than expected, given the relative magnitude of streamflows. Partial upwelling occurs during the spring storms, which bring strong winds in addition to rainfall. The upwelling may induce significant sediment resuspension over the South Lake Tahoe shoals, increasing chlorophyll *a* levels through autochthonous inputs.

Offshore water quality is linked to nearshore water quality via upwelling and spiral eddies, while along-shore transport occurs via large-scale circulation (gyres) and meso-scale eddies (“spiral eddies”). Analysis of high resolution images of Lake Tahoe, paired with MODIS data, indicates that the number of eddies, their direction of rotation, and their locations can change over time, with the eddies shifting between the southwest and southeast shore. They may also disappear altogether, leaving a simple large scale double-gyre system. These eddies themselves might even be transported by the larger-scale clockwise gyre. This would suggest typical large-scale clockwise transport in the southern basin, modified by counter-clockwise eddies, forming counter currents, leading to offshore transport and transport between shores at the corners of the lake. The latter transport mechanism “short-circuits” the along-shore transport, which may help explain the patchiness of the spread of invasive species.

# Contents

<b>Table of Contents</b>	<b>1</b>
<b>List of Tables</b>	<b>3</b>
<b>List of Figures</b>	<b>4</b>
<b>1 Introduction</b>	<b>6</b>
1.1 Overview . . . . .	6
1.2 Background . . . . .	7
1.3 Hypotheses . . . . .	12
1.4 Project Objectives . . . . .	12
1.5 Project Goals and Products . . . . .	13
1.6 Problems Encountered . . . . .	14
1.7 Revisions to Proposed Methodology . . . . .	14
1.8 Summary of Accomplishments . . . . .	14
1.8.1 Web-Accessible Repository of Lake Tahoe Imagery . . . . .	14
1.8.2 RS Acquisition and Storage Tools . . . . .	15
1.8.3 Water Quality Algorithms . . . . .	15
1.8.4 Relation Between Nearshore Clarity and Inputs . . . . .	15
1.8.5 Linkage Between Offshore Clarity and Forcing . . . . .	16
1.8.6 RS Water Quality Reporting System . . . . .	16
1.8.7 Methodology to Study Future Clarity Changes . . . . .	16
1.8.8 Methodology to Study Historical Clarity Changes . . . . .	17
1.8.9 Publication of Findings . . . . .	17
<b>2 Methods</b>	<b>18</b>
2.1 Satellite Data . . . . .	18
2.1.1 Atmospheric Correction . . . . .	18
2.1.2 High Resolution True Color MODIS Images . . . . .	22
2.1.3 MODIS Image Quality Control . . . . .	24
2.1.4 Acquisition and Processing of Lake Tahoe MODIS Data . . . . .	26
2.2 Field Data . . . . .	26
2.2.1 Secchi Depth . . . . .	26
2.2.2 Chlorophyll <i>a</i> . . . . .	26
2.3 Satellite Calibration . . . . .	27
2.3.1 Secchi Depth . . . . .	27
2.3.2 Chlorophyll <i>a</i> . . . . .	27
2.4 Time Series . . . . .	28

<b>3</b>	<b>Results</b>	<b>30</b>
3.1	Web-Accessible Repository of Lake Tahoe Imagery . . . . .	30
3.2	RS Acquisition and Storage Tools . . . . .	34
3.3	Water Quality Algorithms . . . . .	35
3.3.1	Secchi Depth Estimation . . . . .	35
3.3.2	Chlorophyll <i>a</i> Estimation . . . . .	37
3.3.3	Water Quality Match-ups . . . . .	39
3.4	Relation Between Nearshore Clarity and Inputs . . . . .	42
3.4.1	Water Quality Maps . . . . .	42
3.4.2	Stream Inflow . . . . .	47
3.4.3	MODIS Time Series of Nearshore Water Quality . . . . .	49
3.4.4	Stream Water Quality Loadings . . . . .	62
3.4.5	Cyclic Analysis of Nearshore Water Quality . . . . .	66
3.5	Linkage Between Offshore Clarity and Forcing . . . . .	76
3.5.1	Chlorophyll <i>a</i> Maps . . . . .	76
3.5.2	Water Quality Time Series . . . . .	77
3.5.3	<i>In situ</i> Chlorophyll <i>a</i> Profiles: Characterization of Chlorophyll <i>a</i> Variability . . . . .	84
3.6	RS Water Quality Reporting System . . . . .	87
3.7	Methodology to Study Future Clarity Changes . . . . .	87
3.8	Methodology to Study Historical Clarity Changes . . . . .	87
3.9	Publication of Findings . . . . .	87
<b>4</b>	<b>Conclusions</b>	<b>88</b>
	<b>Bibliography</b>	<b>91</b>
	<b>Appendix A</b>	<b>94</b>
A.1	MODIS Time Series Coordinates . . . . .	94
	<b>Appendix B</b>	<b>96</b>
B.1	Spiral Eddies at Tahoe . . . . .	96
B.2	Current Patterns at Tahoe . . . . .	99

# List of Tables

2.1	MODIS Processing Levels . . . . .	19
2.2	Flags and masks that are set during Level 2 and Level 3 processing in SeaDAS. Flags in blue are masked during Level 3 (ocean color) processing. . . . .	20
2.3	User flags for MODIS processing in SeaDAS. . . . .	21
2.4	Primary image categories used by Qview. These identify the quality of images selected for water quality analysis. . . . .	25
2.5	Alternate image categories used by Qview. These identify either the type of rejection or other useful features present in an image. . . . .	25
3.1	List of streams and their corresponding MODIS sampling station(s). . . . .	49
A.1	Coordinates of the locations where time series are extracted from each MODIS water quality map. The “nearshore” stations (NS) are located 750 m from either the shoreline or shoals that are shallow enough for bottom reflectance to contaminate the MODIS reflectance data. Similarly, the “coastal” (CS) and “offshore” (OS) stations are sited 1000 m and 1500 m, respectively, from the shoreline or visible shoals. . . . .	95

# List of Figures

1.1	Tahoe contour and station map . . . . .	7
1.2	Map of LTIMP watersheds . . . . .	8
1.3	Tahoe current vectors, June 2001 . . . . .	9
1.4	Tahoe multi-sensor temperature maps, showing transport, June 2001 . . . . .	10
2.1	MODIS-Aqua high resolution true color images, showing a clear image and images contaminated by clouds, sun glitter, and jet contrails. . . . .	23
2.2	MODIS time series sampling stations . . . . .	29
3.1	Web-accessible repository of Lake Tahoe Imagery. Main window (login or create account). . .	31
3.2	Web-accessible repository of Lake Tahoe Imagery. Product order form. . . . .	31
3.3	Web-accessible repository of Lake Tahoe Imagery. Product order form, showing drop-down list of available products. . . . .	32
3.4	Web-accessible repository of Lake Tahoe Imagery. Sample product delivery page with links to data requested. . . . .	32
3.5	Web-accessible repository of Lake Tahoe Imagery. Sample of a downloaded product. . . . .	33
3.6	Match-ups of <i>in situ</i> and MODIS-predicted Secchi Depth measurements. . . . .	40
3.7	Match-ups of <i>in situ</i> and MODIS-predicted chlorophyll <i>a</i> measurements. . . . .	41
3.8	Secchi Depth and chlorophyll <i>a</i> maps acquired in 2003, Julian Days 152 – 154. . . . .	43
3.9	Secchi Depth and chlorophyll <i>a</i> maps acquired in 2003, Julian Days 157 – 159. . . . .	44
3.10	Secchi Depth and chlorophyll <i>a</i> maps acquired in 2004, Julian Days 100 – 130. . . . .	45
3.11	Bathymetry map of Lake Tahoe, scaled to show the shoals to a depth of 30 m. . . . .	46
3.12	Time series of inflow of Tahoe basin streams, 2002 – 2010. . . . .	48
3.13	Third Creek inflow and time series of MODIS-predicted nearshore Secchi Depth and chlorophyll <i>a</i> at Station 4. . . . .	51
3.14	Incline Creek inflow and time series of MODIS-predicted nearshore Secchi Depth and chlorophyll <i>a</i> at Station 5. . . . .	52
3.15	Glenbrook Creek inflow and time series of MODIS-predicted nearshore Secchi Depth and chlorophyll <i>a</i> at Station 13. . . . .	53
3.16	Glenbrook Creek inflow and time series of MODIS-predicted nearshore Secchi Depth and chlorophyll <i>a</i> at Station 14. . . . .	54
3.17	Logan House Creek inflow and time series of MODIS-predicted nearshore Secchi Depth and chlorophyll <i>a</i> at Station 15. . . . .	55
3.18	Edgewood Creek inflow and time series of MODIS-predicted nearshore Secchi Depth and chlorophyll <i>a</i> at Station 20. . . . .	56
3.19	Trout Creek inflow and time series of MODIS-predicted nearshore Secchi Depth and chlorophyll <i>a</i> at Station 22. . . . .	57
3.20	Upper Truckee River inflow and time series of MODIS-predicted nearshore Secchi Depth and chlorophyll <i>a</i> at Station 22. . . . .	58
3.21	General Creek inflow and time series of MODIS-predicted nearshore Secchi Depth and chlorophyll <i>a</i> at Station 32. . . . .	59
3.22	Blackwood Creek inflow and time series of MODIS-predicted nearshore Secchi Depth and chlorophyll <i>a</i> at Station 36. . . . .	60

3.23	Ward Creek inflow and time series of MODIS-predicted nearshore Secchi Depth and chlorophyll <i>a</i> at Station 37. . . . .	61
3.24	Time series of Upper Truckee River inflow, loadings, and water temperature . . . . .	63
3.25	Time series of Trout Creek inflow, loadings, and water temperature . . . . .	64
3.26	Time series of Edgewood Creek inflow, loadings, and water temperature . . . . .	65
3.27	Mean monthly chlorophyll <i>a</i> (January – April). . . . .	69
3.28	Mean monthly chlorophyll <i>a</i> (May – August). . . . .	70
3.29	Mean monthly chlorophyll <i>a</i> (September – December). . . . .	71
3.30	MODIS-Terra water skin temperature (WST) anomaly maps, showing nearshore temperature patterns along the south shore. . . . .	72
3.31	Mean monthly Secchi Depth (January – April) . . . . .	73
3.32	Mean monthly Secchi Depth (May – August). . . . .	74
3.33	Mean monthly Secchi Depth (September – December). . . . .	75
3.34	Maps showing growth and transport of chlorophyll <i>a</i> in 2003, Julian Days 150 – 157. . . . .	78
3.35	Maps showing growth and transport of chlorophyll <i>a</i> in 2003, Julian Days 159 – 177. . . . .	79
3.36	Maps showing cross-shore transport of chlorophyll <i>a</i> by jets and other currents. . . . .	80
3.37	Maps showing cross-shore transport of chlorophyll <i>a</i> by jets and other currents. . . . .	81
3.38	Water skin temperature (WST) of Lake Tahoe showing large-scale circulation and cross-shore transport of chlorophyll <i>a</i> by currents. . . . .	82
3.39	Maps showing cross-shore and along-shore transport of chlorophyll <i>a</i> by spiral eddies. . . . .	83
3.40	<i>In situ</i> chlorophyll <i>a</i> measured at the LTP station. Both the period of record (1974 – 2010) and the MODIS-Aqua period (2002 – 2010) are shown. . . . .	85
3.41	<i>In situ</i> chlorophyll <i>a</i> measured at the MLTP station. Both the period of record (1974 – 2010) and the MODIS-Aqua period (2002 – 2010) are shown. . . . .	86
B.1	Spiral eddies . . . . .	97
B.2	Drogues, August 2008 . . . . .	98
B.3	Circulation patterns, May 1999 – August 1999 . . . . .	100
B.4	Circulation patterns, May 2000 – June 2001 . . . . .	101
B.5	Circulation patterns, July 2001 – June 2002 . . . . .	102
B.6	Circulation patterns, July 2002 – May 2003 . . . . .	103
B.7	Circulation patterns, June 2003 – August 2003 . . . . .	104
B.8	Circulation patterns, June 2004 – August 2004 . . . . .	105
B.9	Circulation patterns, May 2005 – June 2006 . . . . .	106
B.10	Circulation patterns, June 2006 – August 2006 . . . . .	107
B.11	Drogues, September 2001 . . . . .	108

# Chapter 1

## Introduction

### 1.1 Overview

Remote sensing (RS) technologies are being used worldwide to monitor aquatic, atmospheric, and terrestrial systems. RS provides an instantaneous synoptic overview of these systems which, when coupled with *in situ* measurements, can provide unmatched, cost-effective, quantitative measures of change with spatial resolutions down to the order of meters and temporal frequency better than daily. With a vast repository of RS data extending back almost 30 years, and the guarantee of future data availability, RS data provide the means to understand past changes in the Tahoe Basin, to evaluate the impacts of current activities, and to measure the effectiveness of future management strategies.

Since 1999, NASA has operated a validation site at Lake Tahoe, based on data collected from a network of 4 buoys in concert with U. S., Japanese, and European satellites. The statistical accuracy of the data collected through this system has been tested and found to be extremely high (*Hook et al.* [2003, 2004]; *Hook and Vaughan* [2007]). While the data have been used for monitoring change in other systems, such as the Great Lakes, there has only been limited use of RS in the Tahoe basin restricting our understanding of the complex interplays within Lake Tahoe and associated watershed.

Prior to this study, the knowledge of the decline in water clarity at Lake Tahoe CA/NV was based on the interpretation of data from the UC Davis Tahoe Environmental Research Center's (TERC's) two deep-water measurement sites, referred to as the Index (Lake Tahoe Profile, LTP) and Mid-lake (Mid-lake Tahoe Profile, MLTP) stations (Figure 1.1), the USGS and TERC monitoring of stream conditions from approximately 20% of the streams that flow into Lake Tahoe (e.g., *Hackley et al.* [2005] and Figure 1.2) and more recently, urban runoff measurements (e.g., *Heyvaert and Parra* [2005]). The in-lake measurements, made at intervals from 10 – 30 days, include primary productivity, nutrient concentration (various forms of nitrogen and phosphorus), chlorophyll *a* concentration, light penetration, temperature distribution, and Secchi Depth (or Secchi Disk Transparency, SDT). While these data provide point measurements of what is happening on the lake, they are lacking in both the temporal and spatial detail needed to understand the changes taking place at different parts of the lake (such as the nearshore zone), and the linkage between the lake observations and the input sources. For example, measurements made at the two sites (LTP and MLTP) provide little information about how nutrients and sediment from the streams and intervening zones are transported throughout the lake by surface currents. Such information can be crucial in understanding the processes behind the decline in clarity necessary to predict future changes and can be obtained from remotely sensing data (Figure 1.3). Furthermore, the 10 – 30 day temporal sampling is insufficient to capture changes that take place on the scale of a few days, such as wind-driven upwelling (*Schladow et al.* [2004]; *Steissberg et al.* [2005a], Figure 1.4), which can have a profound effect on the lake clarity measured at these stations. RS data have the potential to provide a synoptic overview of what is happening over the lake at many instances in time, which when coupled with *in situ* data, can provide lake-wide assessments of changes in both near-shore and offshore water quality.

The purpose of this project was to establish a basin-wide RS monitoring network for the Lake Tahoe basin. The establishment of this system should have immediate impacts for many areas of water quality concern, and with further development could address the entire range of environmental monitoring needs.

This first stage focused on the lake itself (rather than terrestrial or atmospheric monitoring), establishing a semi-automated system to evaluate and compare discrete sources of clarity-reducing substances to the lake (streams, storm drains, intervening zones), the effectiveness of best management practices (BMP's) at a sub-watershed scale over time, and changes in lake clarity in both the nearshore and offshore environments. The system capitalized on the local infrastructure developed by NASA, together with the numerous and available satellite datasets.

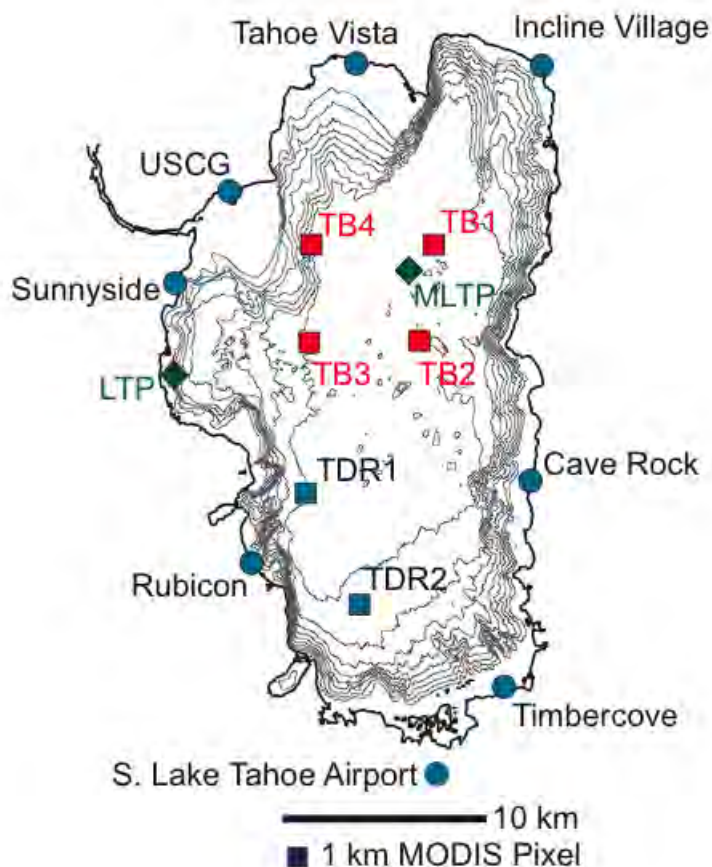


Figure 1.1: Map of Lake Tahoe showing 50 m contours, LTP and MLTP long-term sampling stations, NASA buoys (TB1, TB2, TB3, and TB4), and onshore meteorological stations.

Through this study we put in place a system to utilize remotely sensed and field measurement data to quantify changes in water clarity measurements over the entire lake. Moderate-resolution (1 km, 500 m, and 250 m) satellite data are available several times per day and high-resolution (30 m and 15 m) satellite data are available every 16 days. These data can be used to create maps of water clarity which extend close enough to the shoreline to assess the impacts and fate of key point and non-point pollutant sources. The changes in nearshore clarity at particular areas of interest, such as near stream inflows, can be observed in time series derived from these clarity maps.

## 1.2 Background

Several studies have demonstrated that remotely sensed data can be used to map water quality parameters, such as clarity and chlorophyll *a* concentrations, in lakes (*Horion et al. [2010]*; *Chavula et al. [2009]*; *Wu et al. [2009]*; *Heim et al. [2005]*; *Dall'Olmo et al. [2005]*; *Vos et al. [2003]*). However, the use of remotely sensed data on an operational basis for monitoring water quality in lakes has been limited by either the spatial or temporal resolution of the instrument. For example, the nominal spatial resolution of SeaWiFS (Sea-viewing

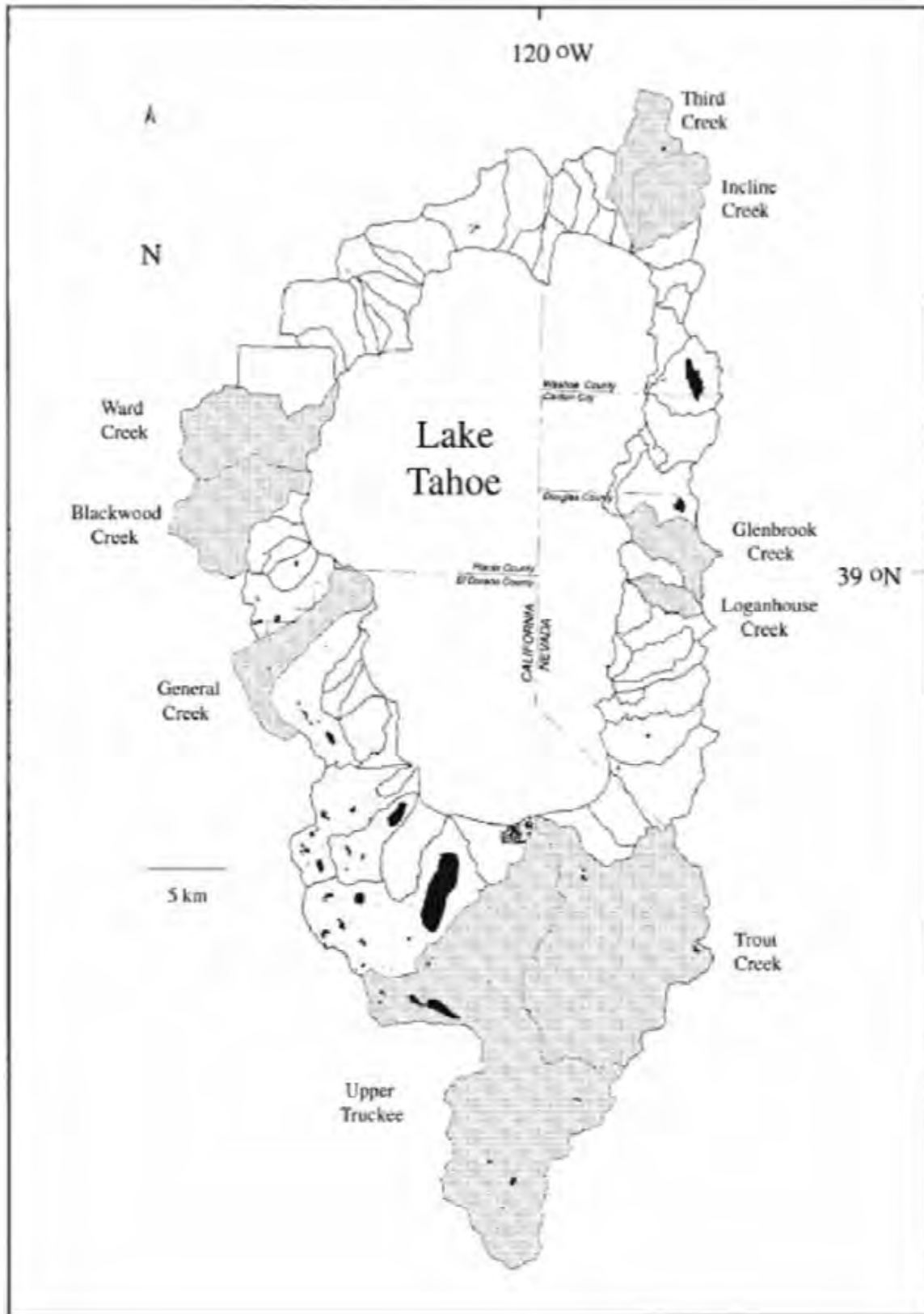


Figure 1.2: Map of the Lake Tahoe basin, delineating the watersheds of the nine Lake Tahoe Interagency Monitoring Program (LTIMP) streams. Source: *Hatch et al.* [2001].

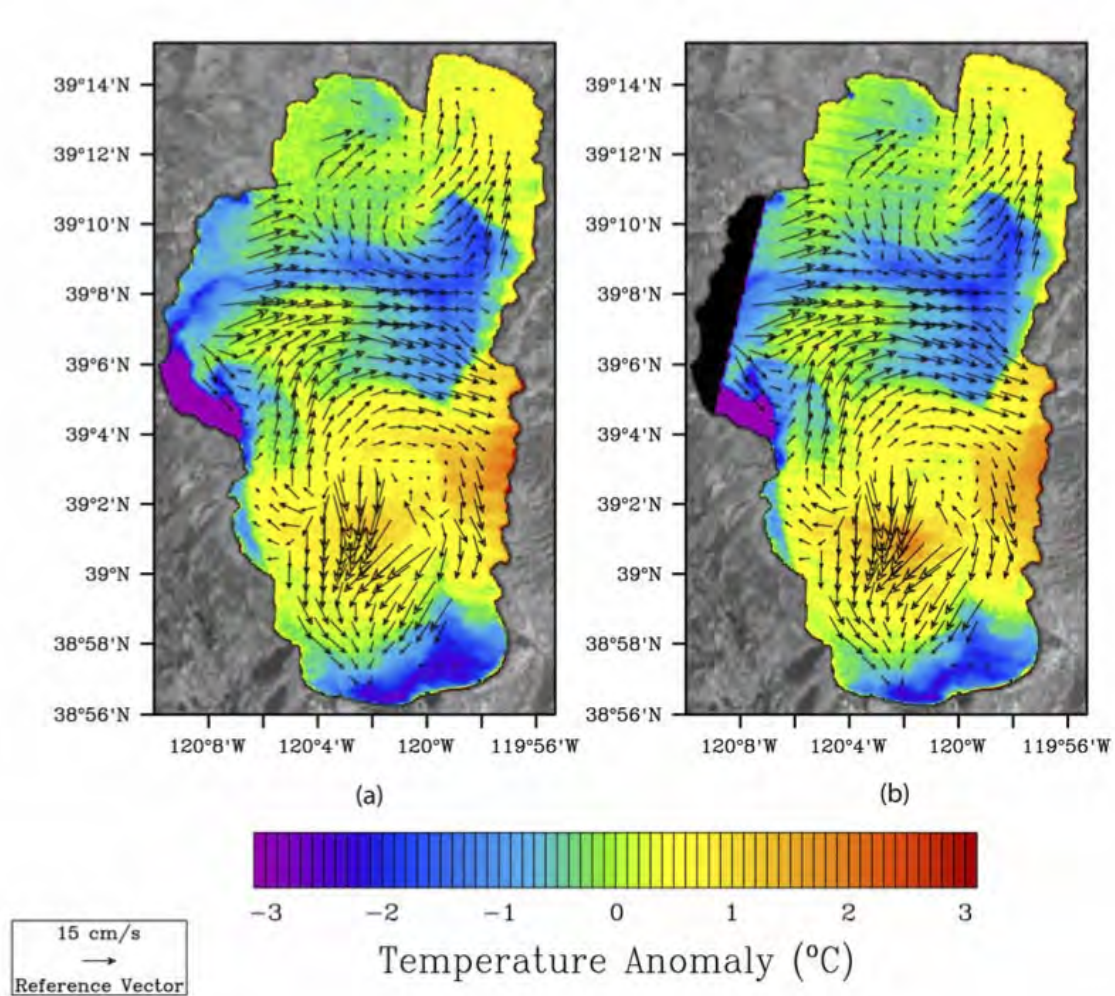


Figure 1.3: Maps of surface temperature anomaly (temperatures minus the spatial median) of Lake Tahoe, collected 38 min. apart, June 3, 2001 (a) Landsat ETM+ (b) ASTER. Strong upwelling of cold (blue) water from the west is shown traveling eastward in the form of a jet. Upwelling is also visible along the southern shore. Source: *Steissberg et al.* [2005b].

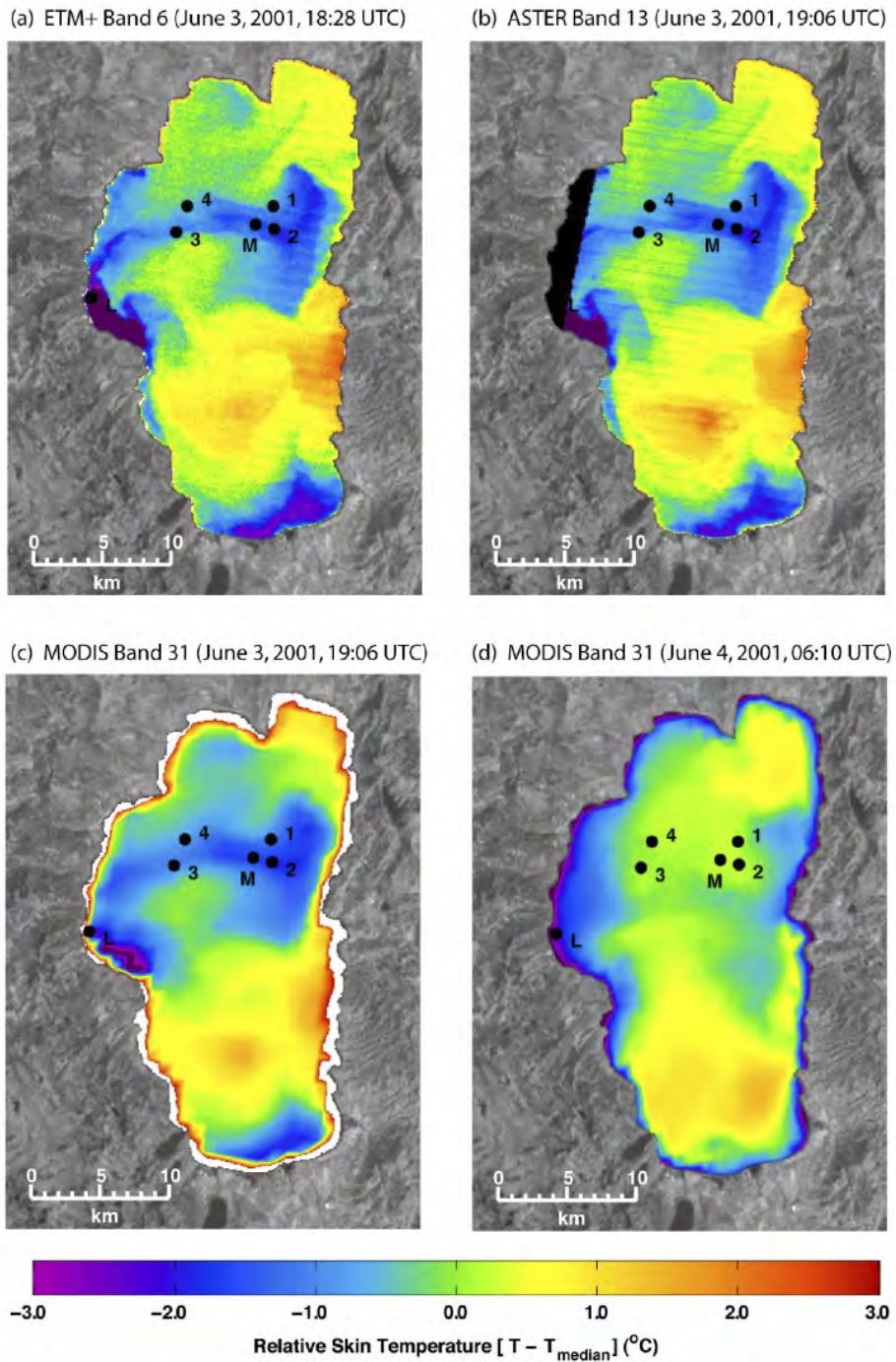


Figure 1.4: Satellite images acquired June 3 – 4, 2001, showing relative skin temperatures. Stations: L = LTP, M = MLTP, 1 – 4 = TB1 – TB4. Strong upwelling is visible along the western shore and transported eastward in a surface jet. Note that this jet intersects both the LTP (Index) and MLTP (Mid-lake) clarity sampling stations, indicating the possibility that measurements at these stations may significantly differ from other sites, depending on lake mixing and surface current patterns. Source: *Steissberg et al.* [2005a].

Wide Field-of-view Sensor), AVHRR, and ATSR-2 is approximately 1 km at nadir. These instruments can retrieve data from mid-latitude sites as often as twice per day (AVHRR collects 4 km data operationally and 1 km data upon request). Therefore, they are capable of mapping large-scale and meso-scale processes in the ocean (e.g., *Wilson and Qiu [2008]*) and basin-scale processes in lakes (*Schladow et al. [2004]*; *Steissberg et al. [2005a]*; *Marti-Cardona et al. [2008]*). However, their data are often too coarse to capture mesoscale processes in lakes and are incapable of mapping nearshore water quality gradients. Therefore, few operational studies (e.g., *Pozdnyakov et al. [2005]*) have been performed. Furthermore, there are a limited number of lake studies that have included nearshore components (e.g., *Heim et al. [2005]*; *Chavula et al. [2009]*; *Xingwei et al. [2009]*; *Wu et al. [2008]*), none of which have been long-term operational studies.

By contrast, high-spatial-resolution sensors, such as ASTER and Landsat are capable of resolving finer scale features. For example, the nominal spatial resolution of the visible and near-infrared (VNIR) bands of ASTER and Landsat-7 Enhanced Thematic Mapper (ETM+) at nadir are 15 m and 30 m, respectively, and the spatial resolution of their thermal infrared (TIR) bands is 90 m and 60 m, respectively. These instruments can capture “snapshots” of meso-scale features in lakes, such as nearshore currents and eddies [*Steissberg, 2008*], as well as basin-scale gyres [*Steissberg et al., 2005b*]. However, the temporal resolution of these instruments is approximately 16 days, limiting retrievals to one or two cloud-free images per month. Previous studies have typically been limited to a small number of images, or even a single image including multiple lakes (*Martinez et al. [2003]*; *Sawaya et al. [2003]*; *Chipman et al. [2004]*; *Brezonik et al. [2005]*). The limited data availability prevents these instruments from measuring short-term water quality variability and inhibits linking changes in water quality to events such as stream pulses, upwelling, or contaminant spills. Furthermore, all Landsat and ASTER images are acquired near nadir. Paired with their late morning overpass time, images acquired from the late spring through the early fall can be significantly contaminated by sunglint.

The Moderate-resolution Imaging Spectroradiometer (MODIS) addresses some of the shortcomings outlined above, particularly when a multi-platform, multi-sensor approach is used. MODIS collects reflected and emitted energy from the Earth surface in 36 spectral bands from 0.4 to 14.4  $\mu\text{m}$ , providing data and derived products for earth’s oceanic, hydrologic, terrestrial, atmospheric, and cryospheric systems. The Terra spacecraft was launched as the first Earth Observing System (EOS) mission on December 18, 1999. A second spacecraft, Aqua, was launched in May 2002. Each spacecraft carries a MODIS sensor.

Terra and Aqua are polar-orbiting satellites in sun-synchronous orbits. The Terra spacecraft crosses the equator at 10:30 AM local time (descending node), and the Aqua spacecraft crosses at 1:30 PM local time (ascending node). Each instrument acquires a daytime scene and a nighttime scene (in the thermal infrared) each day. Combined, MODIS-Terra and MODIS-Aqua provide up to four thermal (temperature) images and two visible and infrared images per day. MODIS-Terra and MODIS-Aqua began providing science data in February 2000 and June 2002, respectively.

High sensitivity radiometric data are recorded at nominal spatial resolutions (at nadir) of 250 m (bands 1 – 2), 500 m (bands 3 – 7), and 1000 m (bands 8 – 36). Nine of the 1000 m bands are traditionally used for ocean color observation. These bands are located in the visible to near infrared (NIR) spectral regime from 412 – 869 nm. These ocean bands were designed with high sensitivity over the range of reflectance typical of open ocean observations under maritime atmospheric conditions. Over highly turbid coastal and inland waters it is possible for this dynamic range to be exceeded, such that the bands saturate and the true signal is unknown.

The 250 m and 500 m bands of MODIS are considered the high-resolution or “HIRES” bands of MODIS (*Franz et al. [2006]*). These were designed for land and cloud observations, which typically have much larger reflectance than the open ocean. Therefore, these bands have a broader dynamic range than the 1000 m bands but reduced sensitivity. These land/cloud bands overlap the spectral range of the ocean bands and extend into the short-wave infrared (SWIR), from 469 to 2130 nm, with a spatial resolution of 250 to 500 meters at nadir. The spectral range of MODIS band 1 is 620 – 670 nm and the range of band 2 is 841 – 876 nm.

Although the sensitivity of the 250 m and 500 m bands is lower than the 1000 m bands of MODIS, it is comparably higher than currently deployed high-resolution sensors and current and previous ocean color sensors. *Hu et al. [2004]* compared these higher resolution MODIS bands with other sensors, including Landsat-7 ETM+, the Coastal Zone Color Scanner (CZCS), and SeaWiFS and concluded that the MODIS HIRES bands provide sufficient sensitivity for water applications. In particular, the MODIS HIRES bands

are 4 – 5 times more sensitive than bands of Landsat-7 ETM+, and the MODIS HIRES blue-green bands are nearly twice as sensitive as the corresponding bands of the CZCS instrument. The great utility of the MODIS HIRES bands is the data they collect can be combined with more sensitive measurements from the ocean bands and temperature data computed from the thermal bands, all acquired concurrently.

### 1.3 Hypotheses

The central hypothesis of this project is that lake clarity, both near-shore and deep-water, can be determined using remote sensing in conjunction with existing *in situ* measurements. These data can be used to derive historical changes in clarity as well as provide a near-real-time measure of clarity throughout the lake.

Other hypotheses include:

1. Nearshore clarity varies around the lake, dependent on land use, stream inflows, non-point-source runoff, and nearshore currents
2. Offshore clarity is affected by mixing events and surface currents, such as during and following wind-driven upwelling

### 1.4 Project Objectives

The objective of this project is to utilize remotely sensed (satellite) data to provide a quantitative management tool for lake-wide assessments of water quality and to link changes in water quality to discrete sources at the sub-watershed (e.g. the Incline Creek watershed) scale.

## 1.5 Project Goals and Products

<b>Products</b>	<b>Goals</b>
1 Web-Accessible Repository of Lake Tahoe Imagery	Create a web-accessible repository of existing Tahoe basin RS imagery, integrated with the COMET cyber-infrastructure system
2 RS Acquisition and Storage Tools	Develop tools for semi-automatically acquiring and storing future RS imagery
3 Water Quality Algorithms	Develop algorithms to characterize the spatial variability of nearshore and offshore water clarity
4 Relation Between Nearshore Clarity and Inputs	Describe the relation between spatial and temporal variability in nearshore clarity and changes in stream, drain, and intervening zone inputs to the lake, following storms
5 Linkage Between Offshore Clarity and Forcing	Describe the relation between spatial and temporal variability in offshore clarity and lake mixing, following wind-driven upwelling, and surface current patterns
6 RS Water Quality Reporting System	Develop a reporting system where RS-derived measures of water quality are made available on a near-real-time basis
7 Methodology to Study Future Clarity Changes	Develop a methodology that can be used to study future changes in nearshore and offshore water clarity for any region of concern around Lake Tahoe, which can be used in water quality management decision-making and design
8 Methodology to Study Historical Clarity Changes	Develop a methodology that can either be directly applied or easily adapted to current and previous measurements acquired by other sensors, including Landsat-5 Thematic Mapper (TM), to create a long-term record of clarity to help understand the historical patterns of clarity change, of importance to present and future basin management
9 Publication of Findings	Publish findings in peer-reviewed journals

## 1.6 Problems Encountered

Lake Tahoe presented considerable challenges, combining the difficulties of very low reflectance signal, typical of the open ocean, with elevated terrestrial atmospheric interference (terrestrial aerosols, absorbing aerosols/pollutants), typical of lake systems. Furthermore, the clarity of Lake Tahoe can far exceed the *maximum* clarity measured in other lakes, even oligotrophic lakes such as Lake Malawi, where Secchi Depths did not exceed 15 m.

Remotely sensed measurements of nearshore data, particularly using high-spatial-resolution satellite sensors, posed problems that were not anticipated. The first problem, which was frequently encountered across the lake, is sun glint contamination. The shallow water creates a surf zone, where white caps can be observed during high winds. The increased roughness of the water in this zone appears to make the water more susceptible to the type of roughness that can exacerbate sun glint contamination. Therefore, this contamination is often present nearshore while the rest of the lake is free of sun glint. The presence of even small amounts of sun glint increases uncertainty in this zone.

The second problem is bottom reflectance. The proposal for this project had a goal to use the bottom reflectance to derive the diffuse light attenuation coefficient. However, the large uncertainty introduced by sun glint prohibits accurate estimates of bottom reflectance.

The third problem is the nearshore region is a high use environment. The nearshore region contains marinas and boat docks, which in turn contain boats and floating buoys. Throughout the nearshore region, boats and boat tracks are far more common than offshore. All of these features can be highly reflective and can contaminate satellite pixels, increasing their brightness.

Errors introduced by these factors can overwhelm the true signal of water leaving radiance. At Lake Tahoe, this signal is very small compared to coastal ocean environments. Since the bands of currently deployed high-spatial-resolution instruments were designed for land sensing, rather than water sensing, their sensitivity is fairly low. Many pixels would need to be averaged together to improve the signal-to-noise ratio, but in the nearshore region, over a sloping bottom, the bottom reflectance can change markedly over a small distance. Therefore, these sensors are not suitable for accurate retrievals of water-leaving radiance in the nearshore zone at Lake Tahoe.

## 1.7 Revisions to Proposed Methodology

To address the problems outlined above, a new methodology was developed, which uses the “high resolution” 250 m and 500 m bands of MODIS to sample water reflectance at three sets of stations sited 750 m, 1000 m, and 1500 m offshore around the lake. These measurements can be used to assess water quality gradients, water quality variability, and to identify potential sources of water quality problems. Patterns visible in the sunglint-contaminated high-spatial-resolution images revealed the presence of several “spiral eddies” in Lake Tahoe, which were previously not known to exist in lakes. These eddies can affect the variability and distribution of water quality. These measurements were combined thermal infrared measurements from ASTER, Landsat, and MODIS to characterize the meso-scale and large-scale circulation patterns at Lake Tahoe, and assess their affects on the variability and distribution of water quality at Lake Tahoe.

## 1.8 Summary of Accomplishments

### 1.8.1 Web-Accessible Repository of Lake Tahoe Imagery

**Goal:** *Create a web-accessible repository of existing Tahoe basin RS imagery, integrated with the COMET cyber-infrastructure system*

A web-accessible repository of satellite data acquired at Lake Tahoe and derived products computed from these data is operational. The database allows the user to search for and download original and processed satellite imagery, including MODIS Level 1B cut-outs, true color images, clarity maps, chlorophyll maps, and supporting data such as water temperature maps. The new system consists of a web-based interface, MySQL database, and PHP scripts to update the database as new satellite data are added. The user interface allows

the user to select the product and date/time range of interest. A product delivery page is created and displayed, with links to each satellite product sorted by date.

### 1.8.2 RS Acquisition and Storage Tools

**Goal:** *Develop tools for semi-automatically acquiring and storing future RS imagery*

Several computer programs were created to process satellite data collected by MODIS. A “cut-out” of Lake Tahoe is extracted from each MODIS image to save processing time and storage space. The bands of each cut-out is atmospherically corrected and corrected for sunglint effects. Three of the MODIS “high-resolution” bands are used to create “true-color” images of Lake Tahoe for quality control and analysis. Then each image is processed to create daily maps and multiple time series of two key water quality parameters: Secchi Depth and chlorophyll *a*.

The coefficients to create the final products were derived by other programs, which were written to process the satellite and field data, perform quality control, select match-ups, and perform the final calibration of remote sensing reflectance values using the long-term records of Secchi Depth and chlorophyll *a* collected at the LTP and MLTP stations.

Additional programs were written to extract time series from sampling “stations” distributed around the lake and compute monthly averages and variability of Secchi Depth and chlorophyll *a* at each station. These stations consisted of three sets of coordinates (45 each) sited in the nearshore, coastal, and offshore regions of the lake.

### 1.8.3 Water Quality Algorithms

**Goal:** *Develop algorithms to characterize the spatial variability of nearshore and offshore water clarity*

Algorithms were developed to predict nearshore and offshore Secchi Depths and chlorophyll *a* from MODIS data. MODIS reflectances, acquired at 1000 m, 500m, and 250 m resolutions, were regressed against *in situ* Secchi Depths and chlorophyll *a* measured at the LTP and MLTP stations from July 2002 – July 2010. The 1000 m bands, which have high sensitivity were calibrated to measure offshore clarity and chlorophyll *a* reduced resolution but higher confidence. The 250 and 500 m bands, which have lower sensitivity but can measure closer to shore, were calibrated to measure nearshore clarity and chlorophyll *a*. An automated atmospheric correction procedure and processing code were developed to produce high quality maps and time series of water quality at Lake Tahoe.

### 1.8.4 Relation Between Nearshore Clarity and Inputs

**Goal:** *Describe the relation between spatial and temporal variability in nearshore clarity and changes in stream, drain, and intervening zone inputs to the lake, following storms*

Time series of stream inflow, Secchi Depth, and chlorophyll *a* were compared at the inflow points of ten basin streams around the lake. The time series of stream inflows and nearshore clarity time series indicate that streamflow, and therefore sediment input, is the major contributor to short-term decreases in clarity. The lowest Secchi Depths were obtained nearest the streamflow locations around the lake, and the Secchi Depth troughs occurred coincident with peak inflows.

The chlorophyll *a* maps and the nearshore/offshore chlorophyll *a* cycle derived from them reveal a significant seasonal pattern. Coincident with spring runoff, chlorophyll *a* begins to increase along the southern shore, concentrated near Stateline, and along the eastern shore, extending just north of Glenbrook Bay. The elevated chlorophyll *a* concentrations observed in the satellite-derived maps were found along the southern and eastern shores in all but two years of this study, 2002 and 2008, which were low flow years. Patches of elevated chlorophyll *a* concentrations appeared during spring runoff and appear to be concentrated along the southern shore adjacent to the Upper Truckee River, Trout Creek, and Edgewood Creek inflows. Elevated concentrations were also observed near Incline Village and Glenbrook. The elevated concentrations appear

to spread around the lake via large-scale circulation (gyres), with flow reversals and shore-to-shore (south-to-south or south-to-west) transport via smaller-scale (“spiral”) eddies 3 – 5 km in diameter. Chlorophyll *a* was observed to spread offshore in plumes or jets following upwelling events. The plumes and eddies may contribute to offshore diffusion.

Around the shoreline, the region adjacent to the Trout Creek and Upper Truckee River inflows showed the greatest variability, and highest peaks of opacity (low Secchi Depths) and chlorophyll *a* concentrations. Surprisingly, the lowest typical water quality measurements were recorded to the east of this point, adjacent to the Edgewood Creek inflow, despite significantly lower flows in Edgewood Creek. Higher temperatures and nutrient concentrations have been found in Edgewood Creek, possibly associated with the Edgewood-Tahoe Golf Course, as well as due to urban pollution affects. However, Edgewood Creek’s flows are low enough that computed loadings indicate a significantly lower impact than the Upper Truckee River. The lower water quality observed at this location may be due to currents transporting the Upper Truckee River and Trout Creek inputs eastward. In addition, there may be significant sediment resuspension from the shoals, which are only approximately 2 m deep between the Trout Creek and Edgewood Creek inflows, which may be transported eastward. Surface current analysis from satellite images and drogue data indicate that a spiral eddy is often found in the southeast corner of the lake. This eddy may concentrate and retain nutrients in this area.

### 1.8.5 Linkage Between Offshore Clarity and Forcing

**Goal:** *Describe the relation between spatial and temporal variability in offshore clarity and lake mixing, following wind-driven upwelling, and surface current patterns*

Upwelling was found to have a strong affect on chlorophyll *a* levels in the fall. In the spring, chlorophyll *a* levels increased along the southern shore following spring inflows. The patches of chlorophyll *a* appear to spread around the lake via large-scale circulation (gyres), with flow reversals and shore-to-shore (south-to-south or south-to-west) transport via smaller-scale (“spiral”) eddies 3 – 5 km in diameter. Chlorophyll *a* was observed to spread offshore in plumes or jets following upwelling events. The plumes and eddies may contribute to offshore diffusion.

### 1.8.6 RS Water Quality Reporting System

**Goal:** *Develop a reporting system where RS-derived measures of water quality are made available on a near-real-time basis*

A reporting system has been developed to provide near-real-time RS-derived measurements of water quality. MODIS images can be easily ordered and downloaded at no cost. Then the scripts developed for this project can be applied in automated fashion to product chlorophyll *a* and Secchi Depth maps from the satellite images. The processed satellite data may be sampled at points of interest to generate time series and monthly averages of chlorophyll *a* and Secchi Depth. Sets of multiple images can be processed as simply as individual images. Prior to generation of water quality maps and time series, manual inspection of the true color images should be performed for QA/QC using the Qview program.

### 1.8.7 Methodology to Study Future Clarity Changes

**Goal:** *Develop a methodology that can be used to study future changes in nearshore and offshore water clarity for any region of concern around Lake Tahoe, which can be used in water quality management decision-making and design*

A methodology was developed during this study for use with MODIS-Aqua that can directly applied to MODIS-Terra to augment the data set. This methodology can continue to be applied to MODIS until both sensors cease operations. This method can then be applied to data collected by future ocean color sensors.

### 1.8.8 Methodology to Study Historical Clarity Changes

**Goal:** *Develop a methodology that can either be directly applied or easily adapted to current and previous measurements acquired by other sensors, including Landsat-5 Thematic Mapper (TM), to create a long-term record of clarity to help understand the historical patterns of clarity change, of importance to present and future basin management*

A methodology was developed during this study for use with MODIS-Aqua that can directly applied to MODIS-Terra to augment the data set and extend it back by 1.5 years. This methodology can be easily adapted to current and previous measurements acquired by other ocean color sensors. These sensors include SeaWiFS (1997 – present), MERIS (2002 – present), OCTS (1996 – present), and CZCS (1978 – 1986). This methodology employs SeaDAS for atmospheric correction and processing. SeaDAS was specifically designed for use with these sensors. These sensors do not possess high resolution bands, so they would be better suited to studying offshore water quality. It may be possible to develop a methodology to predict average weekly or monthly nearshore water quality using offshore water quality measurements acquired by these sensors.

### 1.8.9 Publication of Findings

**Goal:** *Publish findings in peer-reviewed journals*

A draft of a paper describing this research has been written. This is being reviewed by the co-authors in preparation for submission to *Limnology and Oceanography*.

# Chapter 2

## Methods

### 2.1 Satellite Data

The Moderate Resolution Imaging Spectroradiometer (MODIS) was selected to measure Secchi Depth and chlorophyll *a* at Lake Tahoe. There are currently two MODIS sensors in orbit, one aboard the Terra satellite and one aboard the Aqua satellite. MODIS-Aqua was selected for this study due to its greater radiometric accuracy and support of the oceanographic community, leading to better radiometric calibration and processing methods. The 250 and 500 m “high resolution” (HIRES) bands were selected to acquire nearshore measurements. Striping exists in one of the bands due to uneven calibration of the sensors. A destriping algorithm exists for MODIS-Aqua, but does not currently exist for MODIS-Terra due to a lack of calibration data. Therefore, MODIS-Aqua is the ideal choice. In future work, MODIS-Terra data can be added to augment the analysis and study short-term transport effects.

#### 2.1.1 Atmospheric Correction

Spaceborne radiometers, such as MODIS, measure the spectral distribution of radiance exiting the top of the atmosphere. To retrieve water quality measurements, it is necessary to derive the spectral distribution of radiance upwelling from below the water surface. Only a small fraction of the radiance measured at the sensor is water-leaving radiance. Over oligotrophic waters, the atmosphere can contribute approximately as much as 90 – 99% of the signal received by the satellite sensor, due to molecular (Rayleigh) and aerosol (Mie) scattering of direct and reflected sunlight. In addition, there can be large surface contributions from the water surface, such as specular reflection (sun glitter) and white-caps. Therefore, it is essential that atmospheric correction be performed on each satellite image to remove these contributions and adjust for atmospheric attenuation of the water-leaving radiance signal.

The NASA Ocean Biology Processing Group (OBPG) produces a standard set of Level 2 ocean color products for MODIS. However, these products are derived using assumptions that are not valid at Lake Tahoe, which differs from the open ocean in three important aspects. First, the standard ocean color algorithm assumes a maritime atmospheric composition over the open ocean, in which aerosols are comprised primarily of water vapor and salt. The atmosphere at Tahoe contains terrestrial aerosols, such as soil particles, as well as atmospheric pollution, which have more complex scattering and absorption properties. Second, the atmosphere at Tahoe is significantly thinner than the oceanic atmosphere, since the lake surface is 1900 m above mean sea level. Third, despite its great clarity, Tahoe’s waters are optically more complex than the open ocean, due to significant terrigenous inputs. Therefore, important properties do not covary with chlorophyll *a*. This complicates the atmospheric correction process, as described below.

#### SeaDAS

The SeaWiFS Data Analysis System (SeaDAS) Version 6.1, was used to atmospherically correct the MODIS data acquired at Lake Tahoe. SeaDAS is a comprehensive software package designed for the processing, display, analysis, and quality control of ocean color data (*Fu et al. [1998]; Gohin et al. [2002]*). SeaDAS

was designed for use with all of the satellite sensors supported by the OBPG, including MODIS-Aqua, MODIS-Terra, SeaWiFS, OCTS, and CZCS. SeaDAS supports processing sensor data from raw (Level 0, L0) through scientific-level (Level 2 or 3) data products (see Table 2.1). Satellite images may be sub-scened using SeaDAS, allowing small areas of interest to be extracted from large satellite scenes. This can save considerable processing time and storage capacity. SeaDAS can read many image formats and display the images using a number of color maps, along with coastlines and gridlines. SeaDAS can project images, perform various band operations, such as spatial filtering, and can output the data in ASCII format for processing and viewing using other software packages. SeaDAS is designed to run on UNIX or UNIX-based operating systems, such as Linux, Mac OSX, SGI IRIX, or Sun Solaris. It may be run on Windows using Cygwin or a virtual appliance <http://seadas.gsfc.nasa.gov>. The SeaDAS package consists of binaries and libraries, UNIX shell scripts, and IDL programs. IDL (Interactive Data Language) is a scientific programming language made by ITT Visual Solutions (ITT VIS), which contains numerous functions for the display and analysis of gridded and time series data. IDL contains a no-cost run-time mode, allowing end users to run existing compiled IDL programs without having to purchase a software license. Version 7.0 of IDL was used for this study.

Table 2.1: MODIS Processing Levels

Level	Description
Level 0	Raw data.
Level 1A	Level-1A products contain the raw radiance counts from all bands as well as spacecraft and instrument telemetry. Calibration and navigation data, and instrument and selected spacecraft telemetry are also included. Level-1A data are used as input for geolocation, calibration, and processing.
Level 1B	The Level 1B data set contains calibrated and geolocated at-aperture radiances generated from Level 1A sensor counts. Additional data are provided, including quality flags, error estimates, and calibration data.
Level 2	Each Level-2 product is generated from a corresponding Level-1A product. The main data contents of the product are the geophysical values for each pixel, derived from the Level-1A raw radiance counts by applying the sensor calibration, atmospheric corrections, and bio-optical algorithms. Each Level-2 product corresponds exactly in geographical coverage (scan-line and pixel extent) to that of its parent Level-1A product and is stored in one physical HDF file. The standard Ocean Color product contains 12 geophysical values derived for each pixel: six water-leaving radiances for bands 1 to 6, the chlorophyll a concentration, the diffuse attenuation coefficient at band 3, the epsilon value for the aerosol correction of bands 7 and 8, the angstrom coefficient for bands 4 and 8, and the aerosol optical thickness at band 8. The standard SST product contains 11-micron and 4-micron (nighttime only) SST for each pixel. In addition, 32 flags are associated with each pixel indicating if any algorithm failures or warning conditions occurred for that pixel.

## Level 2 Processing Flags

As data are processed (using the l2gen program, which is part of SeaDAS) from Level 1 to Level 2, checks are made for different defined conditions, such as the presence of clouds or sunglint. When tests are met for a particular condition, a flag is set for that pixel for that condition. Each pixel in an image is assigned a 32-bit integer mask, where each bit corresponds to a flag, allowing up to 32 flags to be defined and stored for each pixel. These Level 2 processing flags are stored as the “l2.flags” product. These flags are listed in Table 2.2.

For Level 1 to Level 2 processing (l2gen), masked pixels are not processed and are typically set to zero so as to eliminate them from future analysis. For products where zero could be a valid data value, a number outside the possible data range is substituted. For MODIS, l2gen currently has eight predefined L1A processing masks (each comprised of only one flag) that can be turned on (1) or off (0) by the user. These masks are listed in Table 2.3. For this study, all masking was turned off, and select masks were applied during post-processing.

Table 2.2: Flags and masks that are set during Level 2 and Level 3 processing in SeaDAS. Flags in blue are masked during Level 3 (ocean color) processing.

Bit	Name	Description
01	ATMFAIL	Atmospheric correction failure
02	LAND	Pixel is over land
03	PRODWARN	One or more product warnings
04	HIGLINT	High sun glint
05	HILT	Observed radiance very high or saturated
06	HISATZEN	High sensor view zenith angle
07	COASTZ	Pixel is in shallow water
08	<i>Spare</i>	<i>Spare Bit</i>
09	STRAYLIGHT	Straylight contamination is likely
10	CLDICE	Probable cloud or ice contamination
11	COCCOLITH	Coccolithofores detected
12	TURBIDW	Turbid water detected
13	HISOLZEN	High solar zenith
14	<i>Spare</i>	<i>Spare Bit</i>
15	LOWLW	Very low water-leaving radiance (cloud shadow)
16	CHLFAIL	Derived product algorithm failure
17	NAVWARN	Navigation quality is reduced
18	ABSAER	Possible absorbing aerosol (disabled)
19	<i>Spare</i>	<i>Spare Bit</i>
20	MAXAERITER	Aerosol iterations exceeded max
21	MODGLINT	Moderate sun glint contamination
22	CHLWARN	Derived product quality is reduced
23	ATMWARN	Atmospheric correction is suspect
24	<i>Spare</i>	<i>Spare Bit</i>
25	SEAICE	Possible sea ice contamination
26	NAVFAIL	Bad navigation
27	FILTER	Pixel rejected by user-defined filter
28	SSTWARN	SST quality is reduced
29	SSTFAIL	SST quality is bad
30	HIPOL	High degree of polarization
31	PRODFAIL	Derived product failure
32	<i>Spare</i>	<i>Spare Bit</i>

Table 2.3: User flags for MODIS processing in SeaDAS.

Mask Name	Description
maskland	Mask land pixels
maskcloud	Mask clouds or ice
maskhilt	Mask saturated pixels (hilt)
maskbath	Mask shallow-water pixels, as determined by bathymetry map
maskglint	Mask pixels contaminated by sunglint
masksatzen	Mask pixels where satellite zenith angle $> 60^\circ$
masksunzen	Mask pixels where the solar zenith angle $> 70^\circ$
maskstlight	Mask pixels contaminated by stray light from nearby land or clouds

### Aerosol Correction

The contribution of Rayleigh scattering is well known and can be accurately estimated (*Gordon [1978]*), after adjusting for the atmospheric pressure at Tahoe. However, the aerosol contributions can be variable and difficult to estimate. SeaDAS contains several atmospheric correction models to correct for the scattering induced by aerosols. Several candidate models were evaluated to identify the best model for correcting Lake Tahoe data. Maritime, coastal, and tropospheric models were tested using different humidities, but these failed to produce accurate results. This may be due to either the highly variable humidity at Tahoe, or the particle content of the water interfering with aerosol estimation.

For open ocean waters, it is common to assume that the water-leaving radiance in the red or near-infrared (NIR) parts of the spectrum is negligible. Known as the “dark pixel assumption,” any signal received in the red or NIR wavelengths is assumed to be contributed by aerosol scattering alone. This allows the aerosol reflectance to be extrapolated from the red or NIR bands to shorter wavelengths (blue and green). This technique is valid for Case 1 waters, where chlorophyll content is low and particulate content is negligible.

However, these conditions are not satisfied in inland and coastal waters, which can contain elevated levels of chlorophyll and, more significantly, significant concentrations of inorganic suspended matter. This leads to non-negligible radiance in the NIR and introduces considerable errors into the retrievals. The current default SeaWiFS/MODIS algorithm has implemented a method to account for the NIR ocean contributions, using an iterative approach based on a model of the spectral shape for particle backscattering coefficient in coastal waters. However, due to model limitations for complex (Case 2) turbid waters, significant errors can still exist in satellite-derived products. Two alternative procedures were found to significantly improve the retrieval accuracy.

*Wang and Shi [2007]* developed a correction algorithm employing the shortwave infrared (SWIR) bands of MODIS. Even in fairly turbid water, the SWIR bands remain optically dark. Although the SWIR method shows improved ocean color products in the coastal regions, its performance in non-turbid ocean waters is usually worse than the standard (NIR) method, introducing noise into the derived products. This is due to the fact that the MODIS SWIR bands are designed for the land and atmosphere applications with substantially lower sensor band signal-noise ratio (SNR) values. Therefore, SeaDAS implements a switching procedure that uses NIR correction where possible, switching to SWIR correction when the NIR reflectance exceeds a specified threshold. This threshold was often exceeded at Tahoe, particularly in the spring and summer. Another problem encountered with this method, is an excessive quantity of pixels were masked, indicating failure of this algorithm.

The second procedure, derived by the Management Unit of the North Sea Mathematical Models (MUMM) [*Ruddick et al., 2000*], avoids the need for iteration by assuming a simple linear relationship between the water-leaving radiances in the visible and NIR. The MUMM algorithm consists of regressing the NIR radiances between two bands, which are located at 748 nm and 869 nm on MODIS. The slope of the line (epsilon) is controlled by aerosol scattering. This line is then extrapolated to the visible to correct for the aerosol scattering contribution. Manual curve fitting is highly inefficient for processing large quantities of satellite images. Therefore, we developed and implemented an automated curve-fitting algorithm to derive epsilon for each image. This required each image to be processed twice. First, the image was processed using the default atmospheric correction algorithm to correct the NIR and SWIR radiances for Rayleigh scattering.

Then the Rayleigh-corrected NIR/SWIR reflectances were extracted over the water surface. Analysis of the data showed that the optimal curve-fitting data fell into a range 0.004 reflectance values in width, starting above the smallest nonzero reflectance value. Values less than 0.0001 and greater than 0.0200 were removed, along with any erroneous data. The minimum value was then identified, and values greater than a linear distance of 0.004 from this value were eliminated. If more than four points remained, a regression line was fit to the filtered data set. The slope of the regression line between two NIR or SWIR bands is the epsilon parameter. This parameter was then input into the second processing iteration of the satellite image. If no epsilon value was found, the image was not be corrected, unless an option was selected to set the epsilon parameter to 1.0. For this study, using the 500 m resolution SWIR bands slightly improved the retrieval accuracy. By using the 500 m SWIR bands, nearshore masking was deactivated, enabling measurements as close as 500 m from shore.

### 2.1.2 High Resolution True Color MODIS Images

Three of the “high resolution” 250/500 m bands of MODIS can be combined to create true color images. MODIS bands 1, 4, and 3 respectively record reflected radiance in the red (620 – 670 nm), green (545 – 565), and blue (459 – 479 nm) part of the atmospheric spectrum. These bands can be combined to form a red-green-blue (RGB) composite, forming a true color image similar to a photograph or what would be seen by a person observing the earth’s surface from space. The 500 m blue and green bands are first interpolated to 250 m to match the resolution of the red band. Each band is corrected for Rayleigh scattering and then projected to a UTM grid. Next, the bands are combined to form a true color (RGB) composite. Finally some brightness and contrast adjustments are performed.

Many atmospheric and surface features can be observed from these images, including clouds, fog, sun glitter, haze, smoke, jet contrails, and sediment plumes. The true color images can be used for scientific analysis for image QA/QC. Due to the relatively low water leaving radiance at Tahoe, high accuracy of atmospheric correction and calibration is required. The true color images were used to manually pre-screen the satellite data, as detailed in the next section, to identify high quality scenes and to remove scenes that might otherwise pass automatic screening algorithms.

Figure 2.1 shows six true color images derived at Lake Tahoe. Figure 2.1(a) shows a high quality image that is perfectly clear of surface and atmospheric interference. Figure 2.1(b) shows an otherwise high quality image that contains two very small clouds in the southwest basin, over and adjacent to Meeks Bay. These can cause sub-pixel contamination of 1 km MODIS data while possibly evading automatic cloud detection. It is possible that they could pass high-resolution screening as well. Therefore these pixels can be identified from the true color image and avoided or masked when sampling data from this scene. This scene was included in the calibration set since the clouds did not obscure the LTP and MLTP sampling locations. Figure 2.1(c) shows thin, faint contrails across the lake surface, crossing over the northern part of the lake. Care must be taken when sampling this image. The bottom three panels show high levels of contamination due to sun glitter. Figure 2.1(d) also shows highly visible jet contrails across the western and southern parts of the lake. The sun glitter in Figure 2.1(e) does not extend to the eastern shore. Therefore, the nearshore region extending from north of Marla Bay to Glenbrook can still be sampled from this image. Figure 2.1(f) shows strong eddy patterns in the sun glitter, indicating a counter-clockwise gyre in the northern part of the lake, a clockwise gyre in the southern part of the lake, and a possible counter-clockwise eddy adjacent to the southern shore. This can help interpret water quality patterns in maps derived from uncontaminated images acquired before or after the date of this image.



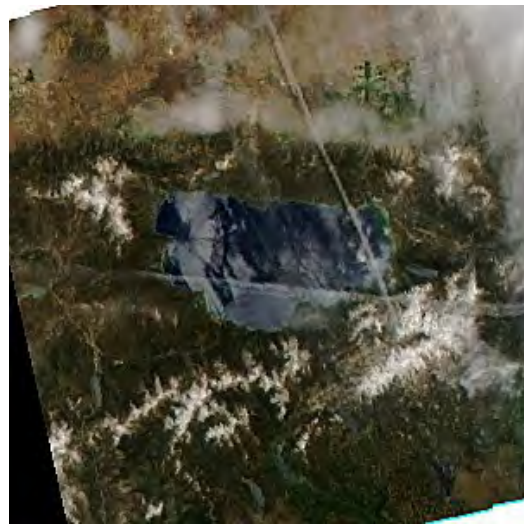
(a) Year: 2002, Day: 245



(b) Year: 2002, Day: 190



(c) Year: 2004, Day: 29



(d) Year: 2004, Day: 152



(e) Year: 2004, Day: 166



(f) Year: 2004, Day: 184

Figure 2.1: MODIS-Aqua high resolution true color images, showing a clear image and images contaminated by clouds, sun glitter, and jet contrails.

### 2.1.3 MODIS Image Quality Control

Analysis of the long-term time series data showed much greater variability than the *in situ* data set. It was determined that sun glitter and small (sub-pixel-scale) contamination from thin or narrow clouds and jet contrails contribute more error than previously thought. Flyovers, and therefore contrails, are common features above Lake Tahoe. They can partially contaminate an image, but they can be thin enough that they cannot be detected well by cloud masking algorithms. Glint contamination is often not uniform across the lakes surface, and is often greater near the shoreline. Therefore, fully automated processing can lead to significant errors, especially in the nearshore data. An improved method was integrated into the processing chain to assist the operator/scientist identify good images and create a subset of high quality images for further processing and analysis.

A quality control computer program with an interactive image viewer was created to allow the user to quickly index through all high resolution true color images in a given folder. With this program, called Qview, the user can quickly categorize each image.

Each category is assigned to a key on the keyboard. When the user presses a key, the image is labeled in the viewer, and its filename is stored in a database. Then the next image in the sequence is displayed. Forward and back buttons allow the user to view any image and set or change its category. Images that have already been categorized display the category on the image, allowing the user to locate images that have been missed or incorrectly categorized. The database can be saved at any point and is automatically saved at the end of the session. This database can be reloaded to continue unfinished work or make corrections.

After all images in a set are identified, a Python script is created to sort the files into sub-folders based on each file's category. This script can be run immediately or saved for later use. Saving all the commands in a script allows a user to view true color images (which are typically very small and can be quickly downloaded) on a local computer, then upload the script to a server for sorting the MODIS images and their associated files.

Qview contains several primary categories for identifying the quality of images for water quality measurements. These categories and their descriptions are shown in Table 2.4. A secondary set of categories, shown in Table 2.5, allows the user to sort rejected images into one of several categories for other potential uses or for deletion.

Table 2.4: Primary image categories used by Qview. These identify the quality of images selected for water quality analysis.

Category	Description
Excellent	Excellent geometry and image clarity (no more than two clouds, $< 0.5 \text{ km}^2$ total), no sun glitter or haze. These are perfect for automated calibration and/or analysis. These will comprise the main analysis data set.
Good	Very Good geometry and image clarity. Slight contamination is acceptable ( $< 2 \text{ km}^2$ ), if it can be safely ignored and/or masked in automated processing. These will comprise the secondary analysis data set and will be analyzed with more care.
Fair	Slight flaws, e.g., a few small clouds ( $< 10 \text{ km}^2$ contamination total), which may require masking or operator viewing, or larger viewing angle. These may still be used for automated analysis, but must be analyzed with more care. If true color image appears to be anomalously bright, but the image is otherwise clear, it may be categorized as “Fair” or “Undecided”.
Marginal	Degraded quality over significant part of the lake, or large viewing angle, but image has potential for providing useful data. These images are likely not suitable for automated processing or analysis.
Poor	Poor image quality and/or clouds exist over lake to the point that little or no data may be obtained, but the image may yield other useful information. This category contains cloudy images that are not overcast and that show interesting features.
Bad	Partial or blank image or other severe flaws.

Table 2.5: Alternate image categories used by Qview. These identify either the type of rejection or other useful features present in an image.

Category	Description
Glint	Image contains sun glitter, which may be useful for current analysis, or may not obscure part of the image, but must be interpreted with care. Images that are partially contaminated with sun glitter may be treated the same as images rated as “Marginal”, i.e., targeted sampling may be performed.
Smoke	Image partly or completely obscured by smoke and/or pollution/haze.
Fog	Fog over lake.
Overcast	Completely overcast over lake and watershed. These images may be deleted in the future, so it should be noted that no ground data could be obtained for the lake or its watershed.
Undecided	Mark for future evaluation. This may be necessary when an image of the lake appears too bright. This may indicate real problems, such as sun glitter or very large solar zenith angle, but it also may be an artifact due to poor selection of brightness stretching parameters.

## 2.1.4 Acquisition and Processing of Lake Tahoe MODIS Data

Since standard land and ocean MODIS products could not be used in this study, MOD01 (Level 1A, uncorrected data) products were ordered from the Level 1 Atmosphere Archive and Distribution System (LAADS, <http://ladsweb.nascom.nasa.gov/data/search.html>). Data orders were grouped by month, and concurrently downloaded via the “wget” utility. The MOD03 geolocation product is not required, since that can be quickly generated from the Level 1A product using SeaDAS.

A comprehensive processing script, “mlake”, was written using the Open Source language Python (Version 2.6, [www.python.org](http://www.python.org)) to automate SeaDAS processing of the Level 1A images to Level 1B and then Level 2. Python constructs commands for SeaDAS to execute. Once SeaDAS completes its computations, the data are passed to Python through temporary ASCII files for further processing and analysis. The mlake script can take one or more MODIS images as input and has several input options to customize processing. For example, once Level 1B images are generated, Level 2 processing can start at this step. The first step generates the geolocation file from the Level 1A image. Next, the corners of a box delineating the extent of the Tahoe watershed were used to extract a sub-scene, which was significantly smaller than the full satellite image, saving considerable storage capacity and processing time in the remaining steps. The extracted Level 1A data are then processed to Level 1B data, consisting of 36 bands, and including the 250 m and 500 m bands at their native resolution (i.e., not resampled to 1 km). The Level 1B data are then atmospherically corrected and processed to Level 2. For this study, the MUMM algorithm was selected as the optimal atmospheric correction scheme, as outlined above. This entails first processing the image to generate Rayleigh-corrected NIR/SWIR data. Next, automated linear regression is performed to compute the epsilon parameter. Finally, the MUMM algorithm is used to atmospherically correct the visible bands, and the final products are written to Level 2 files. The corrected reflectance data are extracted from the Level 2 files to Python structures (using the “extractMaps” script) for calibration, plotting water quality maps, and extracting time series data at multiple locations.

## 2.2 Field Data

### 2.2.1 Secchi Depth

Secchi Depth was measured near midday with a 25 cm white disc with a matte finish. To minimize the interference of surface reflectance, all measurements were taken on the shaded side of the boat. Due to Lake Tahoe’s very large Secchi Depth, the disc was fully illuminated by direct sunlight passing underneath the boat. After the adapting to the ambient light conditions, the observer would lower the disc until it disappeared, then raise it until it reappeared, recording each measurement. The average of the two measurements was recorded as the official Secchi Depth. The time, weather, and water conditions were also recorded. From 1969 – October 2004 measurements were taken by the same observer, R. C. Richards. Starting in October 2004, measurements have been taken by B. Allen, with some readings taken by R. Richards. Both observers had 20/20 corrected vision. Regular measurements have been recorded at the LTP station (110 m depth) every 12 days, on average, since July 1967. Measurements have been recorded every 30 days, on average, at the MLTP station (505 m depth) since December 1969. *Jassby et al. [1999]* found that the precision of measurement was approximately  $5 \pm 1\%$  of the Secchi Depth, or up to 1.26 m for typical Secchi Depths.

### 2.2.2 Chlorophyll *a*

Chlorophyll *a* (corrected for phaeophytin) has been measured at Lake Tahoe since November 1987. Samples were collected at the LTP station at depths of 0, 2, 5, 10, 15, 20, 30, 40, 50, 60, 75, 90, and 105 m on every third Secchi Depth sampling date. On the remaining sampling days, a single composite chlorophyll *a* measurement was taken of the water column to 105 m. To determine the chlorophyll *a* concentration, 100 mL of lake water were passed through a Whatman GF/C filter and frozen until analysis. Filtered chlorophyll *a* was extracted in methanol overnight at 4 °C. Extract fluorescence was measured before and after acidification using a Turner 111 fluorometer fitted with a Corning CS5-60 filter for the excitation light and a Corning CS 2-64 filter, in combination with a 10% neutral density filter for the emitted light. The fluorometer was calibrated as described in *Strickland and Parsons [1972]*.

## 2.3 Satellite Calibration

### 2.3.1 Secchi Depth

The *in situ* Secchi Depths collected from July 2002 – July 2010 at the LTP and MLTP stations were used to calibrate the atmospherically corrected MODIS reflectance data to predict Secchi Depth. The viewing conditions during each *in situ* measurement were assigned a quality flag between 1 (Poor) and 7 (Excellent). These conditions include the atmospheric conditions (clouds, haze, wind) as well as the roughness of the water surface. These conditions affect the quality of satellite as well as *in situ* measurements of Secchi Depth. Therefore, only clear-sky readings with ratings of 3 (Fair) or better were used to calibrate the MODIS data in this study. Match-ups were performed with excellent quality MODIS images, identified and sorted using the Qview program. A program, “calibrateSDT”, was written to identify the high quality MODIS image acquired nearest in time to each *in situ* sample, within a specified time period. A maximum time difference of 48 hours between MODIS and *in situ* sampling was found to be optimal. The following Level 2 flags (Table 2.2) were applied to the MODIS data to eliminate bad values:

1. PRODFAIL
2. CHLFAIL
3. HIGLINT
4. ATMFAIL
5. ATMWARN
6. LOWLW

Multiple regression was used to derive a relationship between the natural log of Secchi Depth (or Secchi Disk Transparency, SDT) and the reflectance data. Several band combinations were tested. Two calibration equations were created: one for nearshore data using the higher resolution bands, and one for higher accuracy offshore data, using the 1000 m resolution bands.

### 2.3.2 Chlorophyll *a*

The *in situ* Chlorophyll *a* samples collected from July 2002 – July 2010 at the LTP and MLTP stations were used to calibrate the atmospherically corrected MODIS reflectance data to predict Secchi Depth. Match-ups were performed with excellent quality MODIS images, identified and sorted using the Qview program. A program, “calibrateChla”, was written to identify the high quality MODIS image acquired closest in time to each *in situ* sample, within a specified time period. A maximum time difference of 48 hours between MODIS and *in situ* sampling was found to be optimal. The following Level 2 flags (Table 2.2) were applied to the MODIS data to eliminate bad values:

1. PRODFAIL
2. CHLFAIL
3. HIGLINT
4. ATMFAIL
5. ATMWARN
6. LOWLW

While Secchi Depth measurements set their own variable integration depth, dependent on the Secchi Depth itself, the depth of integration must be determined for chlorophyll *a* to compute the mean concentration from the field data. Integrating chlorophyll over shallow depths (0 – 5 and 0 – 10 m) performed better than integrating over deeper depths. It is evident that the signal is so strongly attenuated below 10 m that chlorophyll *a* below this depth has relatively little influence on the upwelling radiance. The 0 – 5 m integration performed slightly better than 0 – 10 m at the LTP station, but the difference was not significant. Furthermore, chlorophyll *a* was not measured at 5 m depth at the MLTP station. To ensure all samples were compared on the same basis, a constant 0 – 10 m integration depth was used to compute the mean chlorophyll *a* concentration for all *in situ* samples collected at the LTP and MLTP stations.

Multiple regression was used to derive a relationship between the natural log of chlorophyll  $a$  and the reflectance data. Several band combinations were tested. Two calibration equations were created: one for nearshore data using the higher resolution bands, and one for higher accuracy offshore data, using the 1000 m resolution bands.

## 2.4 Time Series

Three sets of stations, 45 each, were selected for extraction of MODIS reflectances to construct time series of Secchi Depth and chlorophyll  $a$ . The stations are displayed on the map in Figure 2.2. The coordinates are listed in Appendix A.1, Table A.1. The “nearshore” stations (NS) are located 750 m from either the shoreline or shoals that are shallow enough for bottom reflectance to contaminate the MODIS reflectance data. Similarly, the “coastal” (CS) and “offshore” (OS) stations are sited 1000 m and 1500 m, respectively, from the shoreline or visible shoals. The map in Figure 2.2 consists of a Landsat ETM+ image acquired October 2002. The shoals along the southern shore and Marla Bay are clearly visible, as are the smaller shoals along the western shore around Sugar Pine Point and along the edge of Rubicon Bay. The extensive shelf adjacent to Tahoe City is faintly visible, as is the shelf along the eastern edge of Agate Bay, on the northwest shore.

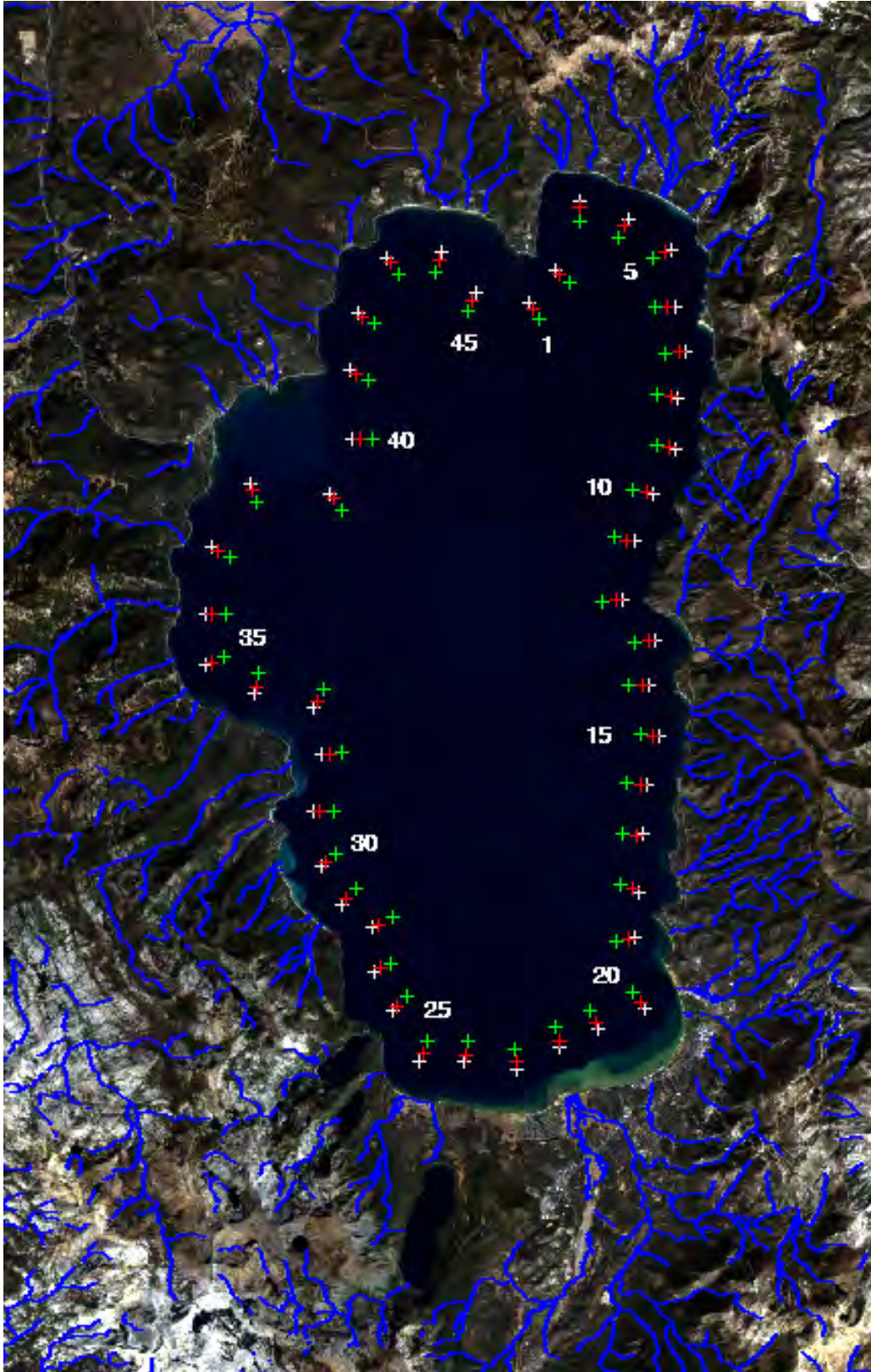


Figure 2.2: Map of Lake Tahoe showing the 135 nearshore (NS), coastal (CS), and offshore (OS) MODIS time series sampling stations.

# Chapter 3

## Results

### 3.1 Web-Accessible Repository of Lake Tahoe Imagery

**Goal:** *Create a web-accessible repository of existing Tahoe basin RS imagery, integrated with the COMET cyber-infrastructure system*

**Accomplishments:**

A web-accessible repository was created to store and distribute processed Lake Tahoe satellite data and derived products. The new system consists of a web-based interface, MySQL database, and PHP scripts set up and update the database as new data are added. Processed satellite imagery served by this system include MODIS Level 1B cut-outs and ASTER Level 1B images. Products derived from the Level 1B MODIS cut-outs include high resolution true color MODIS images, chlorophyll *a* maps, Secchi Depth maps, and 1 km temperature maps.

A MySQL database was created to store, sort, and distribute the satellite data. The database allows the user to search for satellite data by product type and date range. PHP scripts were written for each product. After new data are added to their corresponding server directory, the PHP script for that product run by typing its name into a web browser. The process can be further automated by specifying a system automation process (i.e., “cron job”) to run these scripts at regular intervals.

Figure 3.1 shows the main page, which allows the user to either login or create a new account. After logging in, the user is taken to the product order form (Figure 3.2). The user can specify the date/time search range. The month, day, hour, and minute fields are optional. Then the desired product can be selected from the drop-down list (Figure 3.3). Links to each file matching the search criteria are displayed in the product delivery page (Figure 3.4). Figure 3.5 shows a sample chlorophyll *a* map downloaded from the RS repository.

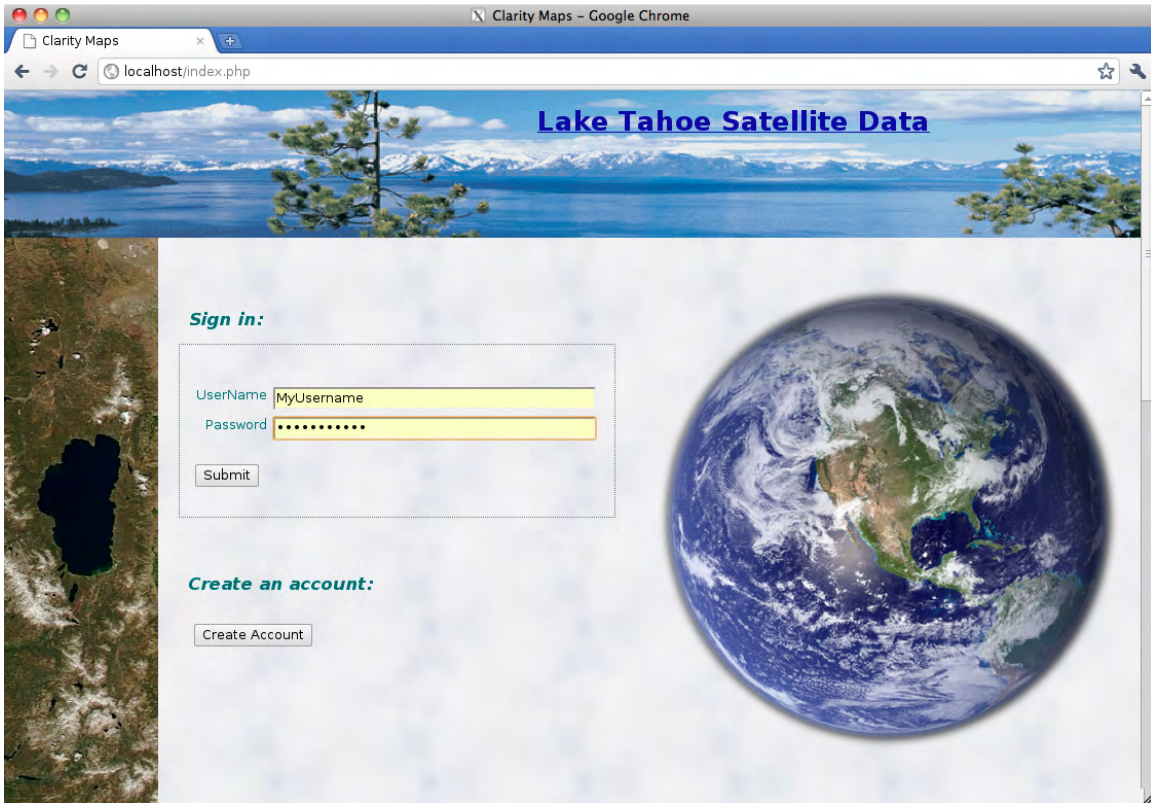


Figure 3.1: Web-accessible repository of Lake Tahoe Imagery. Main window (login or create account).

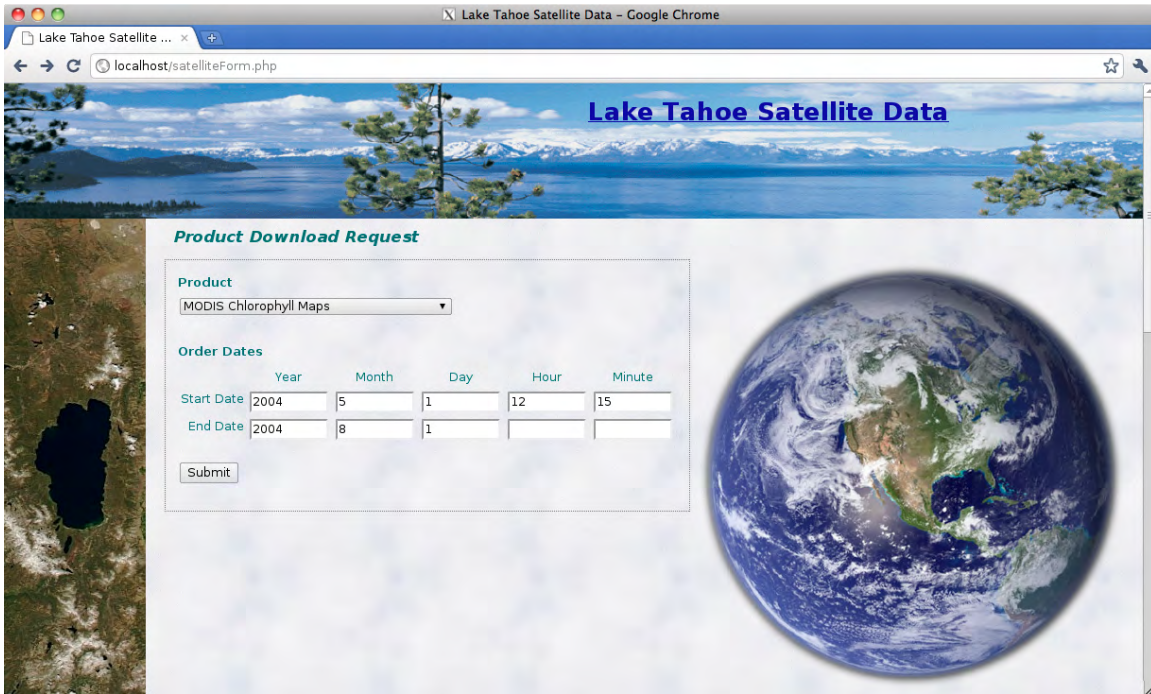


Figure 3.2: Web-accessible repository of Lake Tahoe Imagery. Product order form.

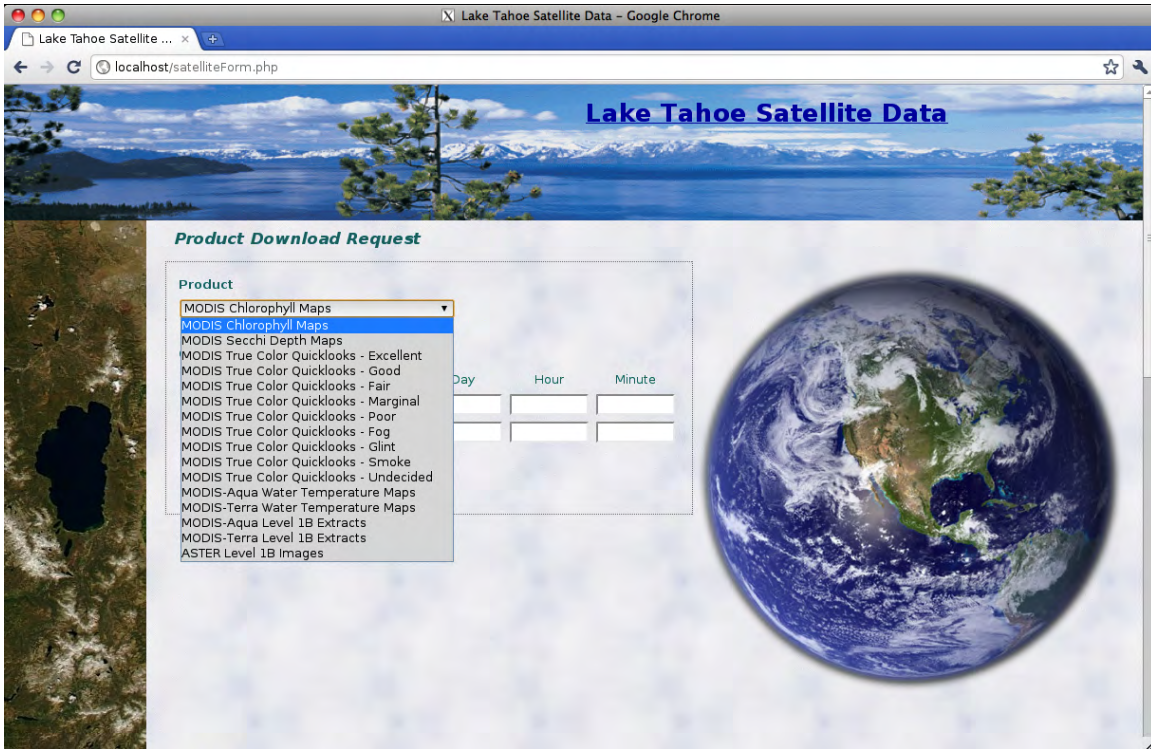


Figure 3.3: Web-accessible repository of Lake Tahoe Imagery. Product order form, showing drop-down list of available products.

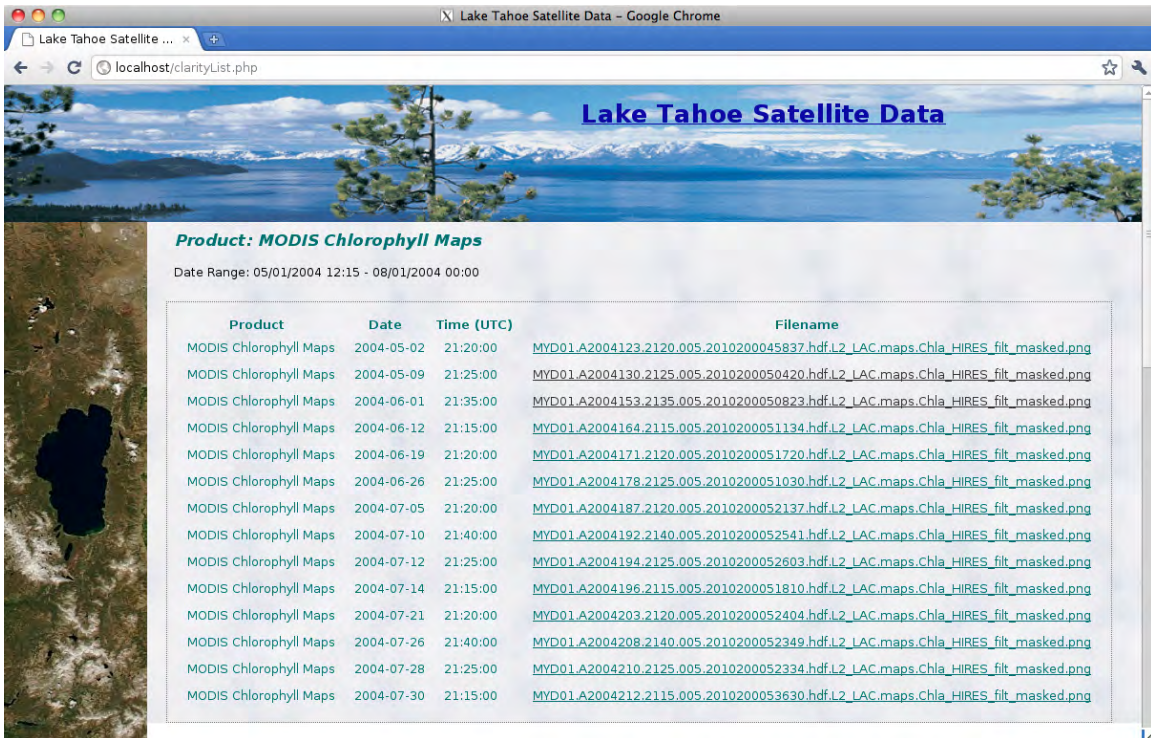


Figure 3.4: Web-accessible repository of Lake Tahoe Imagery. Sample product delivery page with links to data requested.

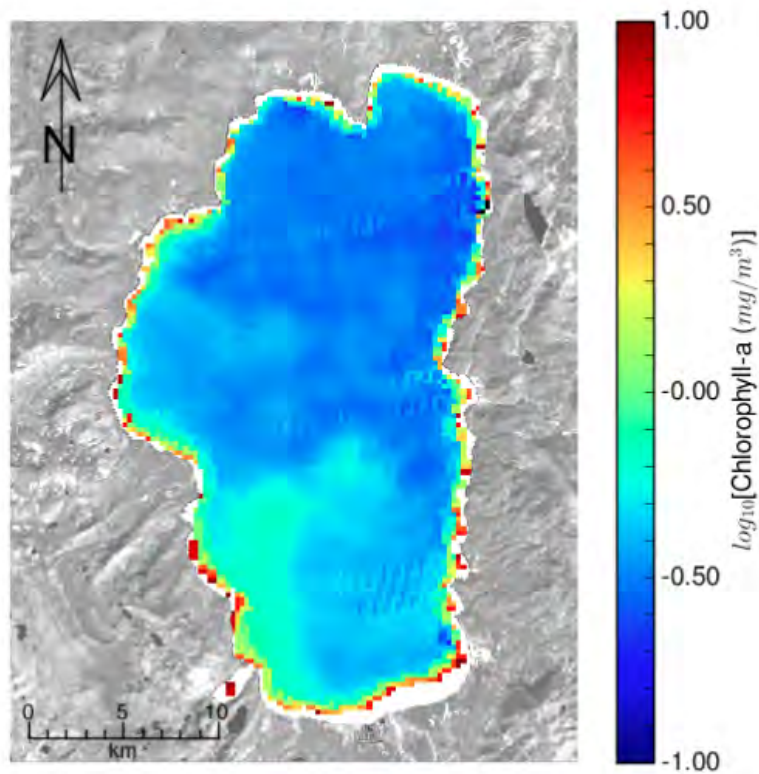
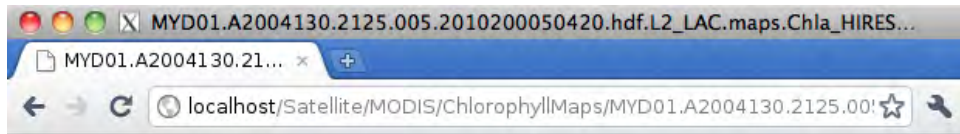


Figure 3.5: Web-accessible repository of Lake Tahoe Imagery. Sample of a downloaded product.

## 3.2 RS Acquisition and Storage Tools

**Goal:** *Develop tools for semi-automatically acquiring and storing future RS imagery*

**Accomplishments:**

Several computer programs were created to process satellite data collected by MODIS. A “cut-out” of Lake Tahoe is extracted from each MODIS image to save processing time and storage space. The bands of each cut-out is atmospherically corrected and corrected for sunglint effects. Three of the MODIS “high-resolution” bands are used to create “true-color” images of Lake Tahoe for quality control and analysis. Then each image is processed to create daily maps and multiple time series of two key water quality parameters: Secchi Depth and chlorophyll *a*.

The coefficients to create the final products were derived by other programs, which were written to process the satellite and field data, perform quality control, select match-ups, and perform the final calibration of remote sensing reflectance values using the long-term records of Secchi Depth and chlorophyll *a* collected at the LTP and MLTP stations.

Additional programs were written to extract time series from sampling “stations” distributed around the lake and compute monthly averages and variability of Secchi Depth and chlorophyll *a* at each station. These stations consisted of three sets of coordinates (45 each) sited in the nearshore, coastal, and offshore regions of the lake (see Figure 2.2).

### 3.3 Water Quality Algorithms

**Goal:** *Develop algorithms to characterize the spatial variability of nearshore and offshore water clarity*

#### 3.3.1 Secchi Depth Estimation

Multiple regression was used to derive a relationship between the natural log of Secchi Depth (or Secchi Disk Transparency, SDT) and the reflectance data. Several band combinations were tested. Two calibration equations were created: one for nearshore data using the higher resolution bands, and one for higher accuracy offshore data, using the 1000 m resolution bands.

##### Nearshore Calibration

Prediction Equation:

$$SDT = e^{(87.678*R469 - 494.785*R555 + 421.263*R645 + 3.371)} \quad (3.1)$$

Regression Summary Statistics:

```

=====
Dependent Variable: lnSDT
Method: Least Squares
# Obs:      121
# Variables: 4
=====
Variable      | Coefficient | Std. Error | t-Statistic | Probability
=====
const         |    3.371373 |    0.057497 |   58.635381 | 0.000000
Rrs_469_filt  |   87.677805 |   18.792591 |    4.665552 | 0.000008
Rrs_555_filt  |  -494.785343 |   70.579274 |   -7.010349 | 0.000000
Rrs_645_filt  |   421.263362 |   58.658755 |    7.181594 | 0.000000
=====
Models stats          | Residual stats
=====
R-squared             0.321860 | Durbin-Watson stat    1.079807
Adjusted R-squared    0.304472 | Omnibus stat          3.483524
F-statistic           18.510280 | Prob(Omnibus stat)    0.175211
Prob (F-statistic)    0.000000 | JB stat               3.370234
Log likelihood        80.145900 | Prob(JB)              0.185423
AIC criterion         -1.258610 | Skew                  -0.406641
BIC criterion         -1.166187 | Kurtosis              2.916051
=====

```

## Offshore Calibration

Prediction Equation:

$$SDT = e^{(-27.849*R469 - 195.216*R555 + 240.839*R645 - 73.823*R412 + 228.994*R443 - 321.460*R531 + 193.337*R678 + 3.471)} \quad (3.2)$$

Regression Summary Statistics:

```

=====
Dependent Variable: lnSDT
Method: Least Squares
# Obs:      121
# Variables: 8
=====
Variable      | Coefficient | Std. Error | t-Statistic | Probability
=====
const         |    3.471417 |    0.063201 |   54.926770 | 0.000000
Rrs_469_filt  |   -27.849375 |   58.296977 |   -0.477716 | 0.633775
Rrs_555_filt  |  -195.215849 |   98.531836 |   -1.981246 | 0.049992
Rrs_645_filt  |   240.838921 |   83.513144 |    2.883845 | 0.004705
Rrs_412       |   -73.823042 |   39.163190 |   -1.885011 | 0.061997
Rrs_443       |   228.993690 |   87.465996 |    2.618088 | 0.010054
Rrs_531       |  -321.459513 |   76.666850 |   -4.192940 | 0.000055
Rrs_678       |   193.337025 |   76.623376 |    2.523212 | 0.013019
=====
Models stats          | Residual stats
=====
R-squared             0.417131 | Durbin-Watson stat    1.351110
Adjusted R-squared    0.381024 | Omnibus stat          3.943068
F-statistic           11.552650 | Prob(Omnibus stat)    0.139243
Prob (F-statistic)    0.000000 | JB stat               3.407827
Log likelihood         89.305024 | Prob(JB)              0.181970
AIC criterion         -1.343885 | Skew                  -0.391902
BIC criterion         -1.159039 | Kurtosis              3.248163
=====

```

### 3.3.2 Chlorophyll *a* Estimation

Multiple regression was used to derive a relationship between the natural log of chlorophyll *a* and the reflectance data. Several band combinations were tested. Two calibration equations were created: one for nearshore data using the higher resolution bands, and one for higher accuracy offshore data, using the 1000 m resolution bands.

#### Nearshore Calibration

Prediction Equation:

$$\text{Chlorophyll} - a = e^{(-459.536 \cdot R_{469} + 372.825 \cdot R_{555} + 315.066 \cdot R_{645} + 0.081)} \quad (3.3)$$

Regression Summary Statistics:

```

=====
Dependent Variable: lnChla
Method: Least Squares
# Obs:      79
# Variables: 4
=====
Variable      | Coefficient | Std. Error | t-Statistic | Probability
=====
const         |    0.081227 |    0.210993 |    0.384977 |    0.701344
Rrs_469_filt  |  -459.536464 |    62.863683 |   -7.310047 |    0.000000
Rrs_555_filt  |   372.825242 |   243.916074 |    1.528498 |    0.130596
Rrs_645_filt  |   315.065536 |   206.120810 |    1.528548 |    0.130583
=====
Models stats          | Residual stats
=====
R-squared             | 0.616556 | Durbin-Watson stat | 1.289631
Adjusted R-squared   | 0.601218 | Omnibus stat       | 2.626635
F-statistic          | 40.198582 | Prob(Omnibus stat) | 0.268926
Prob (F-statistic)   | 0.000000 | JB stat            | 2.264927
Log likelihood        | -30.878050 | Prob(JB)           | 0.322238
AIC criterion         | 0.882989 | Skew                | 0.072838
BIC criterion         | 1.002961 | Kurtosis            | 3.816614
=====

```

## Offshore Calibration

Prediction Equation:

$$\text{Chlorophyll} - a = e^{(-919.614 \cdot R_{469} + 905.723 \cdot R_{555} + 353.584 R_{412} + 980.207 \cdot R_{531} - 1482.211 \cdot R_{547} + 346.793 \cdot R_{667} + 0.298)} \quad (3.4)$$

Regression Summary Statistics:

```

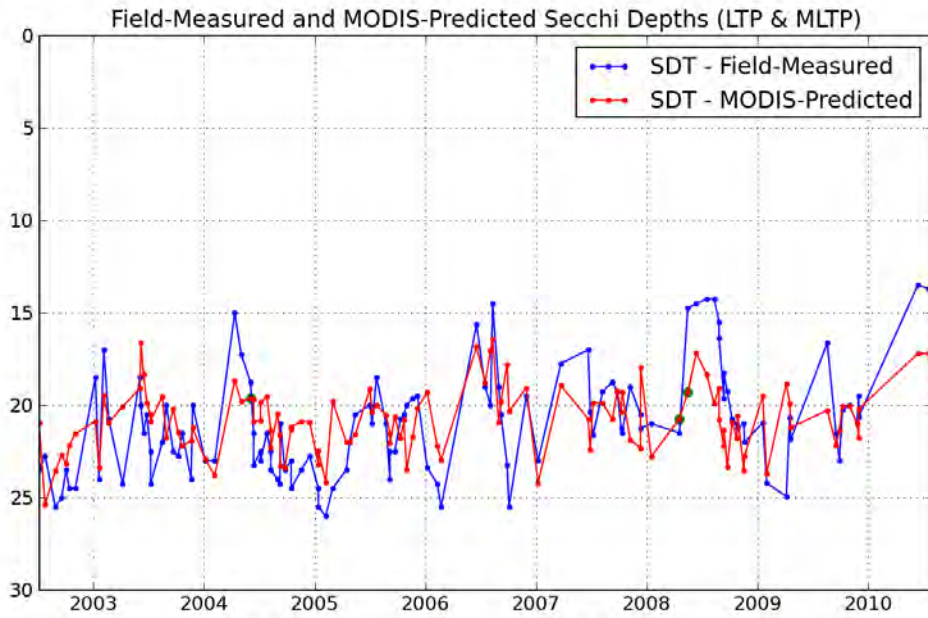
=====
Dependent Variable: lnChla
Method: Least Squares
# Obs:      79
# Variables: 7
=====
Variable      | Coefficient | Std. Error | t-Statistic | Probability
=====
const         | 0.297704   | 0.192389   | 1.547412   | 0.126148
Rrs_469_filt  | -919.613894 | 79.601900  | -11.552663 | 0.000000
Rrs_555_filt  | 905.722931  | 334.622648 | 2.706699   | 0.008480
Rrs_412       | 353.583810  | 59.418055  | 5.950781   | 0.000000
Rrs_531       | 980.207407  | 920.248256 | 1.065155   | 0.290365
Rrs_547       | -1482.211154 | 1057.800606 | -1.401220  | 0.165444
Rrs_667       | 346.792783  | 181.066197 | 1.915282   | 0.059429
=====
Models stats          | Residual stats
=====
R-squared             | 0.792763 | Durbin-Watson stat | 1.568727
Adjusted R-squared   | 0.775493 | Omnibus stat       | 1.664948
F-statistic          | 45.904738 | Prob(Omnibus stat) | 0.434972
Prob (F-statistic)   | 0.000000 | JB stat            | 1.240618
Log likelihood       | -6.572489 | Prob(JB)           | 0.537778
AIC criterion        | 0.343607 | Skew                | -0.302219
BIC criterion        | 0.553558 | Kurtosis            | 3.107479
=====

```

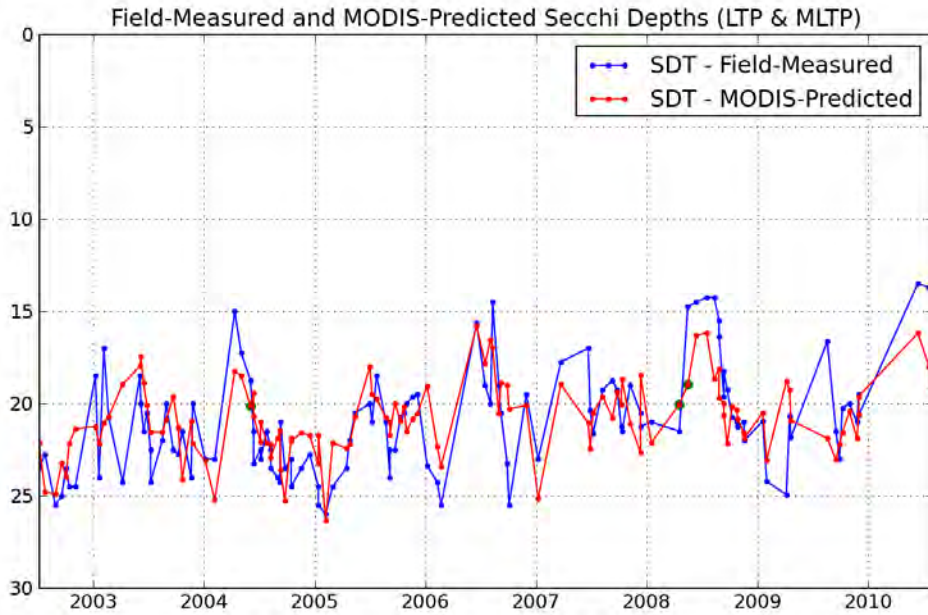
### 3.3.3 Water Quality Match-ups

Match-ups were created between MODIS-predicted and *in situ* water quality. Figure 3.6 shows match-ups between MODIS-predicted and *in situ* Secchi Depths. These comparisons combine MODIS and *in situ* sampling performed at the LTP and MLTP stations. Similarly, MODIS-predicted and *in situ* match-ups of chlorophyll *a* measured at the LTP and MLTP stations are shown in Figure 3.7. While Secchi Depth defines its own integration depth, an integration depth had to be selected for satellite chlorophyll *a* sampling, as outlined in the Methods chapter. An integration depth of 10 m was found to yield optimal performance for MODIS chlorophyll *a* sampling.

The match-ups between MODIS-predicted and *in situ* chlorophyll *a* show significantly better performance of the chlorophyll *a* algorithm. This is in agreement with the superior  $r^2$  values obtained from the chlorophyll *a* calibration. This may be due to higher accuracy of *in situ* chlorophyll *a* sampling, which is a less subjective measurement and is not affected by field conditions. Furthermore, the Secchi Depth maps derived from these equations indicate larger small-scale spatial variability of Secchi Depth than chlorophyll *a*. Both the MODIS-predicted and *in situ* Secchi Depth time series show greater small-scale variability than the chlorophyll *a* data. Furthermore, Secchi Depth appears to have a stronger response to inputs, while chlorophyll *a* shows a stronger dependence on longer-term growth, following inputs, as detailed below. These factors can alter the true value of Secchi Depth between the times of *in situ* and satellite sampling.

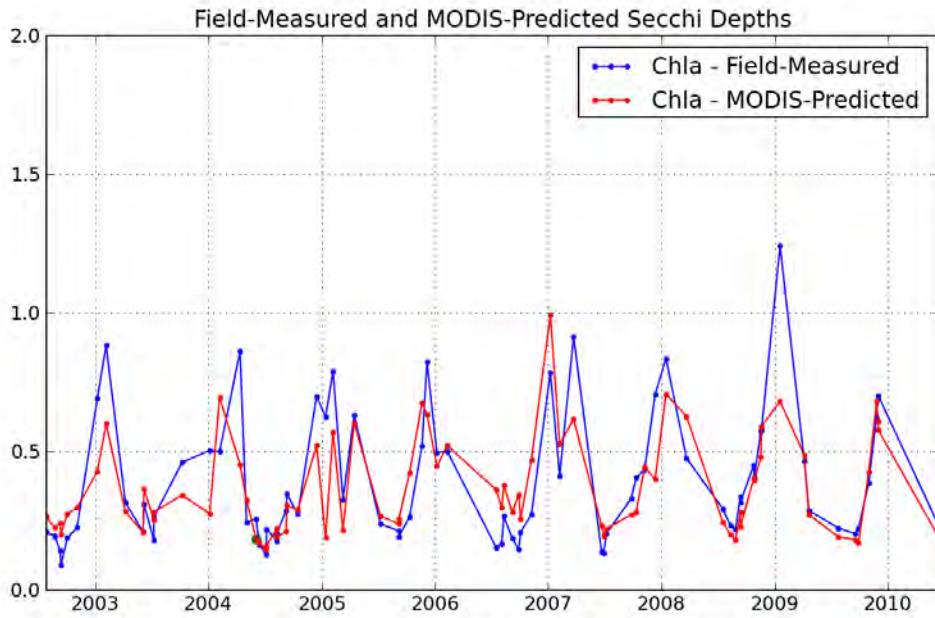


(a) Nearshore MODIS algorithm (higher resolution)

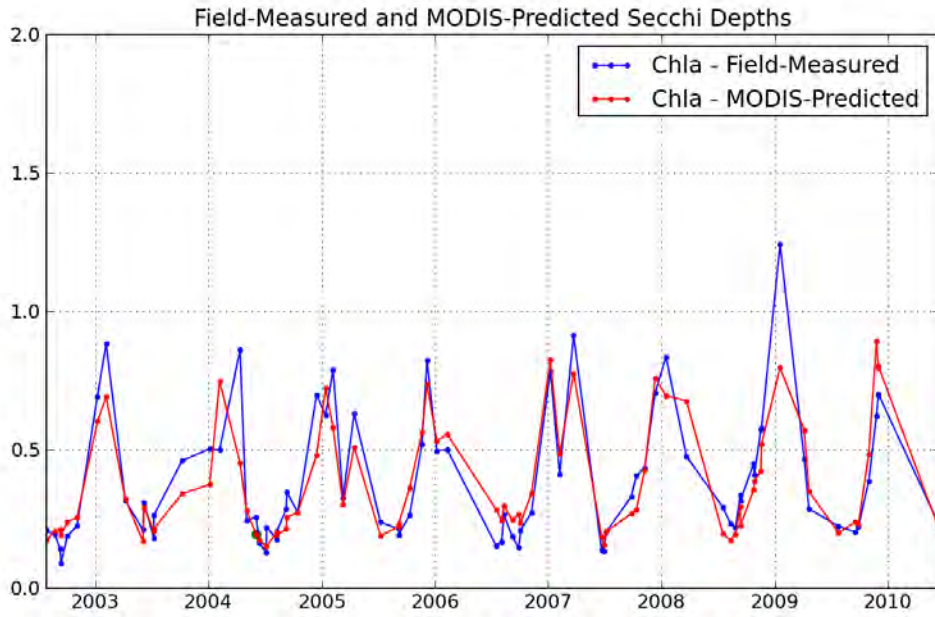


(b) Offshore MODIS algorithm (higher accuracy)

Figure 3.6: Match-ups of *in situ* and MODIS-predicted Secchi Depth measurements.



(a) Nearshore MODIS algorithm (higher resolution)



(b) Offshore MODIS algorithm (higher accuracy)

Figure 3.7: Match-ups of *in situ* and MODIS-predicted chlorophyll *a* measurements.

## 3.4 Relation Between Nearshore Clarity and Inputs

**Goal:** Describe the relation between spatial and temporal variability in nearshore clarity and changes in stream, drain, and intervening zone inputs to the lake, following storms

Maps of water quality (Secchi Depth and chlorophyll *a*) and nearshore time series extracted these maps were analyzed to identify spatial and temporal patterns of Secchi Depth and chlorophyll *a* and their variability. *In situ* streamflow, nutrient, Secchi Depth, and chlorophyll *a* data were paired with the satellite data to determine the effects of streamflow, upwelling, currents, circulation (gyres and spiral eddies), and other factors on the seasonal and spatial changes in lake clarity and chlorophyll *a*.

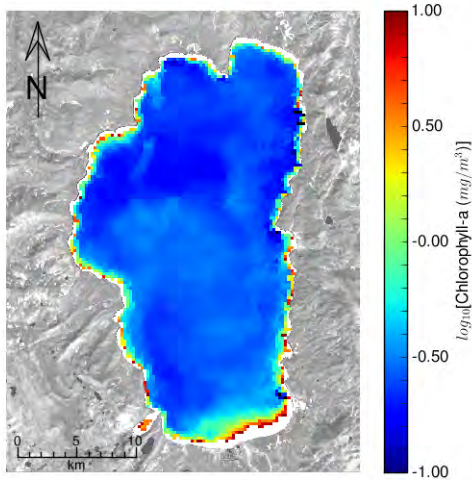
### 3.4.1 Water Quality Maps

Secchi Depth and chlorophyll *a* maps were plotted for every clear, high quality MODIS-Aqua image acquired during the 2002 – 2010 study period. A sample of these maps is shown in Figures 3.8 – 3.10. Care must be taken when interpreting these maps, since shallow nearshore waters can emit significant quantities of bottom reflectance, contaminating the signal. For Secchi Depth sampling, the minimum sampling distance from shore is determined by the bathymetry (Figure 3.11) and the true Secchi Depth. A striking feature of the Secchi Depth and chlorophyll *a* maps is that there is a large difference in the quantity of detectable shoals. For example, the shelves adjacent to Tahoe City and South Lake Tahoe are visible to a depth of 15 – 20 m. The Tahoe City shelf is absent from the chlorophyll *a* maps, and only the shallowest portion of the South Lake Tahoe shelf is evident, to a depth of approximately 5 m. This is due to the fact that the Secchi Depth algorithm largely depends on the “green” band, while the chlorophyll *a* algorithm largely depends on the “red” band and, secondarily, the “blue” band. In the absence of water, the shoals would reflect most strongly in the red part of the spectrum, with significant reflectance in the green part of the spectrum. However, water attenuates red light strongly, so the depth of penetration is limited to a few meters. Therefore, the chlorophyll *a* algorithm picks up minimal quantities of bottom reflectance, and measurements can be acquired significantly closer to shore. During low clarity periods, such as during spring inflows, the depth restriction is lessened, and Secchi Depths can be acquired closer to the shoreline.

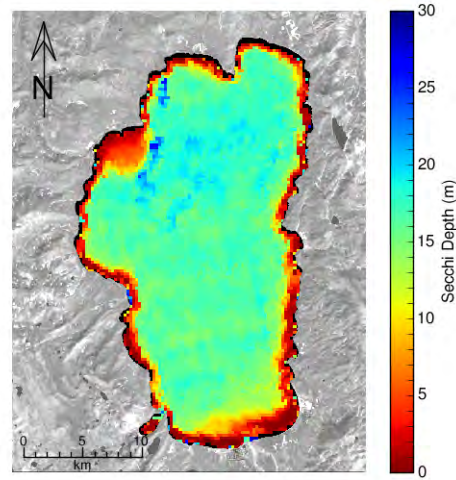
The maps indicate that Secchi Depth and chlorophyll *a* often covary spatially and temporally, even though Secchi Depth itself is much more dependent on light scattering due to fine particles [Swift *et al.*, 2006; Jassby *et al.*, 1999]. Figures 3.8 and 3.9 show four examples where chlorophyll *a* and Secchi Depth covary. Figure 3.8(a) and 3.8(b) show elevated concentrations of chlorophyll *a* and low Secchi Depths, respectively, along the southern shore on Julian Day 152 of 2003. This image was acquired during spring inflow, two days after a partial upwelling occurred. Figure 3.8(c) and 3.8(d) show this plume spreading offshore two days later. The plume translated eastward on Julian Day 157 (Figure 3.9(a) and 3.9(b)) and appears to spread northward along the eastern shore, before dispersing westward in a plume or jet as the extent of the patch along South Lake Tahoe diminishes, apparently moving shoreward (Figure 3.9(c) and 3.9(d)). This transport appears to be caused by a counter-clockwise spiral eddy, which has been observed in the southeast corner of the lake (see Appendix B, Figures B.1 and B.2).

Figures 3.10 shows two examples of chlorophyll *a* and Secchi Depth maps that do not covary, acquired on days 100 and 130 of 2004. There is a relatively strong plume of chlorophyll *a*, but there is only a small and variable decrease in Secchi Depth in these regions. These images were acquired during spring runoff, but 2004 was a low flow year, while 2003 was a moderate flow year that followed a low flow year. Presumably sediment had accumulated over the previous year, leading to a disproportionately large effect on lake water quality in 2003 that was absent in 2004. Nevertheless, the chlorophyll *a* concentrations in the plumes of 2003 and 2004 were similar. The most salient feature of the chlorophyll *a* map in Figure 3.10(c) is that the chlorophyll *a* plume strongly affects the western shore. This effect was evident in most of the other years of this study. In fact, the streams along the western shore appear to contribute little to chlorophyll *a* compared to the chlorophyll *a* transported from South Lake Tahoe via currents. The difference in chlorophyll *a* between the western and southern shores prior to transport is large, and may be due to differences in loadings. However, the difference is larger than expected. Partial upwelling occurs during the spring storms, which bring strong winds in addition to rainfall. The upwelling may induce significant sediment resuspension over the South Lake Tahoe shoals, increasing chlorophyll *a* levels through autochthonous inputs.

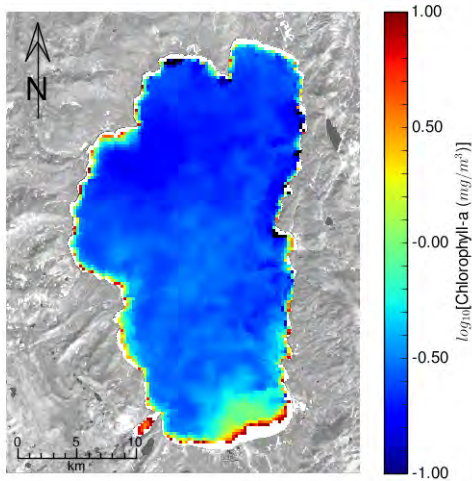
The elevated chlorophyll *a* concentrations shown in these maps were found along the southern and eastern shores in all but two years of this study, 2002 and 2008, which were low flow years. Patches of elevated chlorophyll *a* concentrations appeared during spring runoff and appear to be concentrated along the southern shore adjacent to the Upper Truckee River, Trout Creek, and Edgewood Creek inflows. Elevated concentrations were also observed near Incline Village and Glenbrook. The elevated concentrations appear to spread around the lake via large-scale circulation (gyres), with flow reversals and shore-to-shore (east-to-south or south-to-west) transport via spiral eddies 3 – 5 km in diameter.



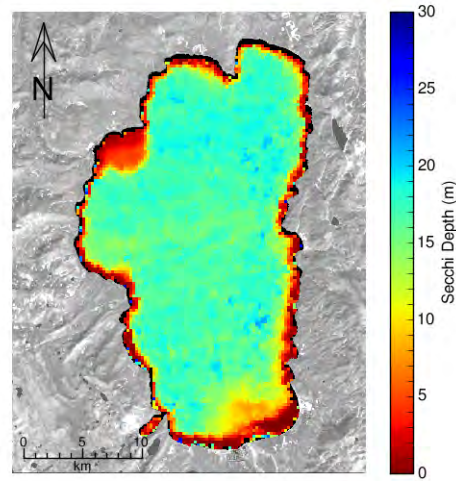
(a) Chlorophyll *a* map, Year: 2003, Day: 152



(b) Secchi Depth map, Year: 2003, Day: 152

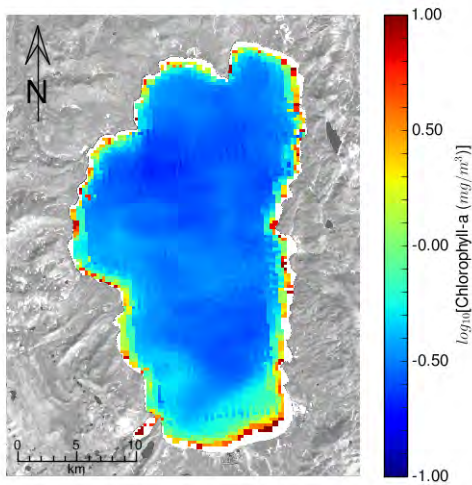


(c) Chlorophyll *a* map, Year: 2003, Day: 154

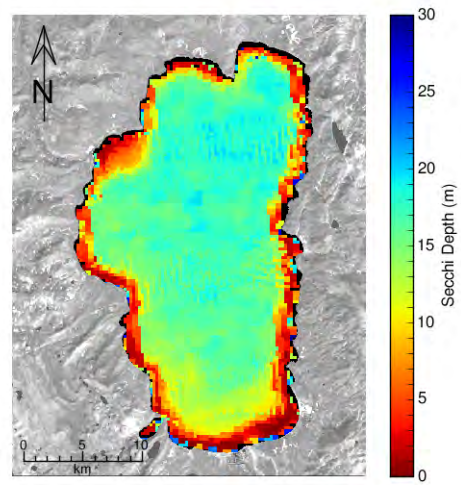


(d) Secchi Depth map, Year: 2003, Day: 154

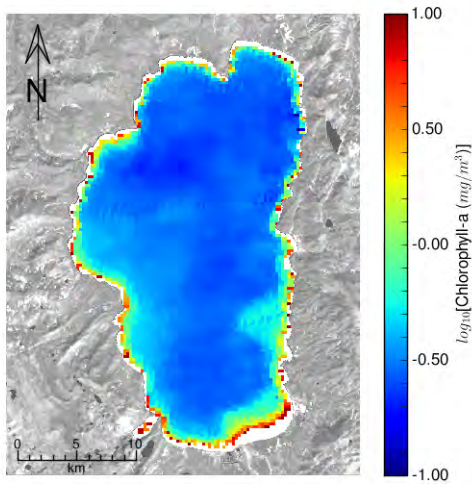
Figure 3.8: Secchi Depth and chlorophyll *a* maps acquired in 2003, Julian Days 152 – 154.



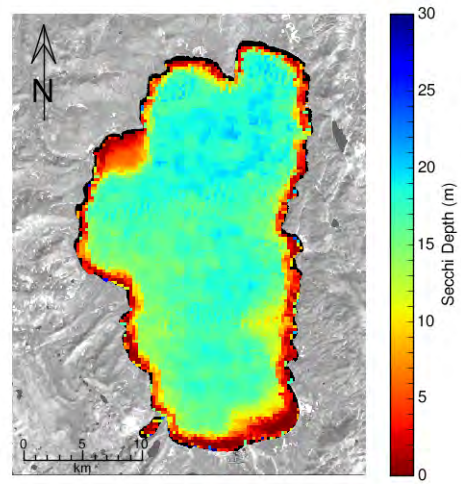
(a) Chlorophyll *a* map, Year: 2003, Day: 157



(b) Secchi Depth map, Year: 2003, Day: 157

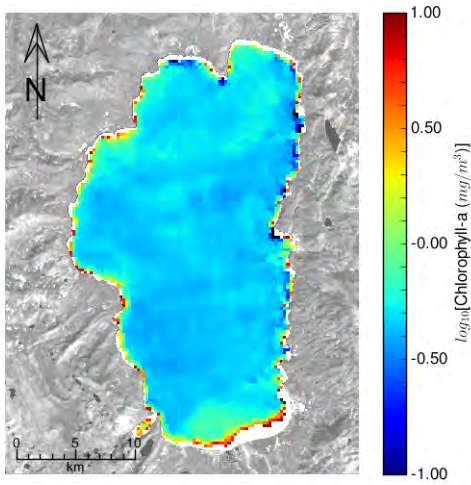


(c) Chlorophyll *a* map, Year: 2003, Day: 159

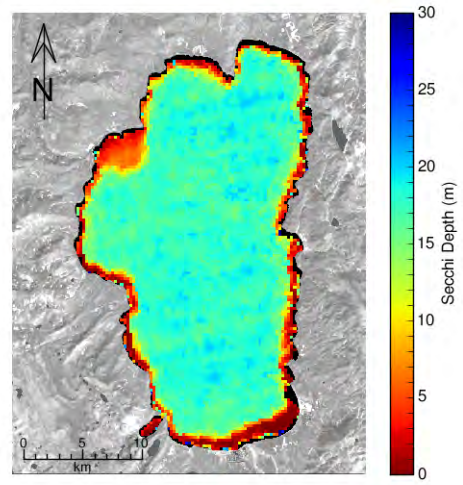


(d) Secchi Depth map, Year: 2003, Day: 159

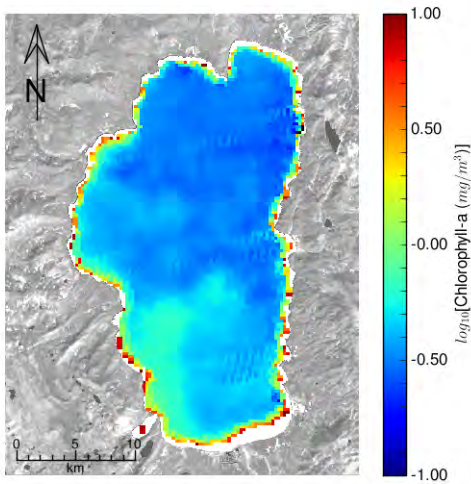
Figure 3.9: Secchi Depth and chlorophyll *a* maps acquired in 2003, Julian Days 157 – 159.



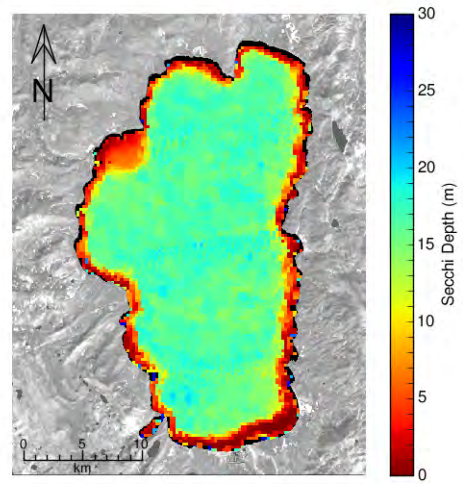
(a) Chlorophyll *a* map, Year: 2004, Day: 100



(b) Secchi Depth map, Year: 2004, Day: 100



(c) Chlorophyll *a* map, Year: 2004, Day: 130



(d) Secchi Depth map, Year: 2004, Day: 130

Figure 3.10: Secchi Depth and chlorophyll *a* maps acquired in 2004, Julian Days 100 – 130.

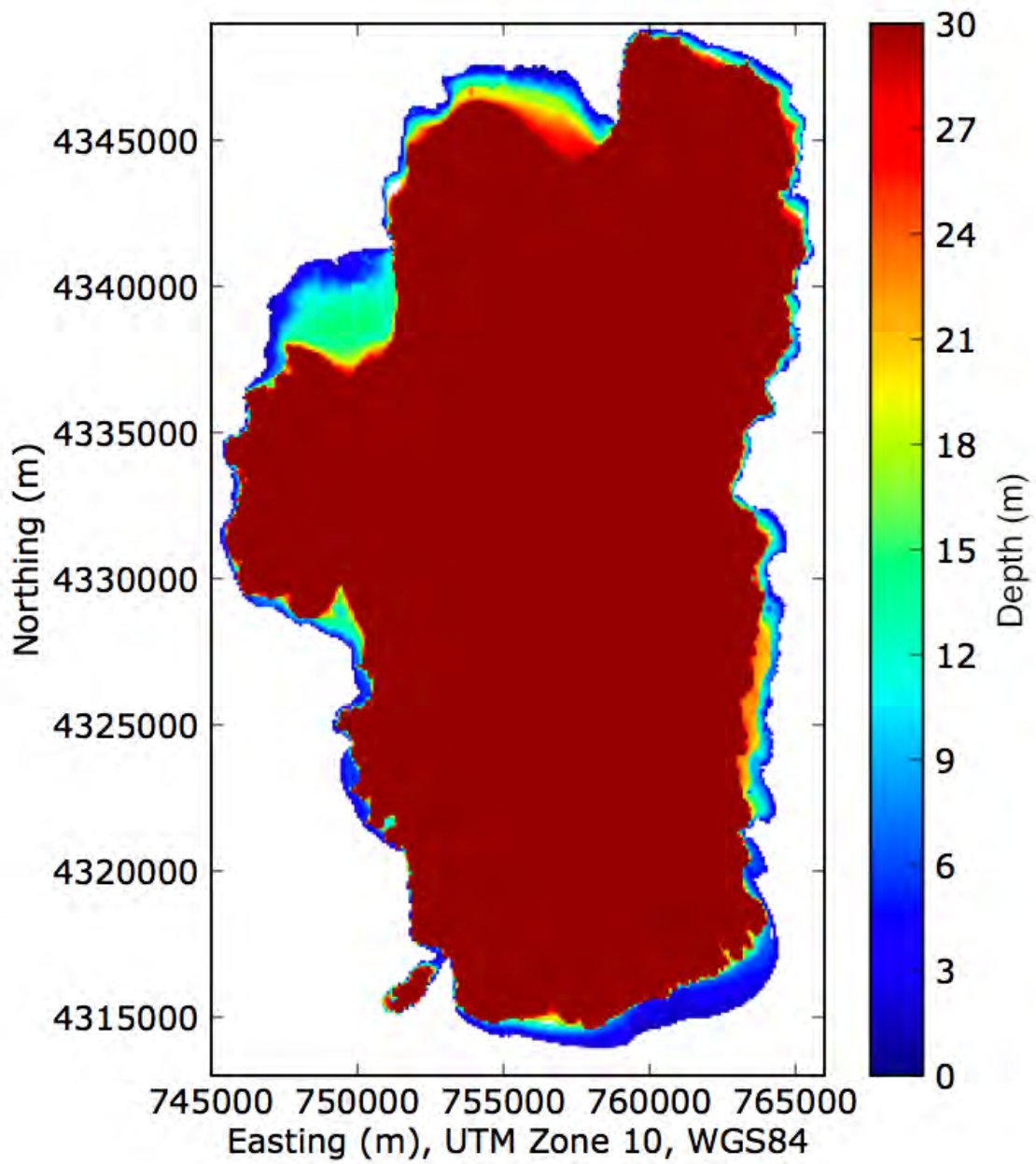


Figure 3.11: Bathymetry map of Lake Tahoe, scaled to show the shoals to a depth of 30 m.

### 3.4.2 Stream Inflow

Stream inflows to Lake Tahoe, recorded at USGS gage stations around the lake, were available for ten basin streams for the 2002 – 2010 study period. These included the nine Lake Tahoe Interagency Monitoring Program (LTIMP) streams shown in Figure 1.2), plus Edgewood Creek, which flows into the southeast corner of the lake at Stateline, NV. In descending order of typical flows, these are:

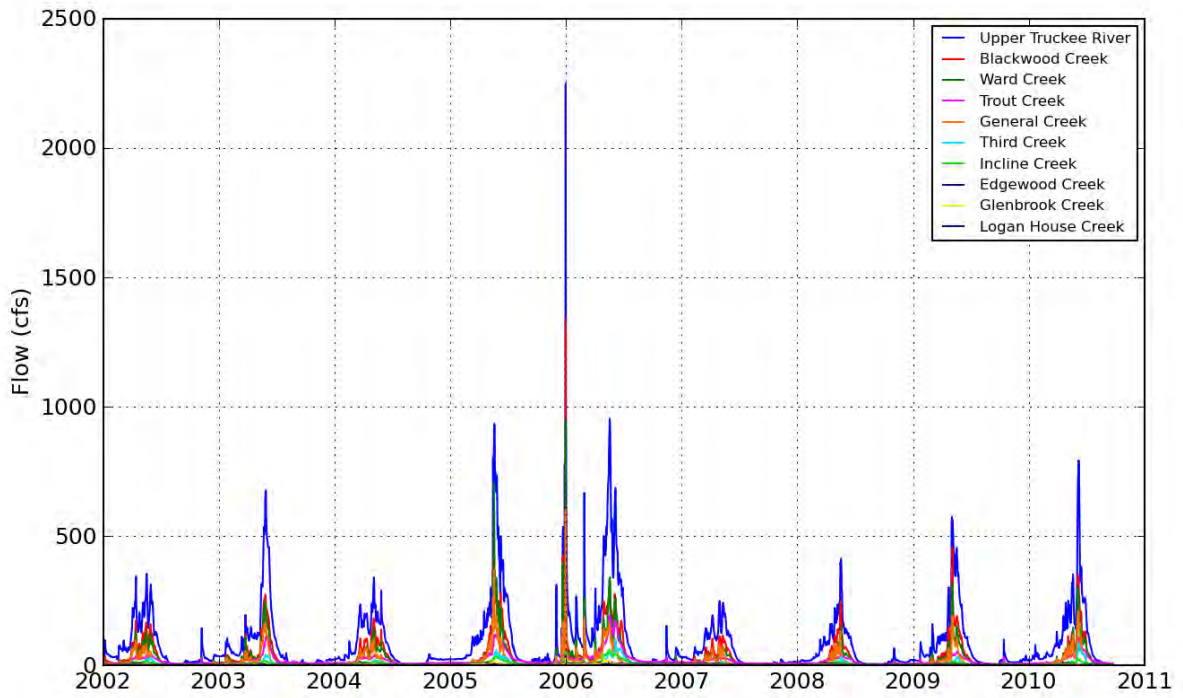
- Upper Truckee River
- Blackwood Creek
- Ward Creek
- Trout Creek
- General Creek
- Third Creek
- Incline Creek
- Edgewood Creek
- Glenbrook Creek
- Logan House Creek

Figure 3.12 shows the measured stream inflows to the lake during the 2002 – 2010 study period. Figure 3.12(a) shows the flows plotted on a linear scale, illustrating the large difference in flows between the Upper Truckee River and the other nine basin streams. The combined inflows of Blackwood and Ward Creeks along the western shore total approximately 70 – 80% of the Upper Truckee River inflow and approximately half of the combined South Lake Tahoe inflow of the Upper Truckee River, Trout Creek, and Edgewood Creek.

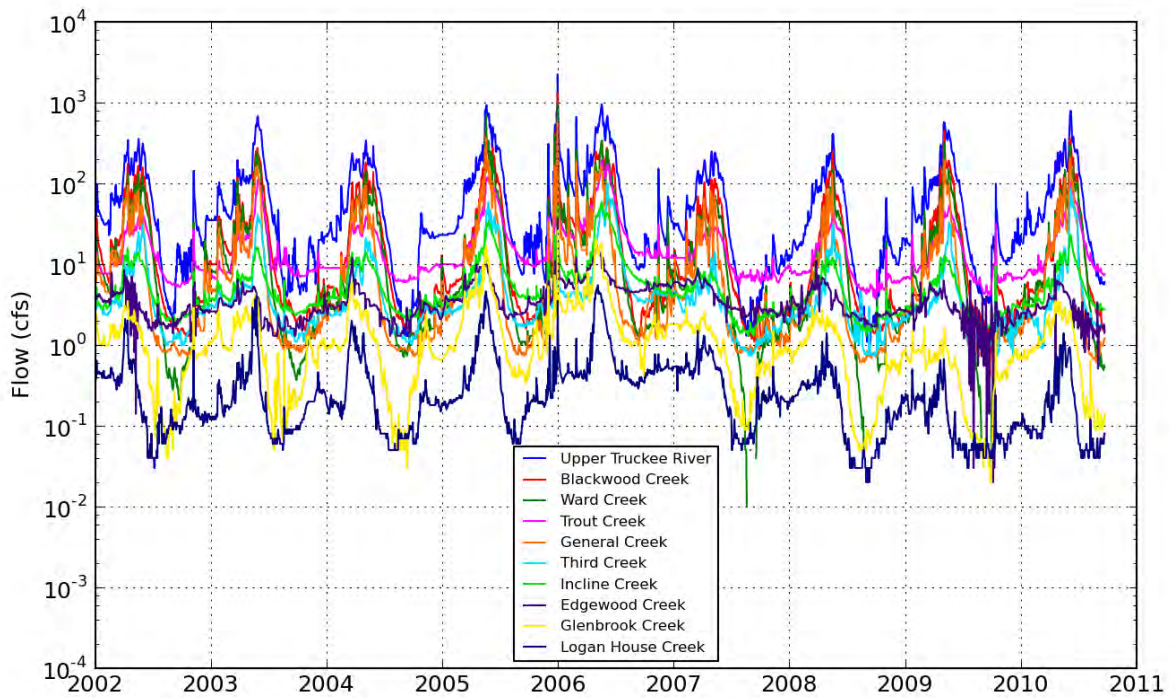
Figure 3.12(b) shows the stream inflows plotted on a log scale. These plots indicate that the timing of the spring inflows is nearly identical for all ten Tahoe basin streams, although the relative magnitudes vary. During low flows, Trout Creek typically provides more inflow than the Upper Truckee River. Similarly, peak Third Creek inflows are higher than Incline Creek inflows, but the low flows of Incline Creek are higher than Third Creek. This may be due to groundwater inputs.

Along the eastern shore, the peaks and low flows of Glenbrook and Logan House Creeks are significantly lower than the inflows of the other basin streams. Based on streamflow and population, in the absence of currents, the water quality along the eastern shore would be expected to be significantly better than other areas of the lake.

Available streamflow data available for other basin streams were compared to these ten streams, using time series and exceedance plots, to identify their contribution to the lake. Of these streams, including Taylor Creek, Martis Creek, Madden Creek, Dollar Creek, and others, Taylor Creek was found to contribute significant inflow; analysis of percent flow exceedance showed the flows to be very similar to Blackwood Creek. However, peak Taylor Creek inflows were typically delayed by one to three days, or even a week or two behind the other basin streams. Taylor Creek drains Fallen Leaf Lake, and the outflow is regulated by a dam. It also flows through what is considered to be the last natural wetland in the basin. The regulated outflow and wetland likely contribute to the inflow delay.



(a) Stream inflow time series: linear scale



(b) Stream inflow time series: log scale

Figure 3.12: Time series of inflow of Tahoe basin streams, 2002 – 2010.

### 3.4.3 MODIS Time Series of Nearshore Water Quality

MODIS-Aqua Secchi Depth and chlorophyll *a* maps were sampled at 135 locations around the lake, distributed in three sets each. The “nearshore” (NS) sampling locations were selected 750 m from the shoreline or visible shoals. Similarly, the “coastal” (CS) and “offshore” (OS) sampling locations were selected 1000 m and 1500 m, respectively, from the shoreline or visible shoals.

The nearshore time series at some locations showed evidence of periodic contamination by bottom reflectance. This was possibly a function of small georeferencing errors in the satellite data. The nearshore and coastal time series exhibited very similar characteristics. Therefore, this analysis will focus on the “coastal” time series as a proxy for nearshore water quality.

Time series of Secchi Depth and chlorophyll *a* measured by MODIS were analyzed at each of the ten streamflow locations. Table 3.1 lists each stream with its corresponding MODIS sampling station(s). Time series of stream inflow, MODIS-predicted Secchi Depth, and MODIS-predicted chlorophyll *a* measured at each of the ten stream inflow locations are shown in Figures 3.13 – 3.23.

Table 3.1: List of streams and their corresponding MODIS sampling station(s).

Stream	Station #
Third Creek	4
Incline Creek	5
Glenbrook Creek	13 / 14
Logan House Creek	15
Edgewood Creek	20
Trout Creek	22
Upper Truckee River	22
General Creek	32
Blackwood Creek	36
Ward Creek	37

Third Creek and Incline Creek flow into the lake on the northern shore, between Stations 4 and 5, at Incline Village, NV. Third Creek (Figure 3.13) is located slightly closer to Station 4, while Incline Creek (Figure 3.14) is located at the midpoint between stations 4 and 5. The Incline Creek inflow (Figure 3.14(a)) was found to correspond better with the Station 5 water quality time series, so these are shown in Figure 3.14(b) and 3.14(c). This correspondence may be due to eastward transport by currents, particularly in the winter. The Glenbrook Creek inflow occurs between Stations 13 and 14. Station 13 captures Glenbrook Bay, while Station 14 captures possible transport-induced effects at the southern outside edge of the bay. Therefore, two figures were created for Glenbrook, one with Station 13 water quality data (Figure 3.15) and one with Station 14 water quality data (Figure 3.16). Each of the remaining seven stream inflows (Figures 3.17 – 3.23) is located adjacent to its respective MODIS sampling station. The Upper Truckee River and Trout Creek both flow into the lake at Station 22.

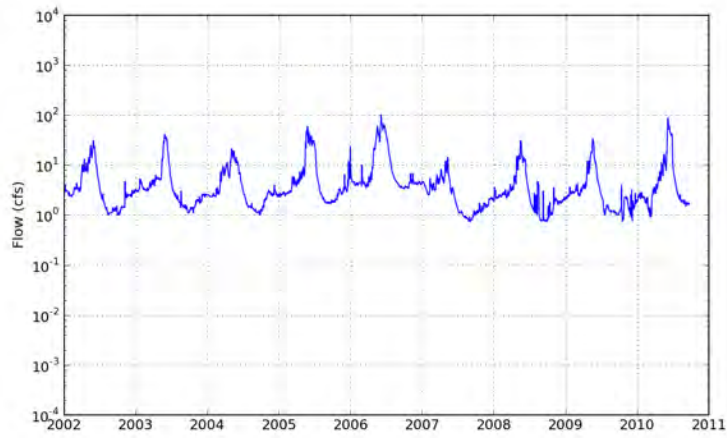
During the 2002 – 2008 study period, the peak spring inflow at Third Creek occurred in 2006 (Figure 3.13(a)). This peak corresponded to a peak in opacity, with a Secchi Depth of 15 m measured at station CS4 (Figure 3.13(b)). A peak in chlorophyll *a* of 1.3 mg/m<sup>3</sup> occurred the following January (Figure 3.13(c)). Similar effects were observed at Incline Creek and Station 5 (Figure 3.14). However, Station 5 showed a peak in opacity of 16.5 m corresponding to a similar winter inflow peak, which occurred a few months prior to this, in December 2005. Third Creek showed a smaller winter inflow peak, and no increase in opacity was observed at Station 4. This confirms the selection of Station 5 for Incline Creek and suggests eastward transport along the northern shore in the winter.

The MODIS-predicted nearshore and coastal Secchi Depth time series indicate that peaks of opacity (low Secchi Depth) correspond very closely to peaks in spring streamflows at all stations (Figures 3.13 – 3.23). This is as expected, since it has been determined that Secchi Depth is primarily influenced by fine particles flowing into the lake [Jassby *et al.*, 1999; Swift *et al.*, 2006]. The MODIS-predicted nearshore and coastal chlorophyll *a* time series indicate a weaker correspondence between chlorophyll *a* peaks and peak spring inflows, with chlorophyll *a* peaks often lagging several weeks or months behind spring inflows. The delay in chlorophyll *a* response is expected, since chlorophyll *a* concentration depends on phytoplankton growth following nutrient inputs, and growth is dependent on other environmental factors.

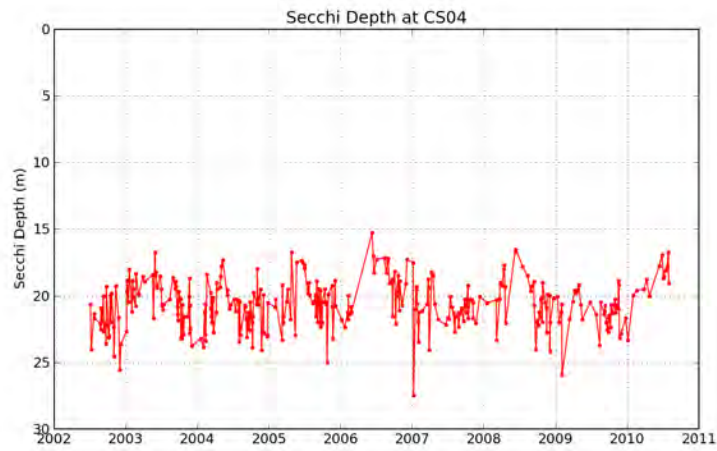
Comparison of the nearshore, coastal, and offshore time series indicated that water clarity was significantly lower and chlorophyll *a* was significantly higher in the nearshore regions than the offshore regions, on average. The variability of these parameters was also much higher nearshore than offshore. In fact nearshore water quality was periodically better than offshore water quality, typically following upwelling.

Around the shoreline, station 22 (adjacent to the Trout Creek and Upper Truckee River inflows) showed the greatest variability, and highest peaks of opacity (low Secchi Depths) and chlorophyll *a* concentrations. Surprisingly, the water quality at Station 20 (adjacent to Edgewood Creek) was typically worse than Station 20 (and the other stations) throughout the year, despite the relatively low flows of Edgewood Creek. Higher temperatures and nutrient concentrations have been found in Edgewood Creek (as detailed below), possibly associated with the Edgewood-Tahoe Golf Course, as well as due to urban pollution affects. However, the flows are low enough that computed loadings appear to be of low significance. The water quality at Station 15, adjacent to the Logan House Creek inflow, was also lower than expected, given its fairly low flows. The water quality at Station 15 typically fell between the levels observed at Stations 13/14 (Glenbrook) and Station 20 (Edgewood Creek).

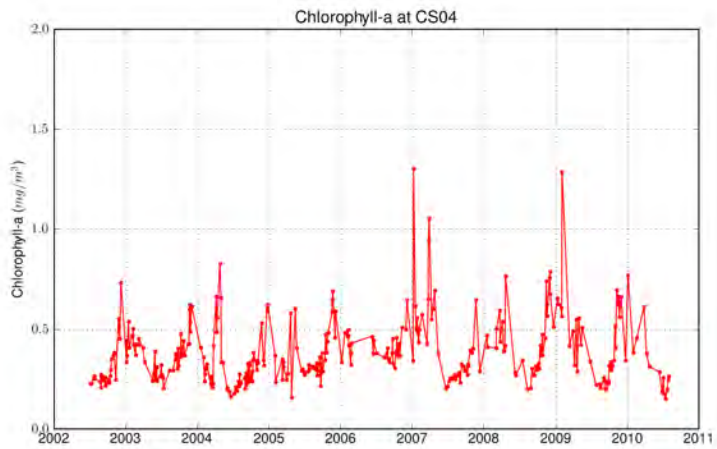
The lower water quality observed at Station 20 may be due to currents transporting the Upper Truckee River and Trout Creek inputs eastward. In addition, there may be significant sediment resuspension from the shoals, which are only approximately 2 m deep between the Trout Creek and Edgewood Creek inflows, which may be transported eastward. Surface current analysis from satellite images and drogue data (see Appendix B, Figures B.1 and B.2) indicate that a spiral eddy is often found in the southeast corner of the lake. This eddy may concentrate and retain nutrients in this area.



(a) Third Creek Inflow

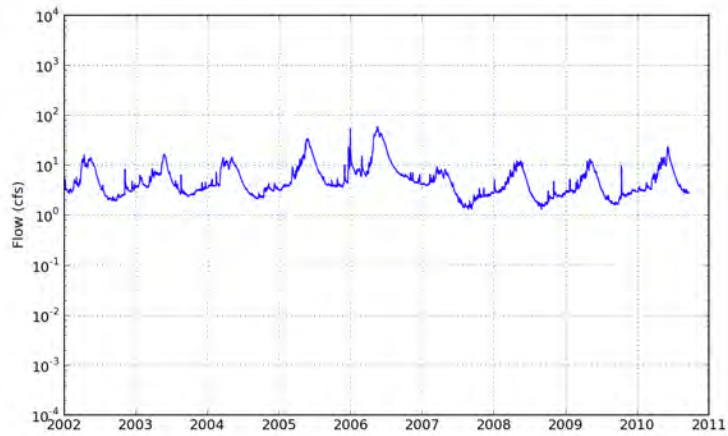


(b) Secchi Depths at Station 4

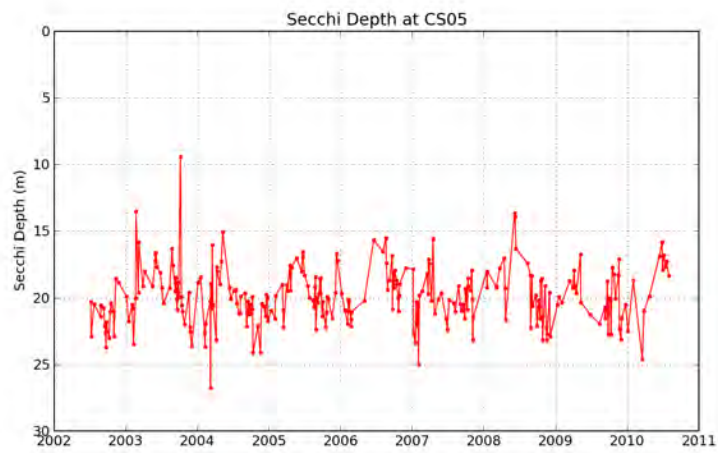


(c) Chlorophyll *a* at Station 4

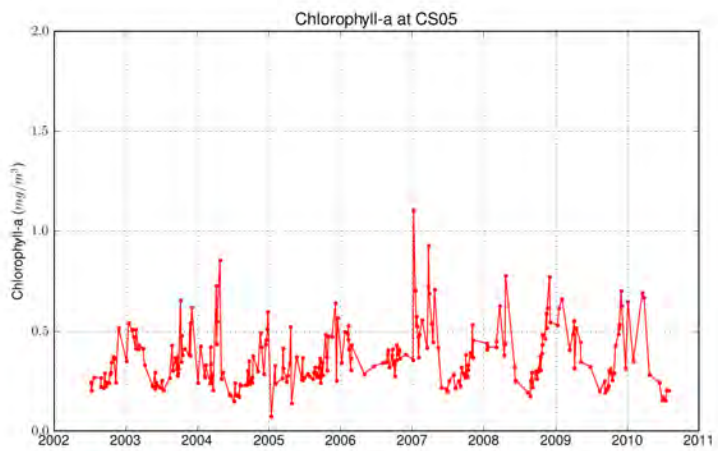
Figure 3.13: Third Creek inflow and time series of MODIS-predicted nearshore Secchi Depth and chlorophyll *a* at Station 4.



(a) Incline Creek Inflow

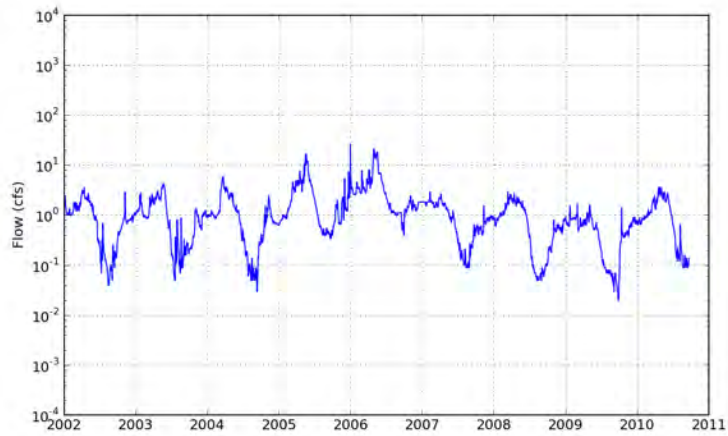


(b) Secchi Depths at Station 5

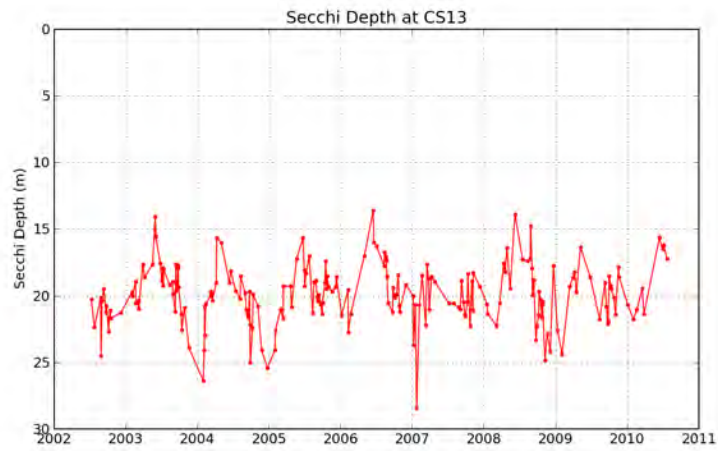


(c) Chlorophyll *a* at Station 5

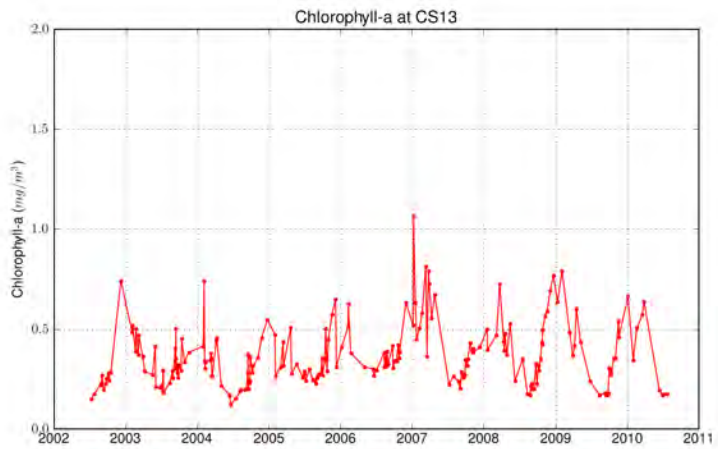
Figure 3.14: Incline Creek inflow and time series of MODIS-predicted nearshore Secchi Depth and chlorophyll *a* at Station 5.



(a) Glenbrook Creek Inflow

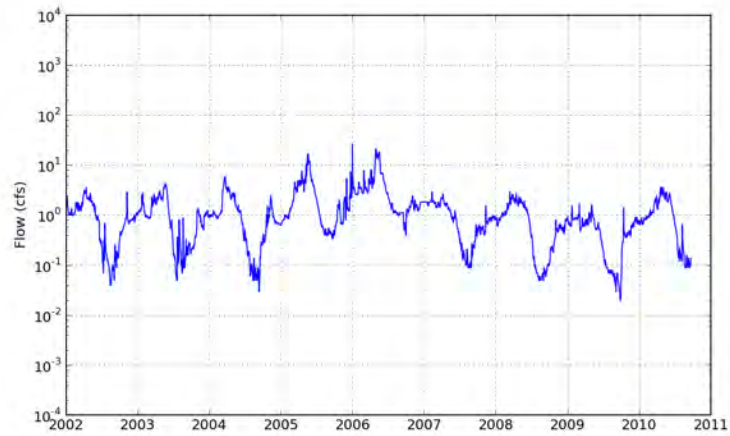


(b) Secchi Depths at Station 13

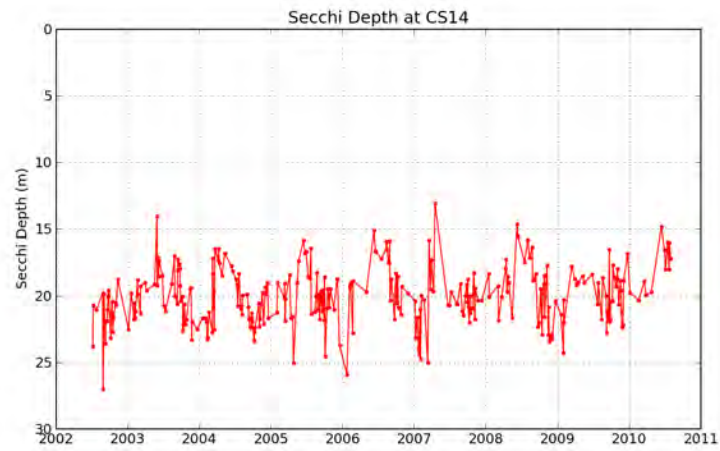


(c) Chlorophyll *a* at Station 13

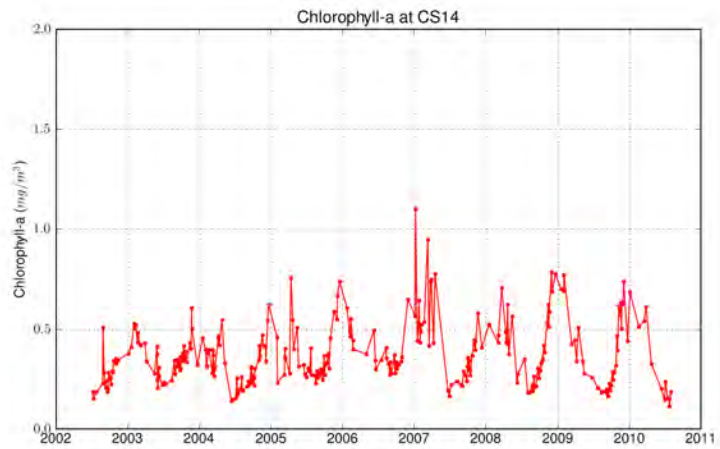
Figure 3.15: Glenbrook Creek inflow and time series of MODIS-predicted nearshore Secchi Depth and chlorophyll *a* at Station 13.



(a) Glenbrook Creek Inflow

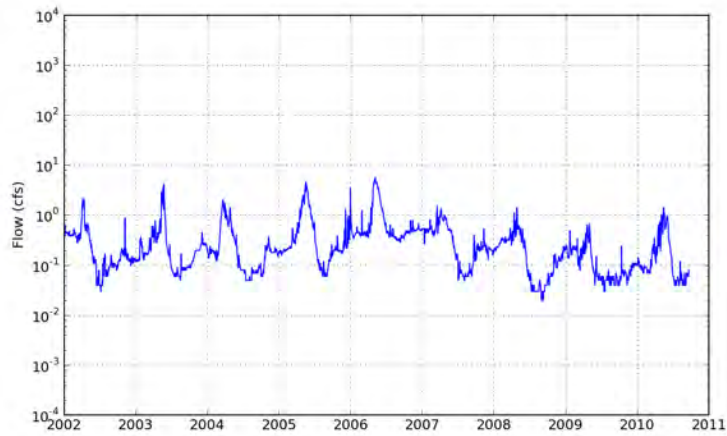


(b) Secchi Depths at Station 14

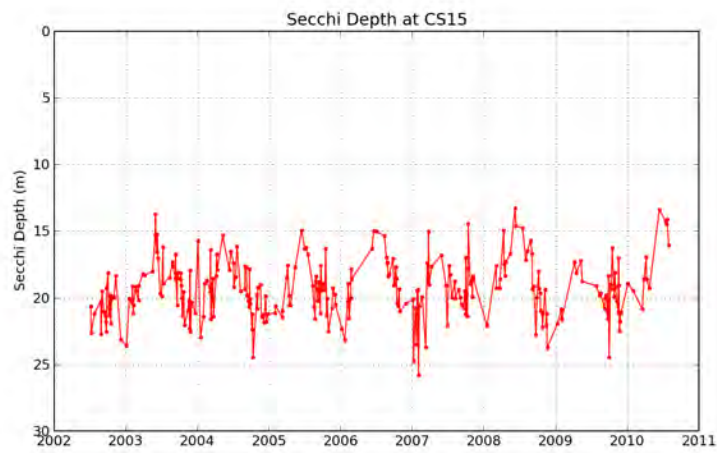


(c) Chlorophyll *a* at Station 14

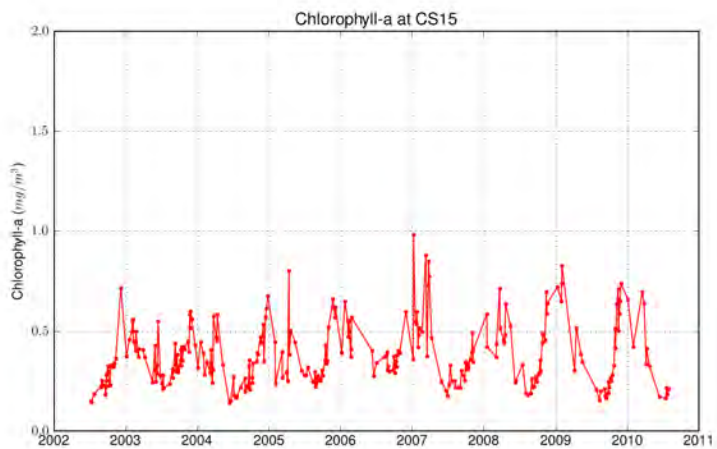
Figure 3.16: Glenbrook Creek inflow and time series of MODIS-predicted nearshore Secchi Depth and chlorophyll *a* at Station 14.



(a) Logan House Creek Inflow

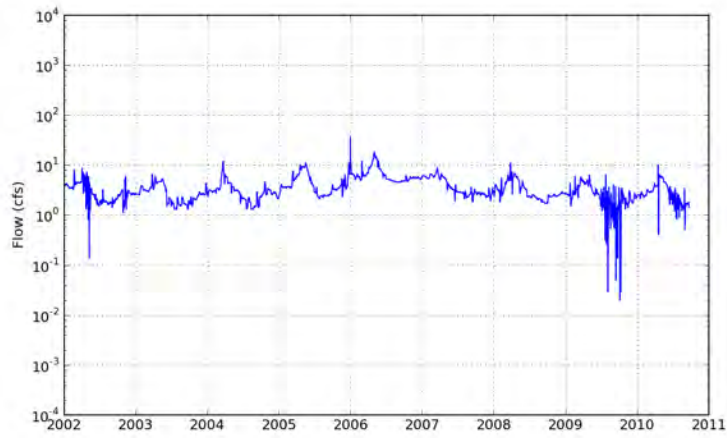


(b) Secchi Depths at Station 15

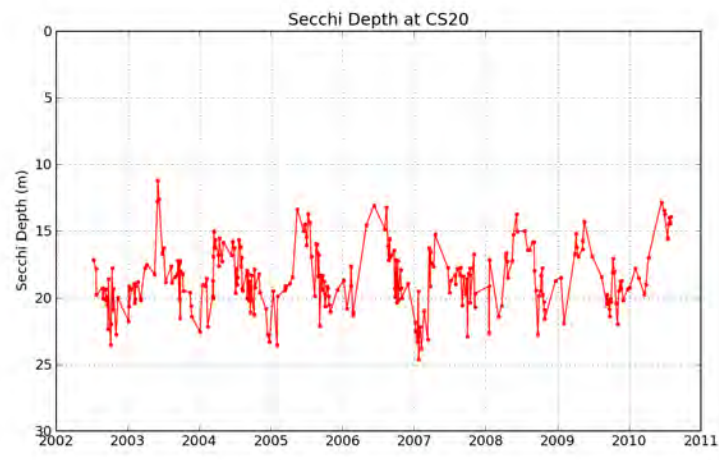


(c) Chlorophyll *a* at Station 15

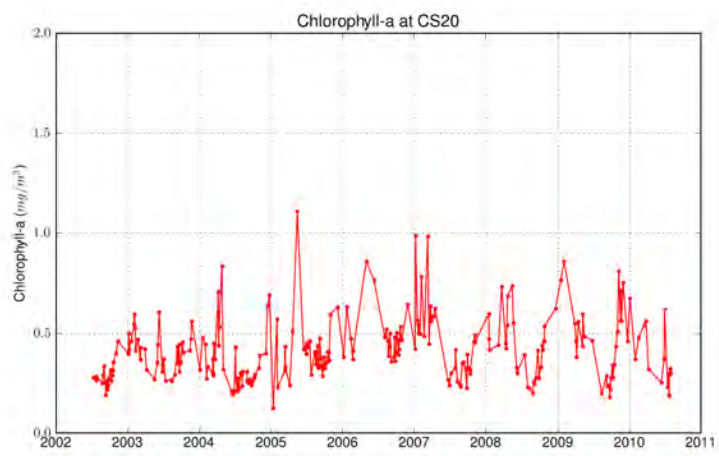
Figure 3.17: Logan House Creek inflow and time series of MODIS-predicted nearshore Secchi Depth and chlorophyll *a* at Station 15.



(a) Edgewood Creek Inflow

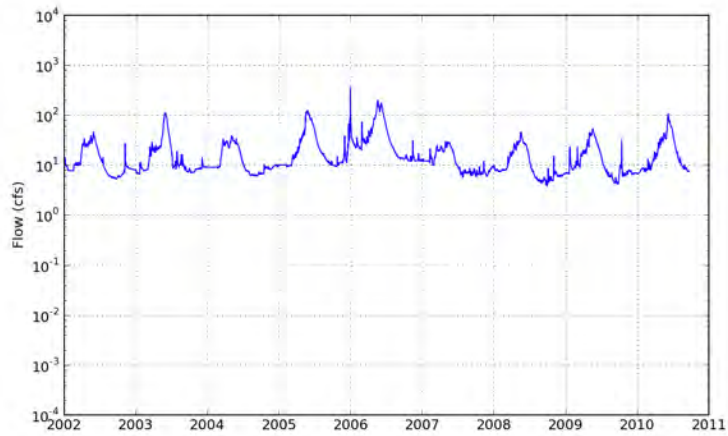


(b) Secchi Depths at Station 20

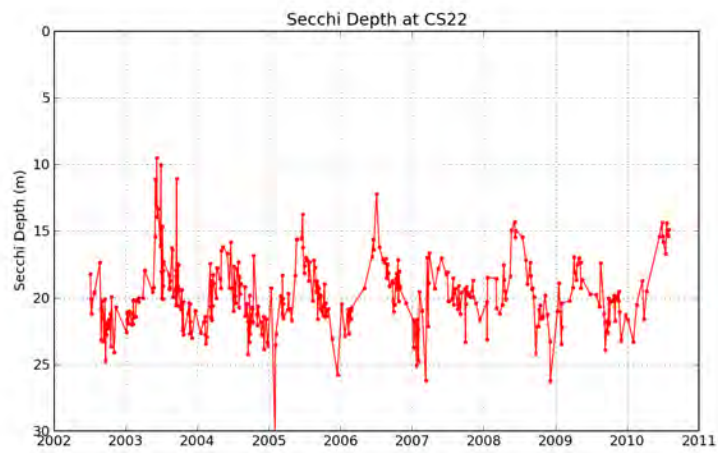


(c) Chlorophyll *a* at Station 20

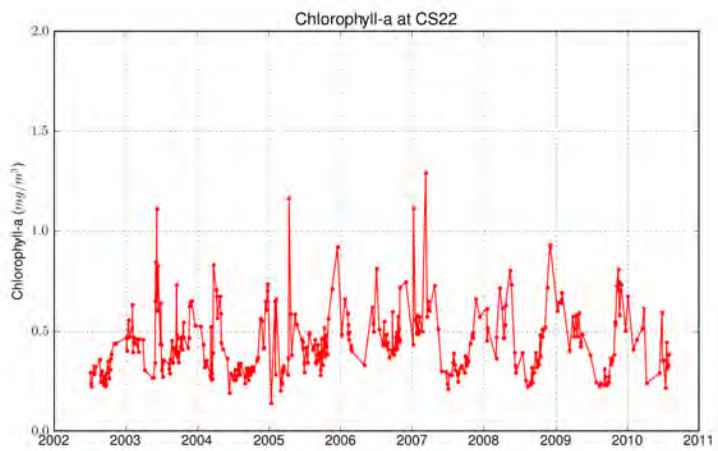
Figure 3.18: Edgewood Creek inflow and time series of MODIS-predicted nearshore Secchi Depth and chlorophyll *a* at Station 20.



(a) Trout Creek Inflow

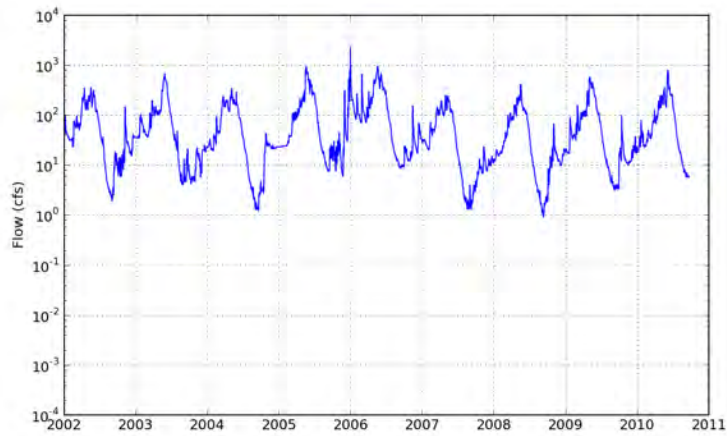


(b) Secchi Depths at Station 22

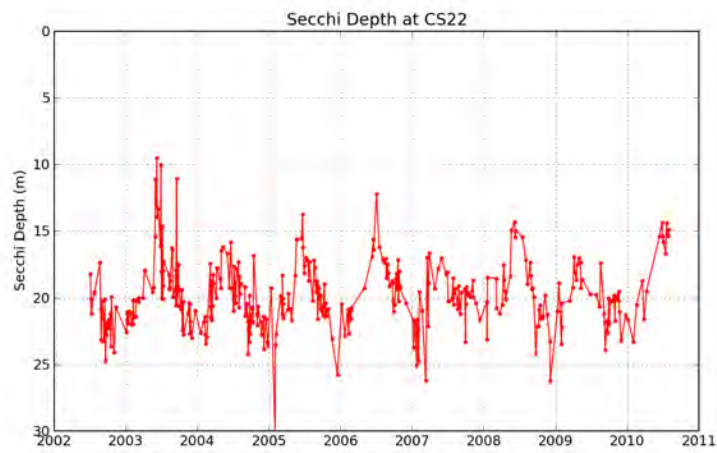


(c) Chlorophyll *a* at Station 22

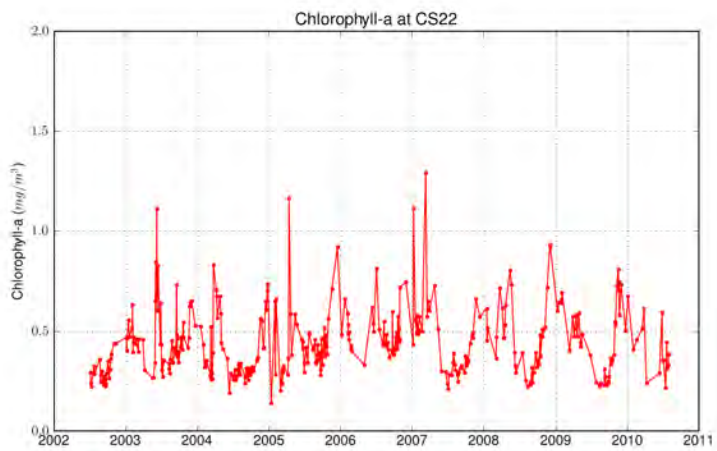
Figure 3.19: Trout Creek inflow and time series of MODIS-predicted nearshore Secchi Depth and chlorophyll *a* at Station 22.



(a) Upper Truckee River Inflow

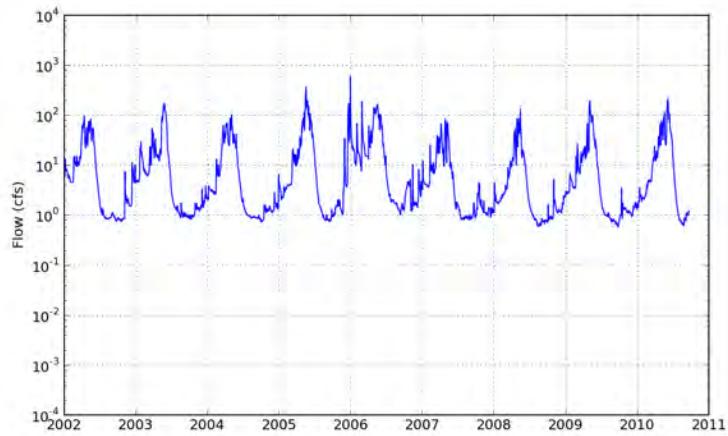


(b) Secchi Depths at Station 22

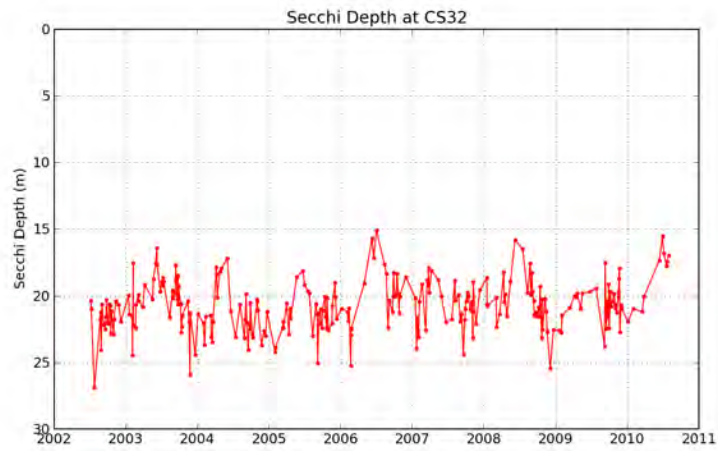


(c) Chlorophyll *a* at Station 22

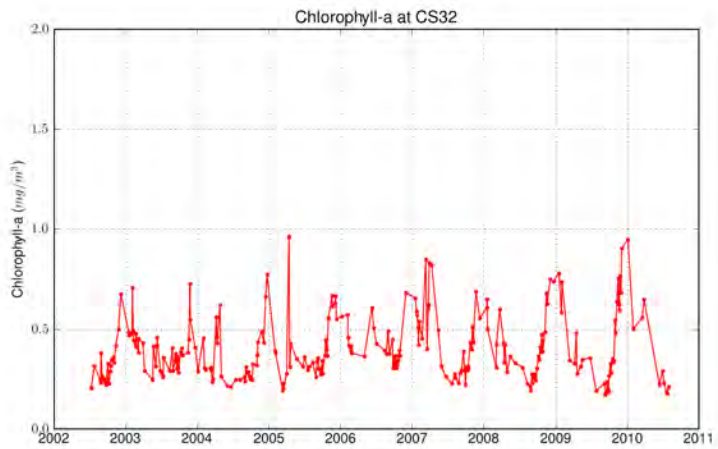
Figure 3.20: Upper Truckee River inflow and time series of MODIS-predicted nearshore Secchi Depth and chlorophyll *a* at Station 22.



(a) General Creek Inflow

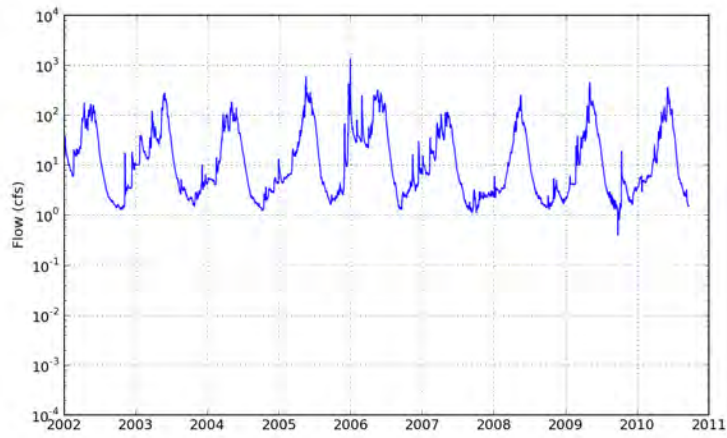


(b) Secchi Depths at Station 32

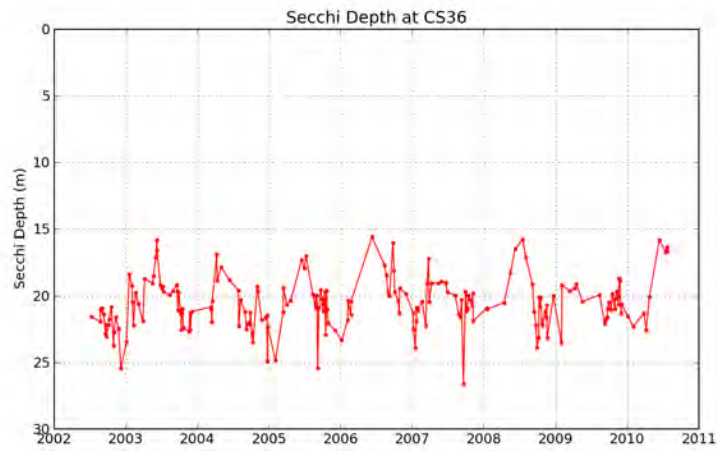


(c) Chlorophyll *a* at Station 32

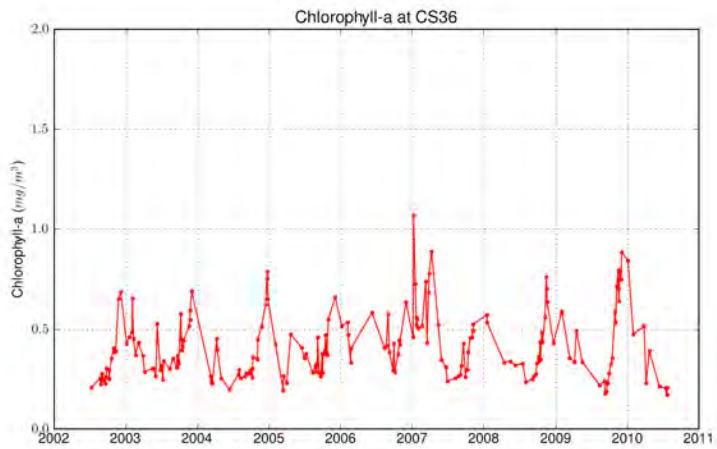
Figure 3.21: General Creek inflow and time series of MODIS-predicted nearshore Secchi Depth and chlorophyll *a* at Station 32.



(a) Blackwood Creek Inflow

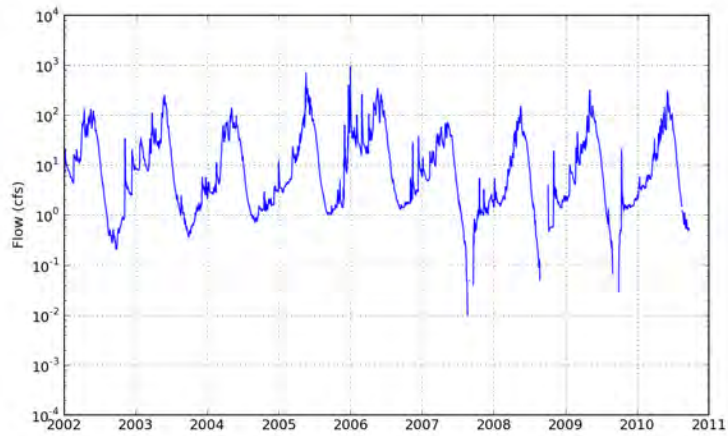


(b) Secchi Depths at Station 36

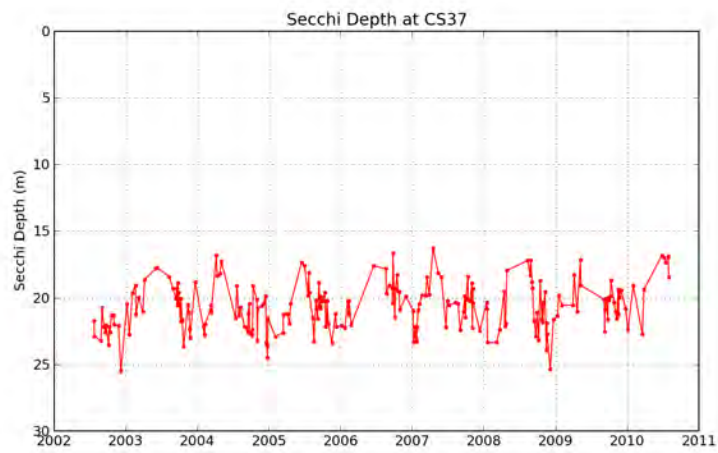


(c) Chlorophyll *a* at Station 36

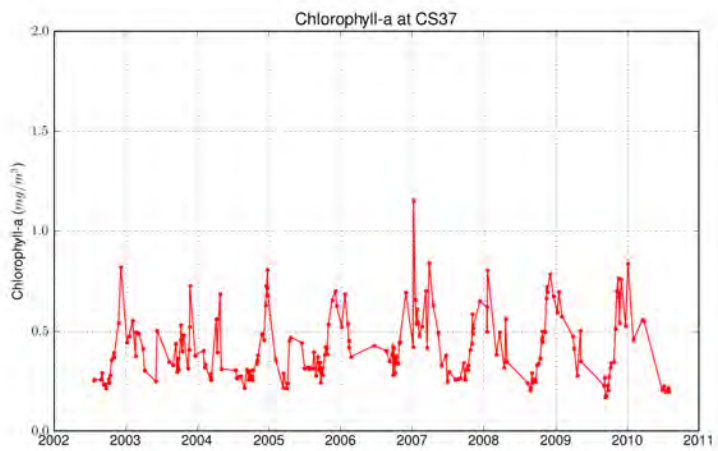
Figure 3.22: Blackwood Creek inflow and time series of MODIS-predicted nearshore Secchi Depth and chlorophyll *a* at Station 36.



(a) Ward Creek Inflow



(b) Secchi Depths at Station 37



(c) Chlorophyll *a* at Station 37

Figure 3.23: Ward Creek inflow and time series of MODIS-predicted nearshore Secchi Depth and chlorophyll *a* at Station 37.

### 3.4.4 Stream Water Quality Loadings

To assess the impact of basin stream inflow on nearshore water quality and its spatial variability, stream inflow and water quality data were obtained from the USGS National Water Information System (NWIS, <http://nwis.waterdata.usgs.gov/usa/nwis/qwdata>). Several parameters were recorded at weekly to monthly frequencies at the three major inflow points at South Lake Tahoe, including the Upper Truckee River, Trout Creek, and Edgewood Creek. Total nitrogen (TN) and total phosphorus (TP) loadings were computed as the product of measured concentrations and the instantaneous streamflow recorded during field sampling. Suspended sediment loads were recorded in tons/day.

The timing of major nutrient and sediment loading events correspond well to spring runoff events, which occur between March and June. There was no difference in timing between the nutrient and sediment loading peaks of the Upper Truckee River and Trout Creek. These watersheds are adjacent to one another, and the streams nearly converge as they flow into the lake. No significant difference in timing of loading was observed between Edgewood Creek and the other two streams. However, some of Edgewood Creek's loading peaks (e.g., 2006 and 2007) were significantly attenuated relative to the other two streams. The TN and TP concentrations were significantly higher at times in Edgewood Creek than the other two streams. Furthermore, Trout Creek contributes more loadings during the winter. However, since the flow of the Upper Truckee River is significantly larger during spring runoff, it appears to contribute the majority of the nutrient and sediment loadings to the southern part of the lake in particular and the whole lake in general.

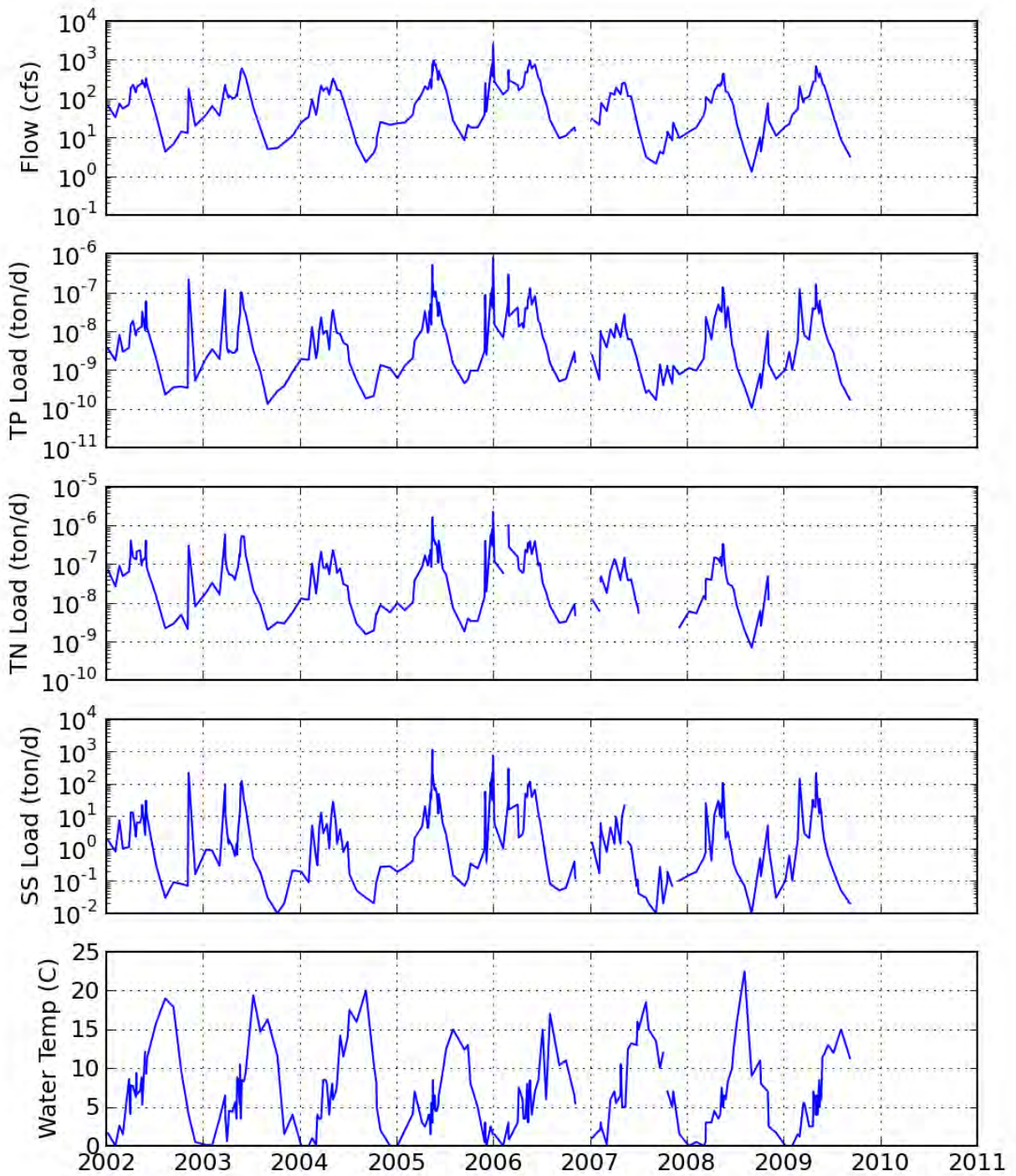


Figure 3.24: Time series of Upper Truckee River inflow, loadings (total phosphorus (TP), total nitrogen (TN), suspended sediment (SS)), and water temperature, 2002 – 2010. Source: <http://nwis.waterdata.usgs.gov>.

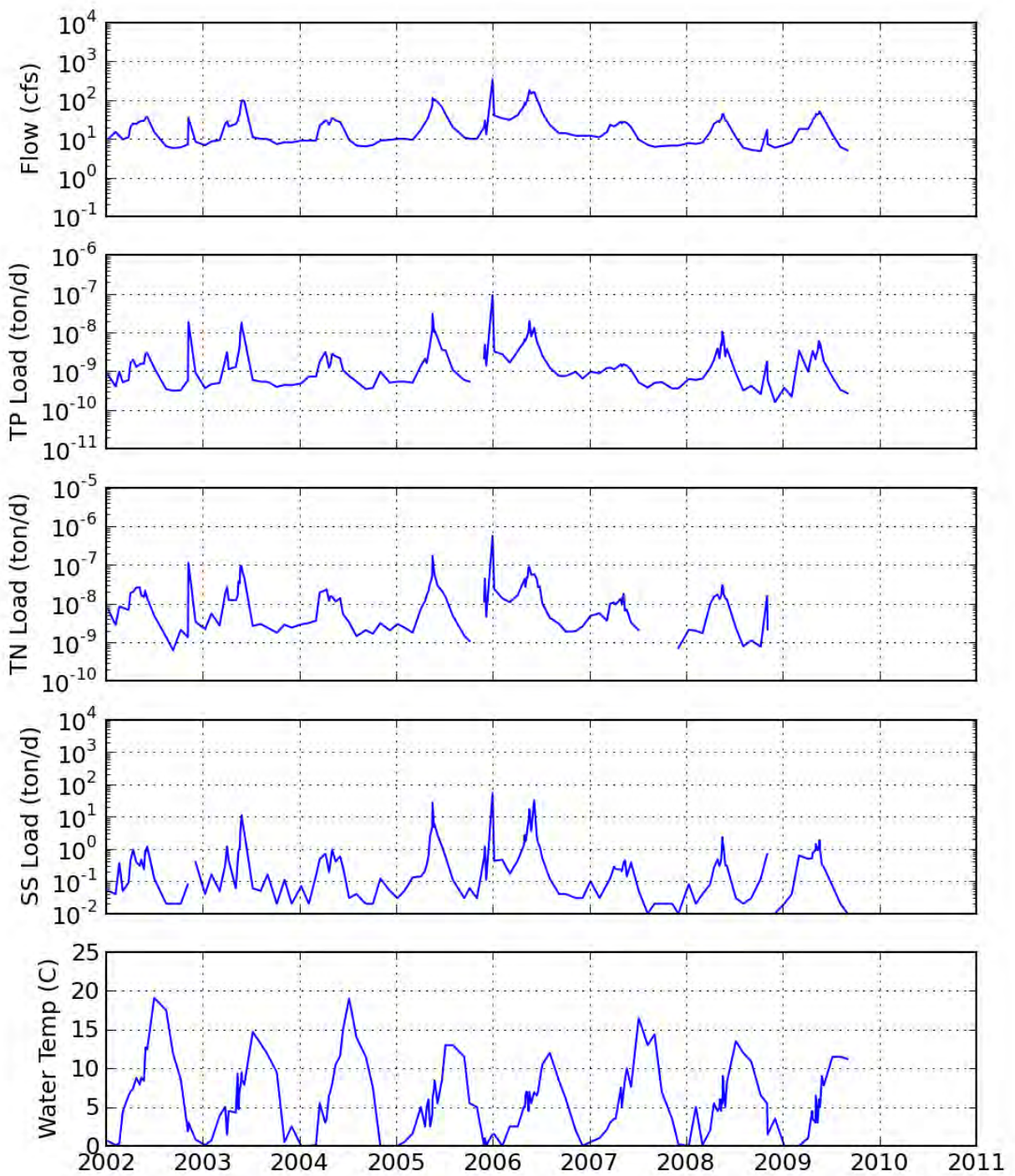


Figure 3.25: Time series of Trout Creek inflow and loadings (total phosphorus (TP), total nitrogen (TN), suspended sediment (SS)), 2002 – 2010. Source: <http://nwis.waterdata.usgs.gov>.

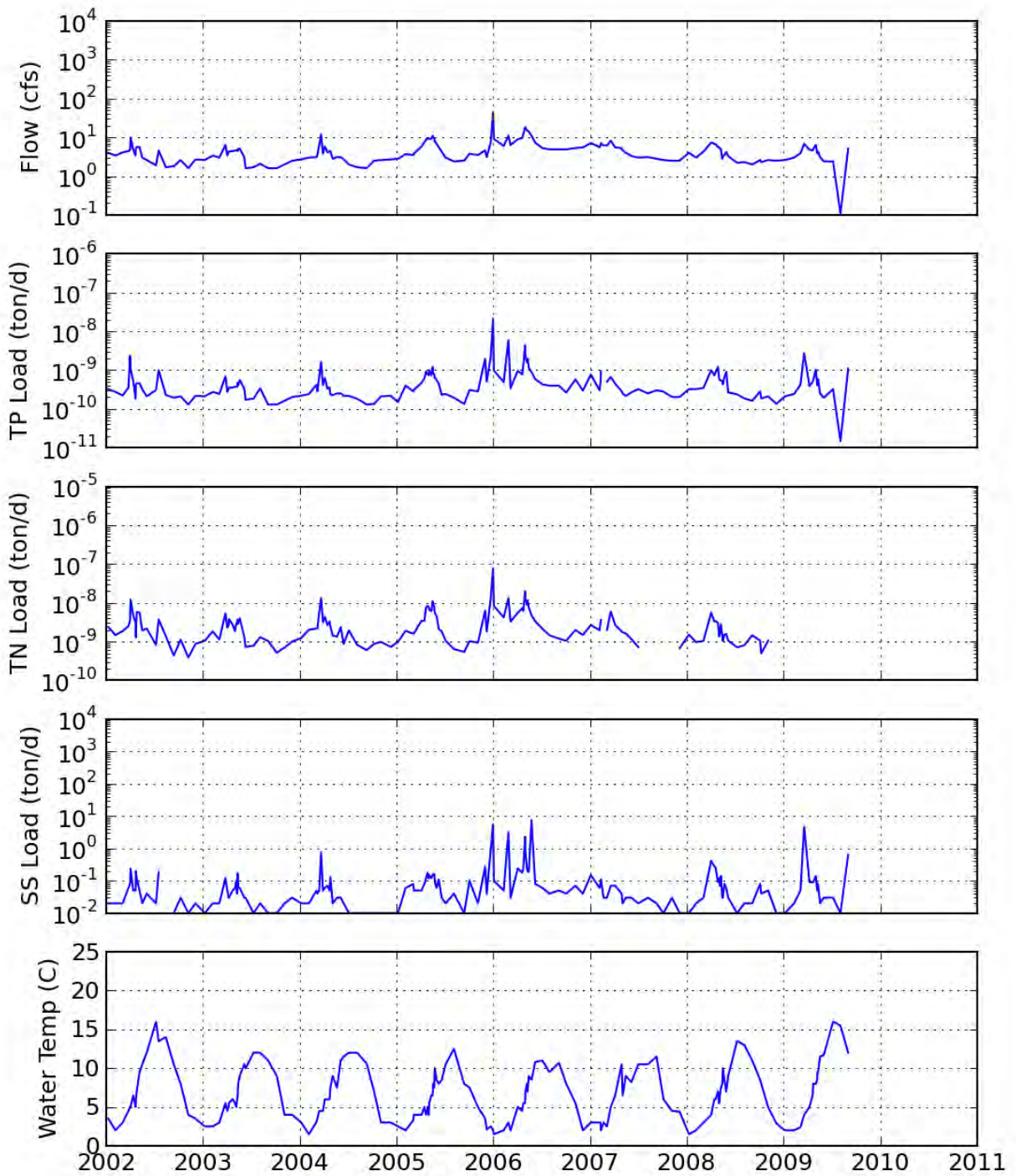


Figure 3.26: Time series of Edgewood Creek inflow and loadings (total phosphorus (TP), total nitrogen (TN), suspended sediment (SS)), 2002 – 2010. Source: <http://nwis.waterdata.usgs.gov>.

### 3.4.5 Cyclic Analysis of Nearshore Water Quality

To quantify the annual cycle of the distribution and changes of nearshore water quality, the combined average monthly chlorophyll *a* concentration and Secchi Depth recorded by MODIS at the nearshore, coastal, and offshore sampling stations were computed over the study period. For example, the June chlorophyll *a* average at NS20 represents the average value of chlorophyll *a* observed at NS20 in the month of June over the 2002 – 2010 study period. This is often referred to as cyclic analysis. The chlorophyll *a* plots are shown in Figures 3.27 – 3.29. The Secchi Depth plots are shown in Figures 3.32 – 3.33.

#### Chlorophyll Cycle

Analysis of the MODIS-derived nearshore mean chlorophyll *a* cycle (Figures 3.27(a) - 3.29(d)) shows complex and changing patterns. Mean chlorophyll *a* concentrations are generally at their highest levels during January (Figure 3.27(a)) and December (Figure 3.29(d)). This is consistent with *in situ* chlorophyll *a* profiles collected offshore at the LTP and MLTP stations (See Section 3.5, Figures 3.40 and 3.41), which show that deep mixing distributes the chlorophyll from the Deep Chlorophyll Maximum (DCM) throughout the water column. This increases the chlorophyll *a* concentrations in the surface layer, where MODIS can detect them.

Mean chlorophyll *a* levels drop around the lake from December through March (Figures 3.29(d), 3.27(a), 3.27(b), and 3.27(c)). This is also evident in the *in situ* chlorophyll *a* profiles, when chlorophyll *a* variously diminishes throughout the water column or begins to concentrate in the DCM. The satellite data show that chlorophyll *a* levels drop more rapidly along the western and northwestern shores, which is surprising, since it was expected that stronger upwelling along the western shore would keep chlorophyll *a* suspended in the surface layer. In April (Figure 3.27(d)), as spring runoff begins, peaks of chlorophyll *a* appear at different locations around the lake, most notably at Station 22, adjacent to the Upper Truckee River inflow, which contributes the largest discharge. Chlorophyll *a* is also elevated along the northern shore, peaking at Station 43, adjacent to Carnelian Bay, California. The reason for this latter peak is not clear.

In May (Figure 3.28(a)), the nearshore mean chlorophyll *a* peak diminishes slightly and broadens significantly, spreading midway up the eastern shore and along the southern shore. As this occurs, coastal and offshore values peak sharply at Station 20, representing a westward shift from April's peak at Station 22. This suggests chlorophyll *a* spreading in the nearshore region while a plume at Station 20 transports chlorophyll *a* offshore. Eddy transport, such as shown by drogoue tracks along the southeast shore (see Appendix B, Figure B.2) could transport the chlorophyll *a* northward along the eastern shore. Westward transport along the southern shore is consistent with a clockwise gyre in the southern basin. Both circulation patterns could co-exist.

The mean chlorophyll *a* peak shifts eastward again in June (Figure 3.28(b)), from Stations 20 to 21, as it diminishes. A sharp chlorophyll *a* peak appears at Station 35, south of Blackwood Creek. In May, There was an offshore peak at Station 34. This peak may have shifted shoreward and northward, which would indicate transport from offshore. This would be consistent with chlorophyll *a* transport from the southern shore, across the lake. A small peak appears again at Station 43.

In July (Figure 3.28(c)), the peaks near the Upper Truckee River (Station 21) and Blackwood Creek (Station 35) diminish, while a second peak appears at Station 25, adjacent to the Taylor Creek inflow in the southwest corner of the lake. Taylor Creek represents a potentially significant source of nutrients. However, since this creek flows through a wetland, it is expected that in-stream nutrient levels would be reduced. While this stream has shown a delay in inflows relative to the other basin streams, this delay is not large enough to account for the delayed peak. One possible explanation for the delayed chlorophyll *a* peak is delayed growth due to differences in water temperature. This site is typically affected more often by upwelling, due to its location near the southwest shore, while strong winds typically originate from the southwest. Furthermore, this site is over deeper water than, e.g., Station 22, rather than a shallow shelf. Upwelling can regularly reduce water temperatures during the spring, while spring and daytime temperatures tend to be higher in shallow-water regions. The lower water temperature may delay phytoplankton growth in the surface layer. These factors are illustrated in the MODIS-derived water temperature maps shown in Figure 3.30. Each image shows the affects of upwelling. A thin band of cool water extends along the southwest shore until it reaches the shelf. The temperatures differ by 2 – 3 °C between the southwest and southeast shores. Another contributing factor could be in-lake nutrient transport. Satellite maps (See Section 3.5, Figure 3.39, and Appendix B) show a counter-clockwise eddy that is commonly in this location. This eddy could regularly

transport nutrients and phytoplankton from the Upper Truckee River to this location, bypassing the stations in between, augmenting the nutrient and chlorophyll *a* levels at this site.

In August (Figure 3.28(d)), mean chlorophyll *a* levels increase along the western, northern, and eastern shores, but they do not increase along the southern shore, where the chlorophyll *a* peak at Station 22, broadens and diminishes. The peak at Station 25 vanishes, as a smaller one appears at Station 29. Two possible explanations exist for the apparent shift of the peak from Station 25 to 29. First, a clockwise gyre could have transported nutrients and chlorophyll *a* northward along the western shore. Second, a counter-clockwise eddy could have shifted or broadened, linking South Lake Tahoe inflows to the western shore. This pattern is evident in the satellite-derived chlorophyll *a* maps (See Section 3.5, Figure 3.39).

In September (Figure 3.29(a)), the peak along the southern shore diminishes, as do the other smaller peaks around the lake. Otherwise, the shape of the mean chlorophyll *a* curve is similar to August, with slightly lower mean chlorophyll *a* levels along the eastern shore and higher levels along the southern shore.

From October through December (Figures 3.29(b) – 3.29(d)), the mean chlorophyll *a* levels increase significantly, approximately 25 percent per month. The peak around the Upper Truckee River inflow remains from June through October. In November (Figure 3.29(c)), the peak appears to shift westward to Station 25. Otherwise, the shape of the mean chlorophyll *a* curve is similar in September and October. In November, peaks appear again. In November, addition to Station 25, there are broad peaks at Stations 3 (Incline Village), 36 (Blackwood Creek), and 43 (Carnelian Bay).

Mean chlorophyll *a* levels increase further in December (Figure 3.29(d)), reaching their highest levels for the year, around the lake. Chlorophyll *a* levels are significantly higher from Station 18 (Zephyr Cove) to 43 (Carnelian Bay), encompassing from more than half the lake, from the southeast shore to the northwest shore.

### Clarity Cycle

The MODIS-derived nearshore mean Secchi Depth cycle (Figures 3.31 - 3.33) shows changing patterns that sometimes covaried with chlorophyll *a*, but at other times were independent of – or inversely related to – chlorophyll *a*. In January, the mean Secchi Depth curve is approximately the mirror image of the chlorophyll *a* curve. This indicates that high chlorophyll *a* is associated with high clarity and that chlorophyll *a* and particles are inversely related. This situation occurs during strong upwelling, when the water column is well mixed. This has a greater likelihood of occurrence in January, when stratification reaches its minimum. Mean Secchi Depths are approximately 1 m lower along the southwestern shore, where upwelling is expected to be greatest, since the strongest winds typically originate from the southwest. There is a peak in opacity of 18.7 m at Station 20. Cyclic analysis of the inflows shows a moderate peak in January. However, sediment resuspension during strong winter storms could be occurring over the shelf adjacent to South Lake Tahoe.

From February through May, mean Secchi Depths decrease approximately 2 m around the lake, with greater decreases along the eastern part of the southern shore and the southern part of the eastern shore, between stations 15 and 23. The mean Secchi Depth decreased by 3 m at Station 20. Surprisingly, a second opacity peak appeared at Station 15, adjacent to the Logan House Creek inflow. It generally has the lowest inflow of the streams evaluated in this study. Given this peak and the peak at Station 20, adjacent to the Edgewood Creek inflow, this areas merit further study. In May, the mean Secchi Depth is higher at Station 25, in the southwest corner of the lake, where there is minimal inflow.

In June, nearshore mean Secchi Depths drop as low as approximately 14 m at Stations 20 and 22, adjacent to the Edgewood Creek and Upper Truckee River inflows, respectively. The lower mean Secchi Depths spread westward to Station 23.

In July, mean Secchi Depths increase by approximately 1.5 m. Mean Secchi Depth does not drop significantly at Stations 29, 35, and 43, creating peaks of Secchi Depth at these stations, in addition to more significant Stations 15, 20, and 22. There is a significant chlorophyll *a* peak at Station 25, with a smaller peak at Station 22, as noted above, showing that chlorophyll *a* and particles are reduced at Station 22 as they increase at Station 25. This further suggests the possibility of westward transport along the southern shore during this period. The lesser chlorophyll *a* peaks at Stations 35 and 43, combined with the other coinciding opacity and chlorophyll *a* peaks, indicate covariance of particles and chlorophyll *a* at these locations, as expected when inflow is the source of nutrients and particles. Stations 29 and 35 are south of the General Creek and Blackwood Creek inflows, respectively. It is possible that a southward current is responsible for

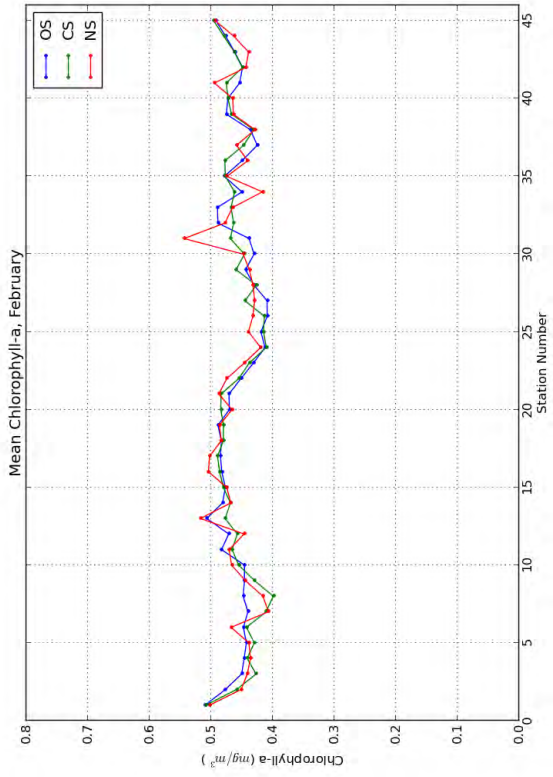
transporting particles from Blackwood and General Creeks southward along the western shore. At Station 35, this would be associated with a counter-clockwise gyre in the northern part of the lake.

In August, mean Secchi Depth levels remain the same at the coastal and offshore stations everywhere around the lake except at between Stations 25 and 30. The mean chlorophyll *a* levels stay nearly the same at these locations, indicating that particles are settling as phytoplankton growth levels off. The nearshore opacity peaks diminish around the lake as well. Inputs from inflow are minimal at this time, and the warm surface layer is relatively stable, leading to a net loss of particles from the surface layer. There is some indication of particle transport, as Secchi Depths increase at Stations 35 and 43, while they increase northward.

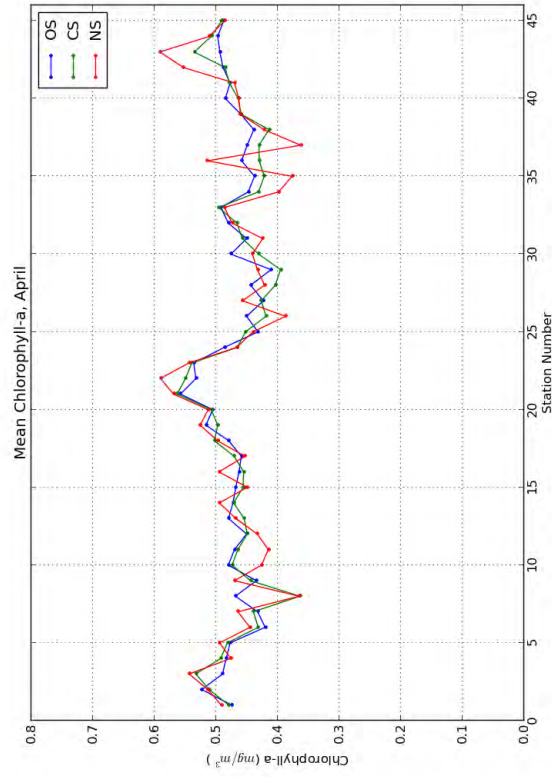
From August to September, mean Secchi Depths markedly increase, particularly along the eastern and southern shores, while chlorophyll *a* levels change only minimally. The mean Secchi Depth remains at a similar level, maintaining Secchi Depth at about 1 m lower than the surrounding stations. This station may be more affected by partial upwelling at this time.

In October, nearshore Secchi Depths increase slightly as Secchi Depths decrease slightly offshore, indicating offshore transport. The lowest mean nearshore Secchi Depth is 18 m at Station 20. In November, Secchi Depths show a very small increase, as chlorophyll *a* levels increase markedly around the lake. The lowest mean Secchi Depth in November is 18.5 m at Station 15, midway up the eastern shore, adjacent to the Logan House Creek inflow. Mean Secchi Depth and chlorophyll *a* levels do not vary during this time period.

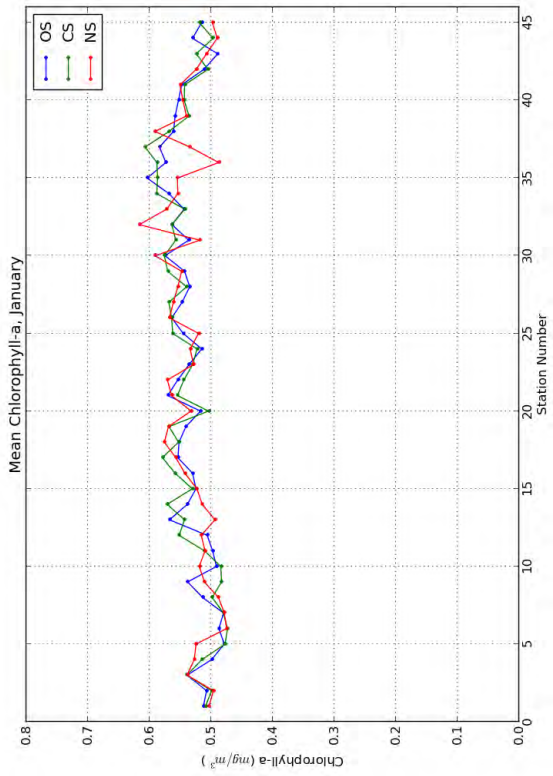
In December, mean Secchi Depth levels increase by 1 – 2 m along the southern and western shore, as chlorophyll *a* levels increase in this region. Upwelling is stronger during this period, so the covariance of chlorophyll *a* and Secchi Depth are likely due to upwelling contributions of chlorophyll *a* and higher clarity water to the surface layer. The lowest Secchi Depth shifts from Station 15 to 13, while the second lowest mean Secchi Depth is located at Station 22. Winter inflows are increasing at this time, leading to fresh nutrient and particle inputs as upwelling increases. However, the inflows are significantly lower than in the spring, so the effects of upwelling on chlorophyll *a* and Secchi Depth levels appears to outweigh the effects of inflow.



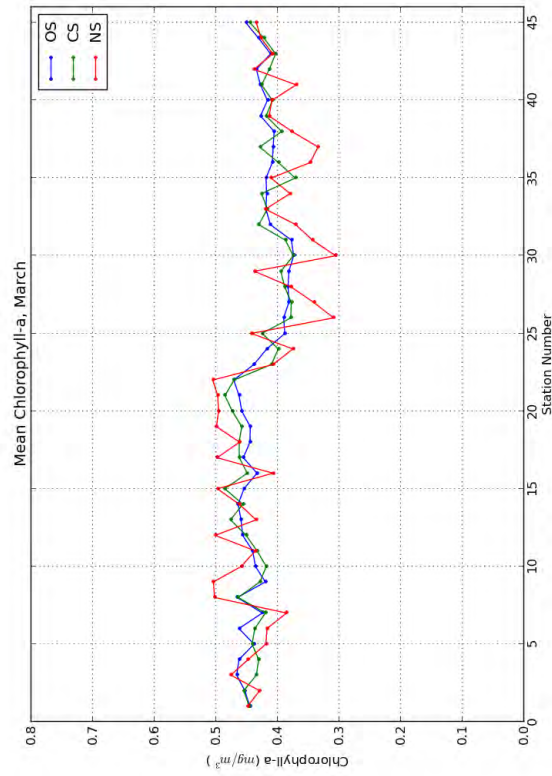
(a) January



(b) February

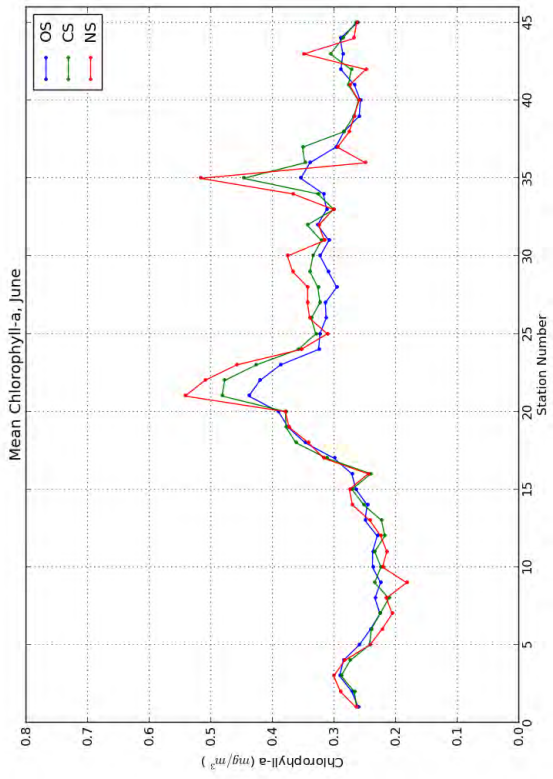


(c) March

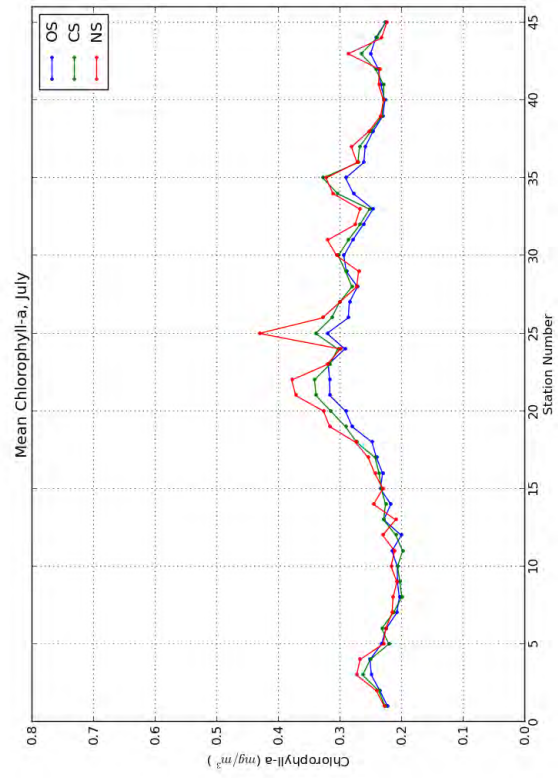


(d) April

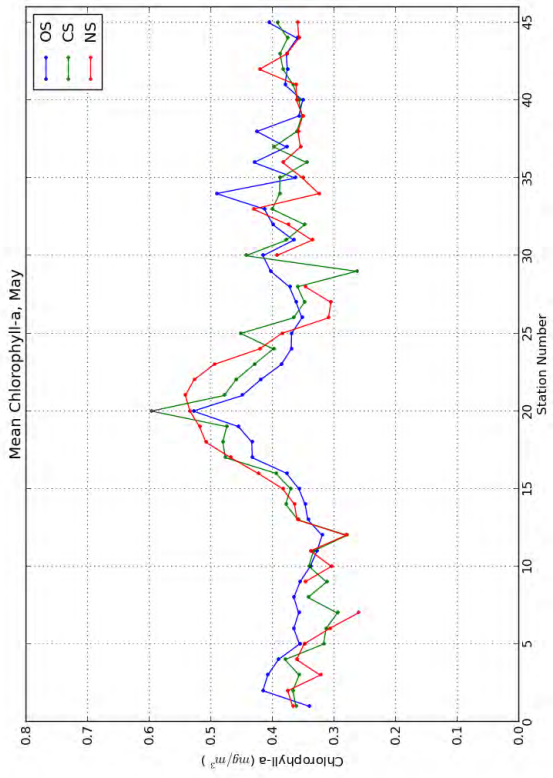
Figure 3.27: Mean monthly chlorophyll *a* (January – April).



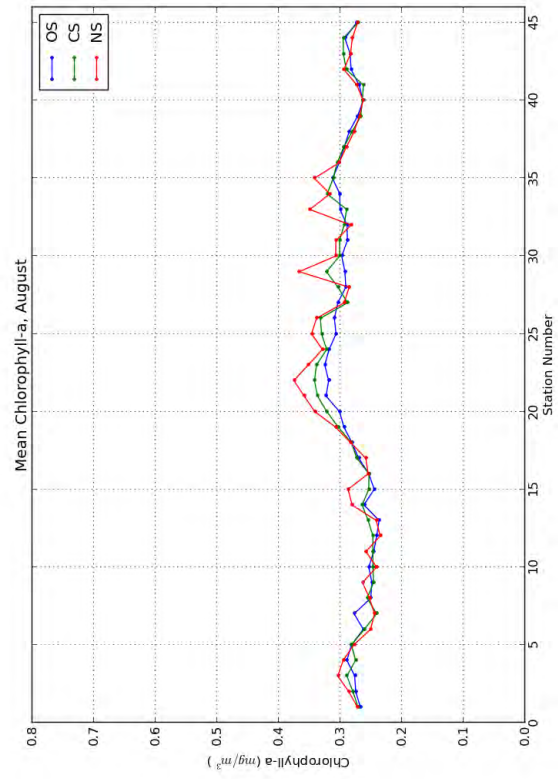
(a) May



(b) June

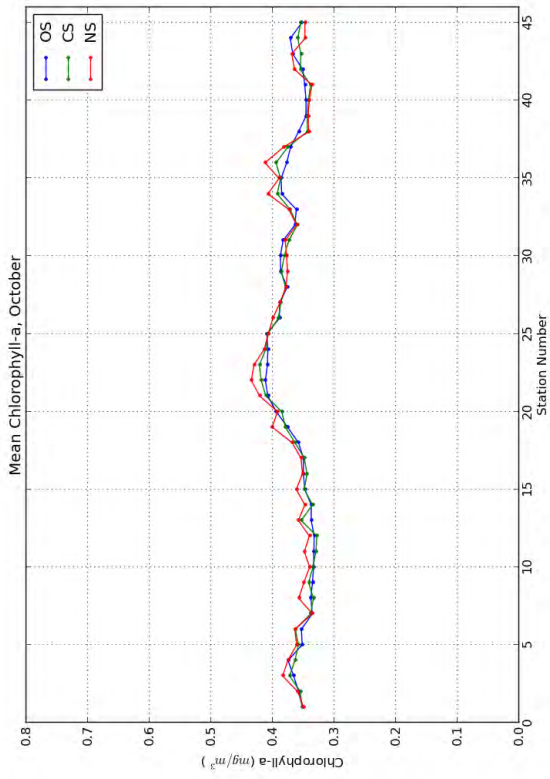


(c) July

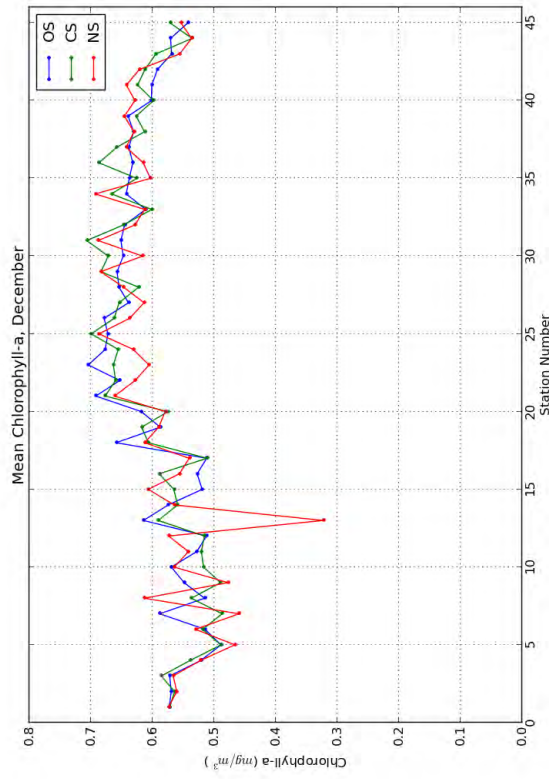


(d) August

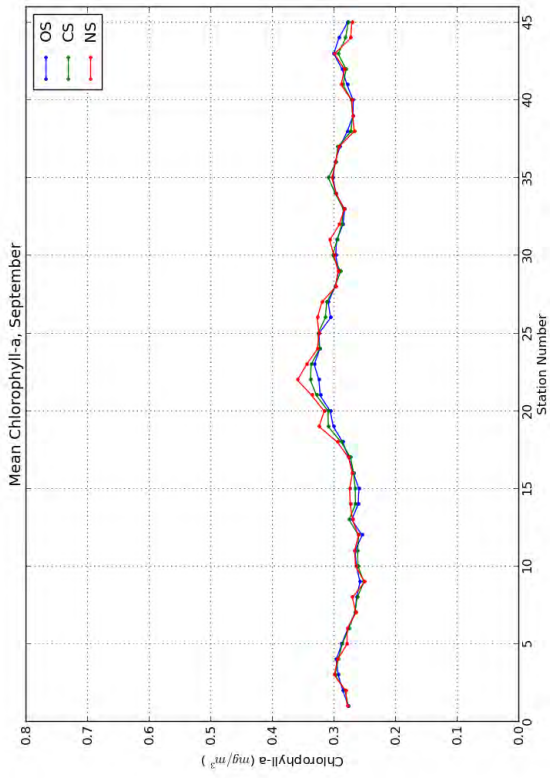
Figure 3.28: Mean monthly chlorophyll *a* (May – August).



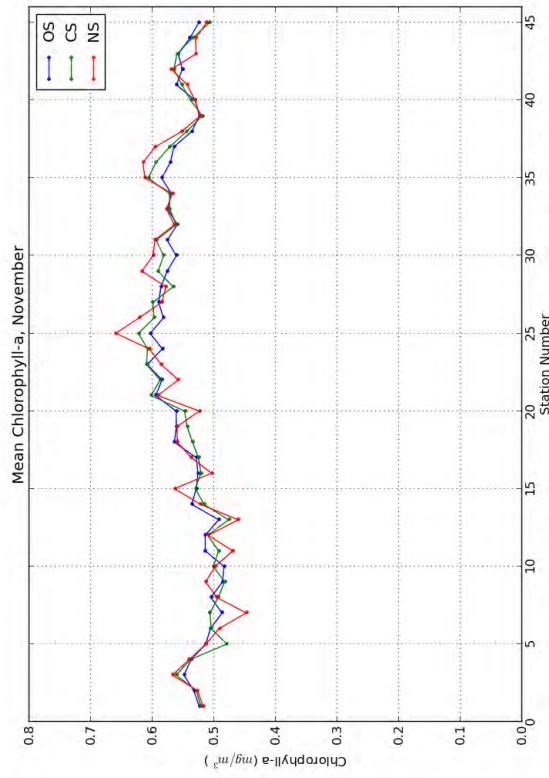
(a) September



(b) October

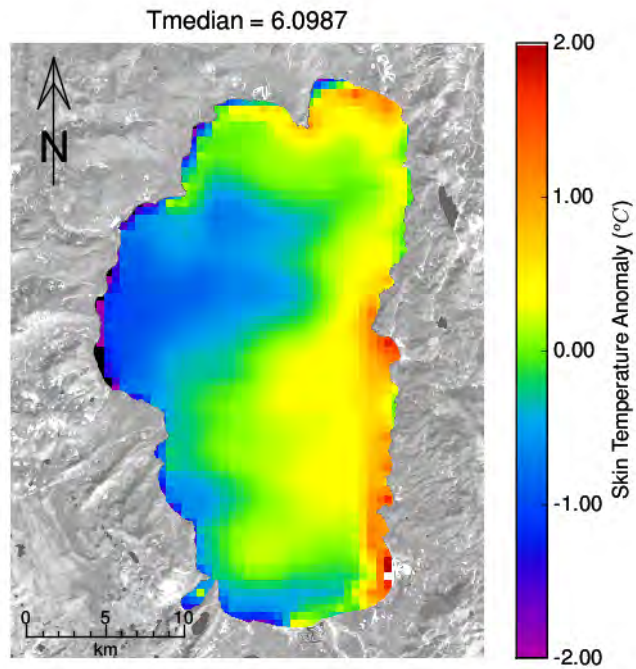


(c) November

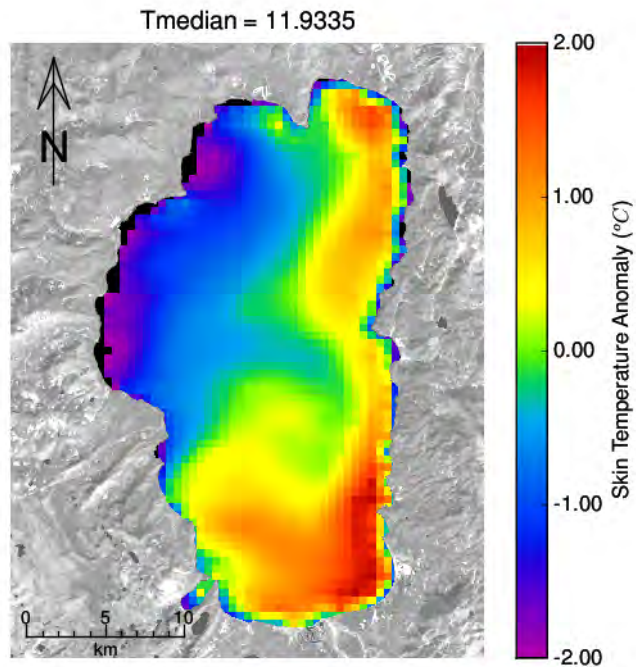


(d) December

Figure 3.29: Mean monthly chlorophyll *a* (September – December).

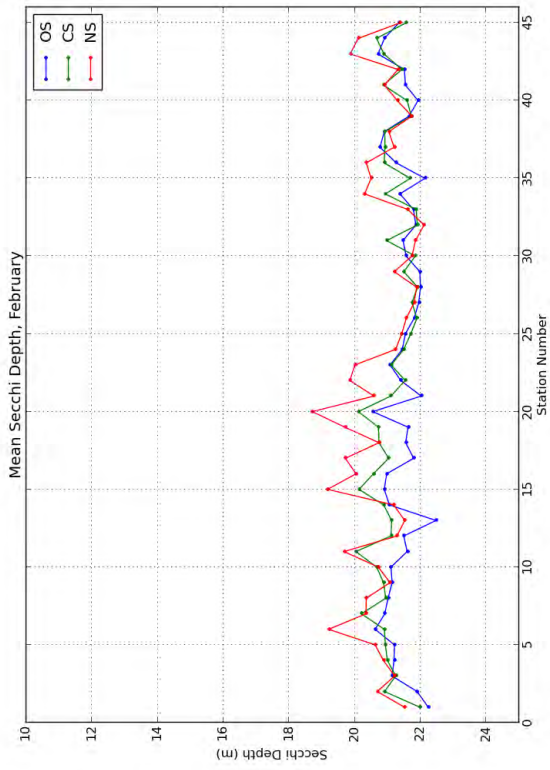


(a) MODIS WST Anomaly Map, Year: 2004, Day 87

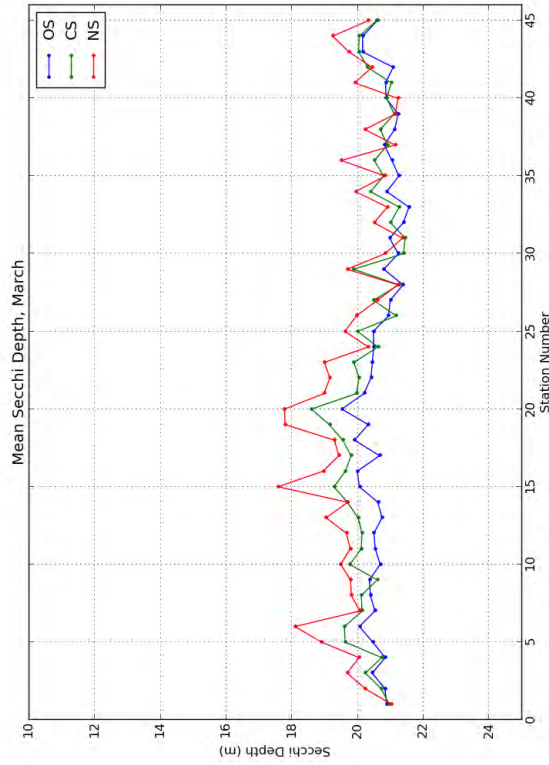


(b) MODIS WST Anomaly Map, Year: 2004, Day 159

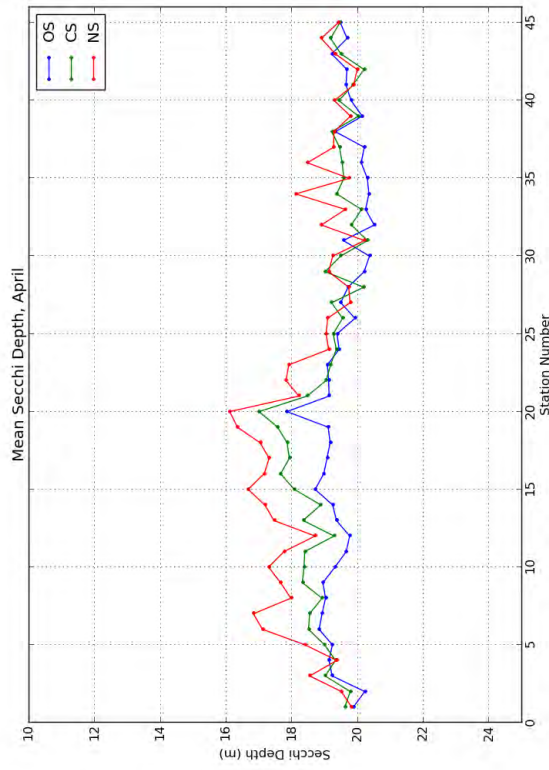
Figure 3.30: MODIS-Terra water skin temperature (WST) anomaly maps, showing nearshore temperature patterns along the south shore.



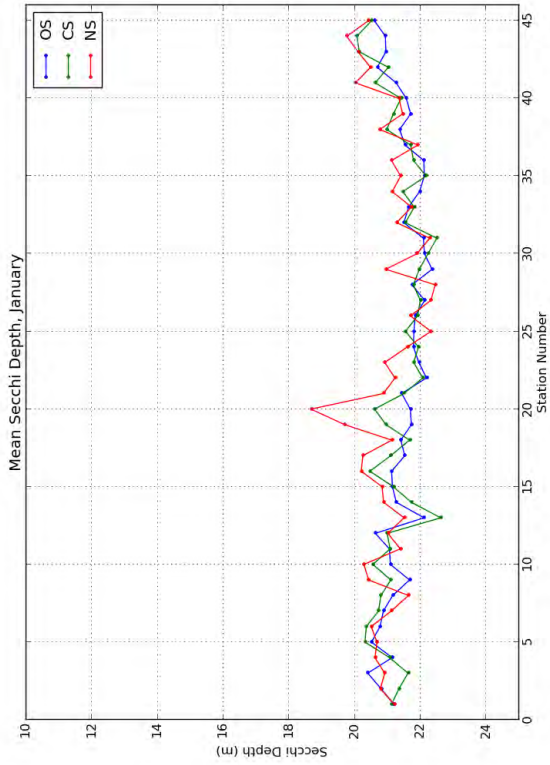
(a) January



(b) February

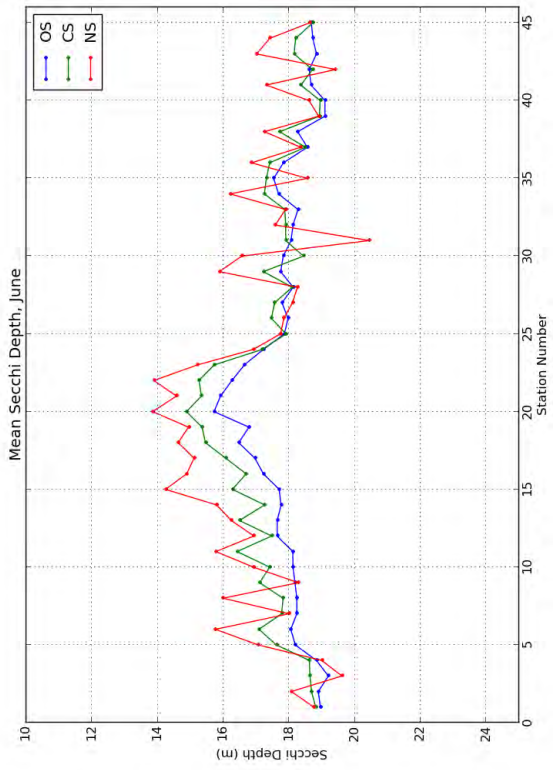


(c) March

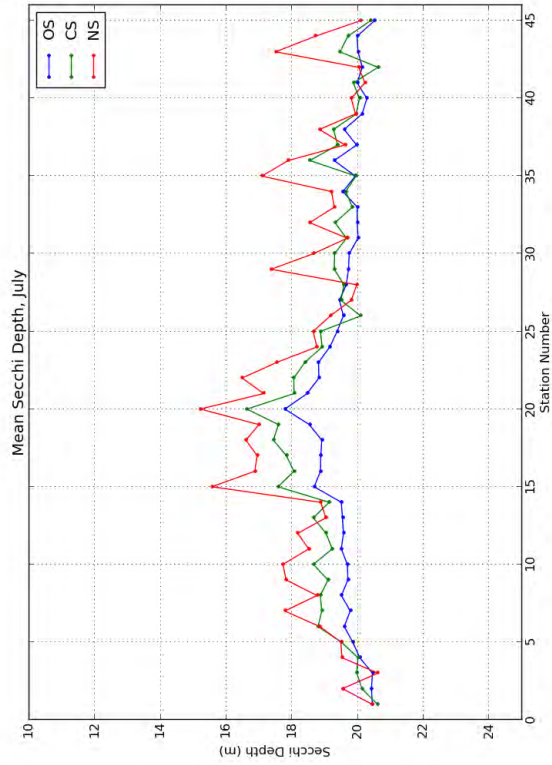


(d) April

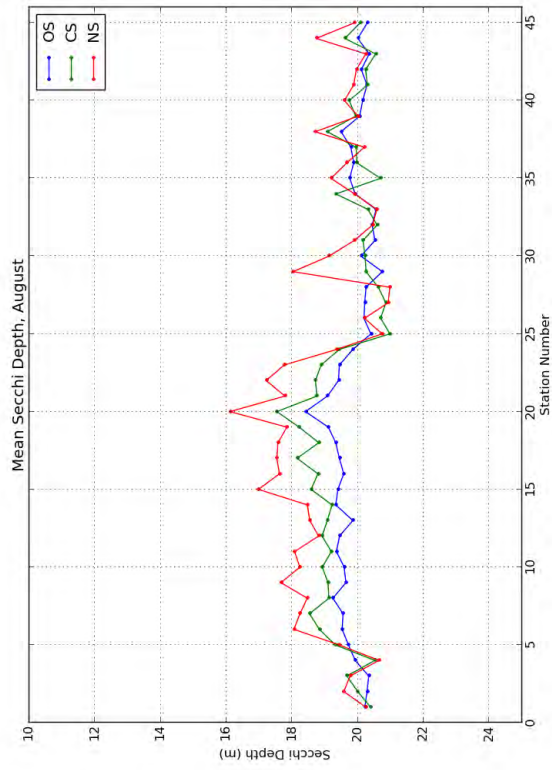
Figure 3.31: Mean monthly Secchi Depth (January – April). Note: the vertical scale is reversed, denoting depth from the surface.



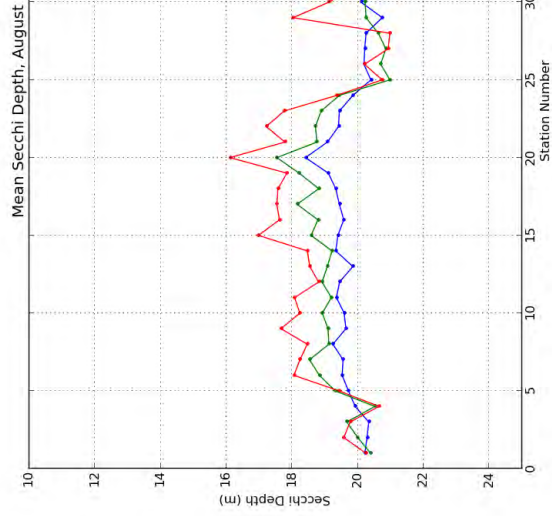
(a) May



(b) June

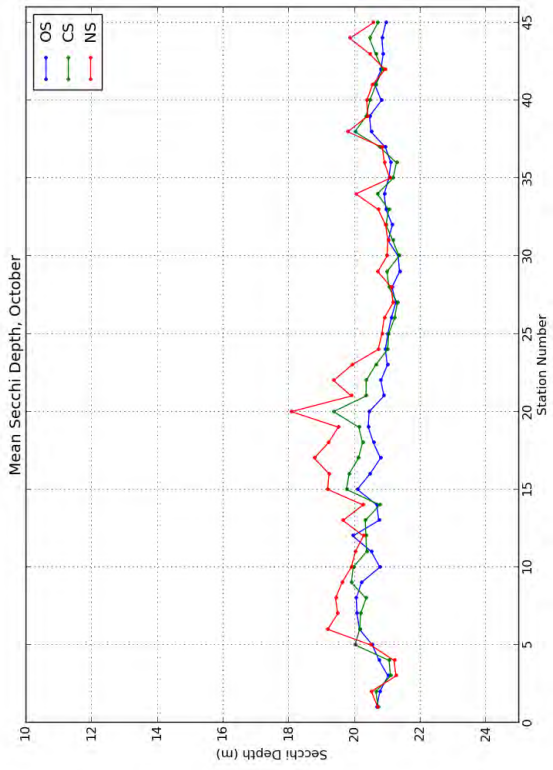


(c) July

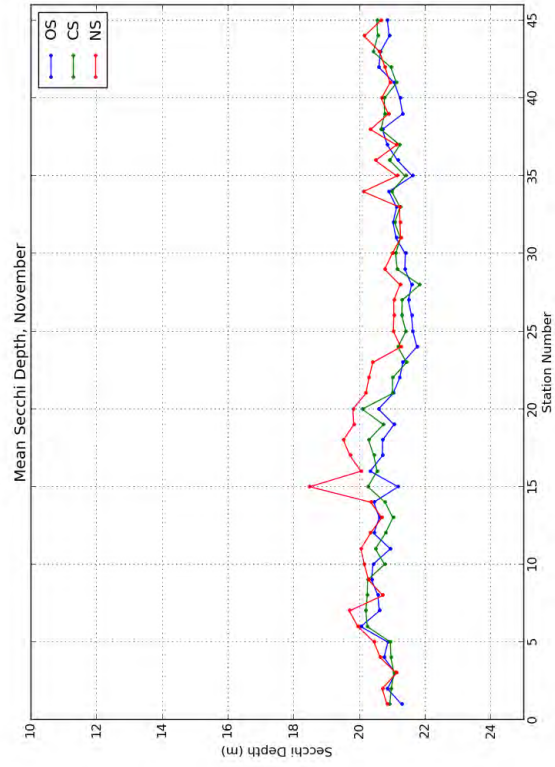


(d) August

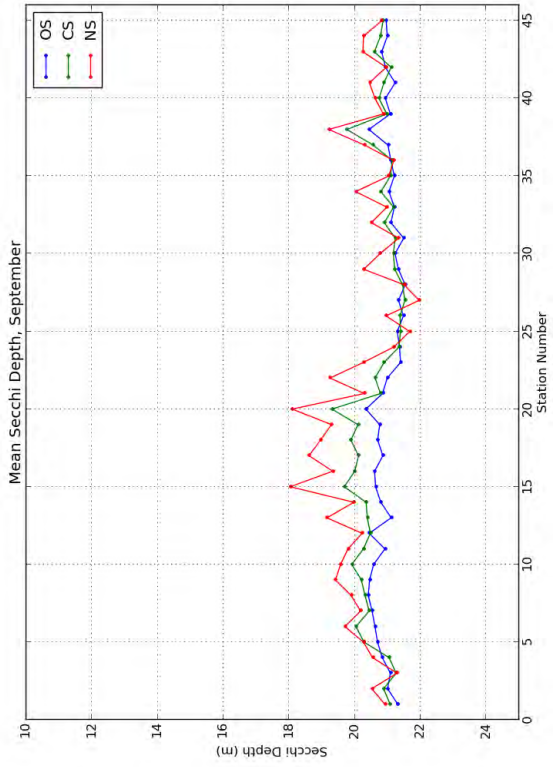
Figure 3.32: Mean monthly Secchi Depth (May – August).



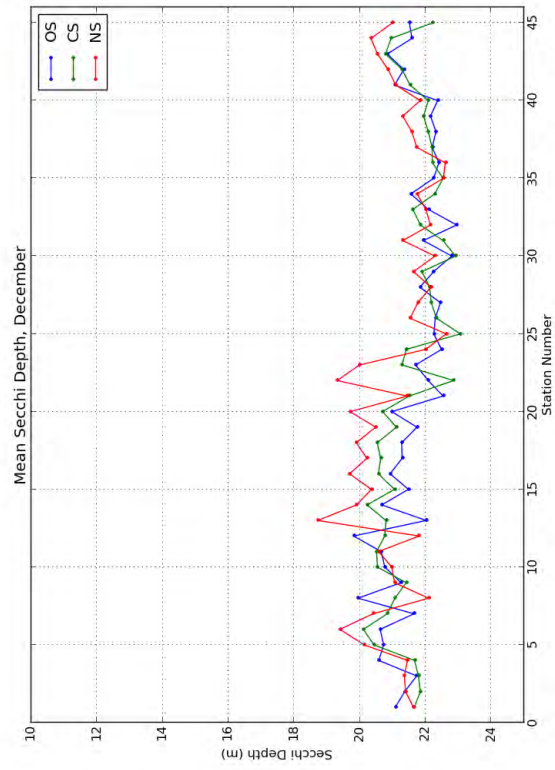
(a) September



(b) October



(c) November



(d) December

Figure 3.33: Mean monthly Secchi Depth (September – December).

## 3.5 Linkage Between Offshore Clarity and Forcing

**Goal:** *Describe the relation between spatial and temporal variability in offshore clarity and lake mixing, following wind-driven upwelling, and surface current patterns*

The previous section examined the effect of streamflow inputs on the distribution and variability of nearshore Secchi Depth and chlorophyll *a*. The data indicate that upwelling can contribute autochthonous inputs and that surface currents distribute particles and chlorophyll *a* around the shoreline and offshore. These mechanisms will be examined in greater detail in this section.

### 3.5.1 Chlorophyll *a* Maps

Figures 3.34 and 3.35 show the growth and transport of chlorophyll *a* in the spring and summer of 2003. Chlorophyll *a* levels increase significantly adjacent to South Lake Tahoe, influenced by the large combined inflows of the Upper Truckee River, Trout Creek, and Edgewood Creek. The patch of elevated chlorophyll *a* appears to translate eastward and then northward along the eastern shore. Then a plume emerges from the eastern shore, flowing westward. Finally, the patch of chlorophyll *a* shifts south again, spreading offshore before it diminishes. Figure 3.36 shows a similar pattern, with different timing, in 2004. Chlorophyll *a* levels are elevated along the western shore, spreading outward from Sugar Pine Point, adjacent to the General Creek inflow. As these concentrations diminish, a fresh input of chlorophyll *a* is provided from the south shore in the form of a jet or plume (Figures 3.36(c) and 3.36(d)). Figure 3.37 shows other evidence of jets or plumes of chlorophyll *a*. Figure 3.37(a) shows chlorophyll *a* spreading from the eastern shore near Marla Bay. Figure 3.37(b) shows chlorophyll *a* spreading from the southeast shore to Meeks Bay and Sugar Pine point, effectively short-circuiting the alongshore transport and missing the Emerald Bay region. A similar pattern is evident in Figure 3.37(c). Finally, a small jet of chlorophyll *a* can be seen leaving the Upper Truckee River inflow location (Station 22), heading west just offshore. These may be induced by eddies located in this region (see Appendix B).

The transport pattern evident between Julian Days 100 (Figure 3.37(b)) and 102 (Figure 3.37(c)) can be better understood by considering MODIS-derived water skin temperature (WST) maps acquired at this time. Figure 3.38 shows four WST anomaly maps acquired by MODIS-Terra and MODIS-Aqua on Julian Days 100 and 102. Each pair of images was acquired four hours apart, allowing enough time for transport patterns to be clearly delineated. Upwelling occurred prior to image acquisition, influencing water quality as well as providing a tracer of cooler water from the metalimnion. The warm patch of water along the east shore in Figure 3.38(a) divides (Figure 3.38(c)), spreading northward and southward, as a cooler patch to the west translates eastward and a warmer patch near Meeks Bay on the southwest shore translates northward. This pattern continues on Julian Day 102 (Figure 3.38(c) and 3.38(d)), tracing a double-gyre system, with a counter-clockwise gyre in the northern part of the basin and a clockwise gyre in the southern part of the basin. This was also observed by *Steissberg et al.* [2005b, a].

Figure 3.39 shows four examples of eddy-induced transport. Figure 3.39(a) shows a clear example of chlorophyll *a* transport induced by a counter-clockwise spiral eddy, transporting chlorophyll *a* from South Lake Tahoe to Marla Bay before turning west and flowing offshore. There is also a plume emitted from the southern shore, possibly indicating a temporary reversal of eddy rotation. Figure 3.39(b) shows a plume of chlorophyll *a* from the Upper Truckee River inflow to D. L. Bliss on the southern part of the western shore. The shape of this plume indicates a counter-clockwise spiral eddy induced this transport. Figure 3.39(c) shows a sharply defined plume between Marla Bay and South Lake Tahoe. Since the nearshore concentrations of chlorophyll *a* are higher adjacent to the Upper Truckee River than at Marla Bay at the time this image was acquired, the transport is evidently northeastward, carried by a clockwise eddy. This closely matches the transport pattern traced by drogues from South Lake Tahoe to Marla Bay in August 2008, as shown in Appendix B, Figure B.2. Figure 3.39(d) shows evidence of a large eddy adjacent to the southern shore. The direction of rotation is not clear, but since a plume westward-flowing plume is visible north of this eddy, it is likely that it is flowing counter-clockwise.

### 3.5.2 Water Quality Time Series

Analysis of the chlorophyll *a* maps and time series reveal a significant seasonal pattern. Coincident with spring runoff, chlorophyll *a* begins to increase along the southern shore, concentrated near Stateline, and along the eastern shore, extending just north of Glenbrook Bay. The chlorophyll appears to be transported clockwise along the shore, spreading offshore in jets following upwelling events. There is some transport between the south and east shores across the lake via a clockwise eddy transport. The eddy transport may contribute to offshore diffusion. It is notable that the peak chlorophyll occurs near Edgewood-Tahoe Golf Course, and the elevated chlorophyll *a* values extend to just north of Glenbrook Golf Course. Clarity is mildly correlated to chlorophyll, at times, but the chlorophyll signal is stronger. Offshore water quality is linked to nearshore water quality via upwelling and spiral eddies, while alongshore transport occurs via large-scale circulation (gyres) and meso-scale eddies (“spiral eddies”).

During the winter periods of years 2004, 2005, 2007, and 2009, peaks in *clarity* (high Secchi Depths) and chlorophyll *a* occurred at several stations. Meteorological and water temperature data (not shown) indicate upwelling occurred during these periods, following strong winds between 10 and 30 m/s. Strong upwelling transports high clarity water to the surface, which contains low levels of particles but high levels of nutrients. If this water is transported from the depth of the deep chlorophyll *a* maximum (DCM), chlorophyll *a* concentrations in the surface layer can increase immediately. Otherwise, chlorophyll *a* concentrations will increase over time, following the upwelling. The 2004 chlorophyll *a* peak occurred approximately five weeks after the upwelling, while the 2007 chlorophyll *a* and clarity peaks coincided with upwelling. It is notable that this upwelling was stronger and that the clarity and chlorophyll *a* peaks were stronger, indicating that water was transported from greater depths. On the eastern shore, Secchi Depth and chlorophyll *a* peaks were observed during the 2004 upwelling in Glenbrook Bay (Station 13, Figure 3.15) and near Logan House Creek (Station 14, Figure 3.17). It is notable that the clarity and chlorophyll *a* peaks were attenuated adjacent to the point south of Glenbrook Bay (Station 14, Figure 3.16(b)). This station was located closer to the shoreline, and the corresponding water quality maps (not shown) indicated that *low* chlorophyll *a* and low clarity water was confined to within approximately 750 m from shore, suggesting that this region was affected by increased streamflow, which was elevated at this time. Within two weeks, this trend reversed, and a band of high chlorophyll *a* water could be seen in this nearshore region in the chlorophyll *a* maps. This can also be seen in the time series; chlorophyll *a* peaks around January 17, 2004 at Station 14, while it drops at Station 13, which is further from shore. The 2004 winter water quality peaks were stronger along the northern and eastern shores, while the 2005 water quality peaks were stronger along the southern and western shores.

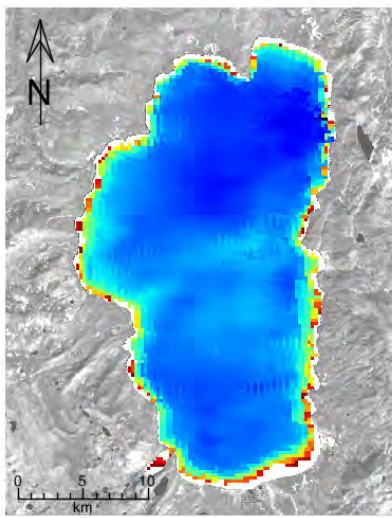
Comparison of the nearshore, coastal, and offshore time series indicated that water clarity was significantly lower and chlorophyll *a* was significantly higher in the nearshore regions than the offshore regions, on average. The variability of these parameters was also much higher nearshore than offshore. In fact nearshore water quality was periodically better than offshore water quality, typically following upwelling.

The peak in chlorophyll *a* appears near the Upper Truckee inflow location in April (Figure 3.27(d)), then shifts eastward from April to May (Figure 3.28(a)). The chlorophyll *a* peak then appears to shift westward as it diminishes, from May (Station 20) through September (Station 31, Figure 3.29(a)). Since the Upper Truckee River has been shown to provide the majority of nutrient and sediment loads to the lake, this is assumed to be the origin of the elevated chlorophyll *a* and particle concentrations. This indicates that the spatial changes in water quality are due to east-to-west transport along the southern shore, as would be the result of a clockwise gyre in the southern basin. This has been observed by drogoue data and satellite images collected in 2001 [Steissberg *et al.*, 2005b, a].

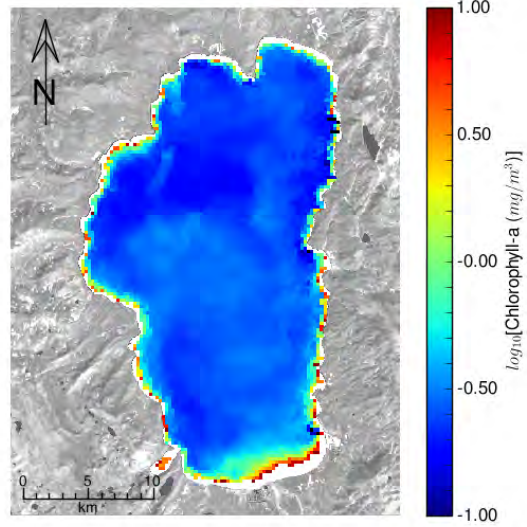
However, drogues deployed in August of 2008 indicated the presence of a 5 km counter-clockwise eddy north of the Upper Truckee River inflow and a 3 km clockwise eddy to the east of this, adjacent to the southeast shore. The former pattern was also observed by satellite images (see Appendix B, Figure B.1(c, g)), but clear evidence of a counter-clockwise eddy adjacent to the southeast shore was shown by satellite images (see Figure B.1(a, e)).

The evidence indicates that the number of eddies, their direction of rotation, and their locations can change over time, with the eddies shifting between the southwest and southeast shore. They may also disappear altogether, leaving a simple large scale double-gyre system. These eddies themselves might even be transported by the larger-scale clockwise gyre. This would suggest typical large-scale clockwise transport

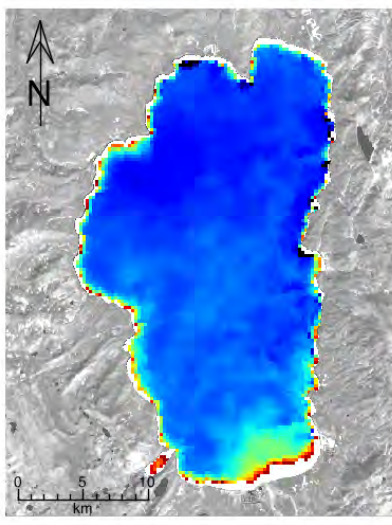
in the southern basin, modified by counter-clockwise eddies, forming counter currents, leading to offshore transport and transport between shores at the corners of the lake. The latter transport mechanism “short-circuits” the along-shore transport, which may help explain the patchiness of the spread of invasive species.



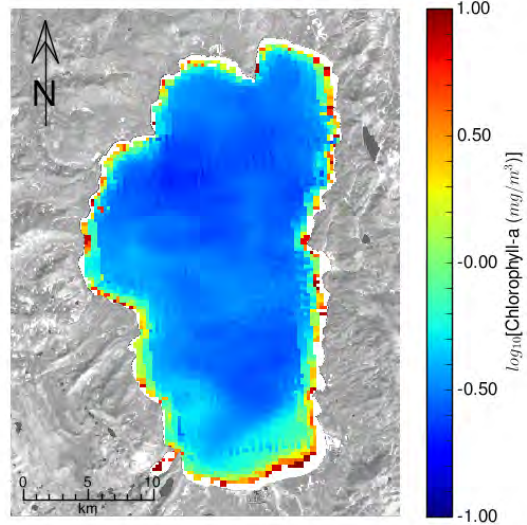
(a) Year: 2003, Day: 150



(b) Year: 2003, Day: 152

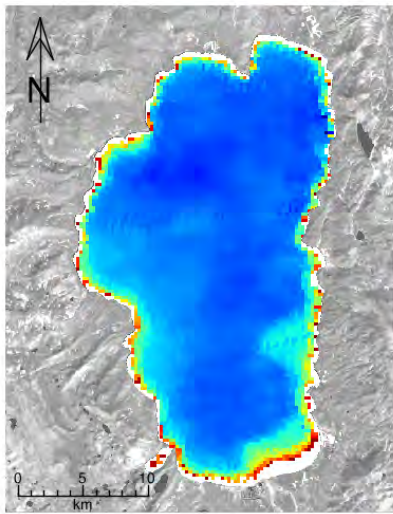


(c) Year: 2003, Day: 154

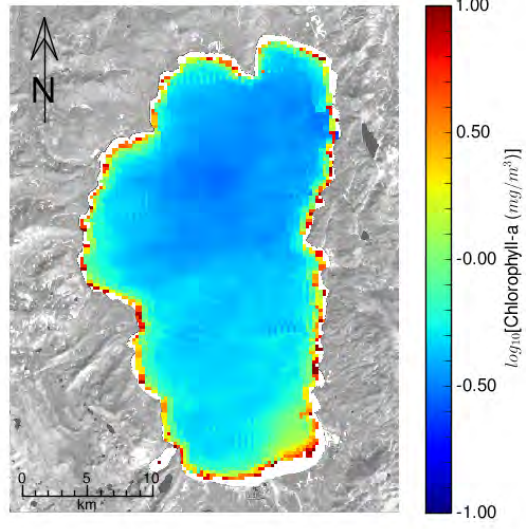


(d) Year: 2003, Day: 157

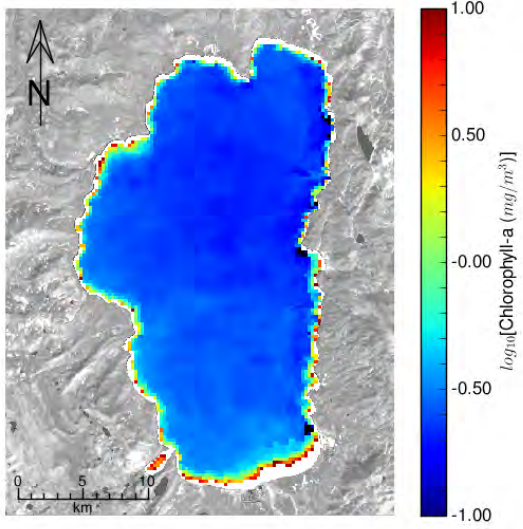
Figure 3.34: Maps showing growth and transport of chlorophyll *a* in 2003, Julian Days 150 – 157.



(a) Year: 2003, Day: 159

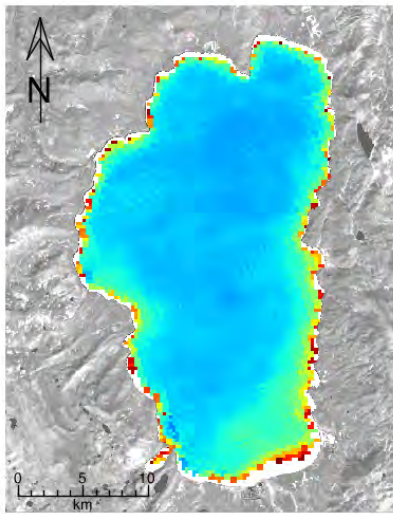


(b) Year: 2003, Day: 166

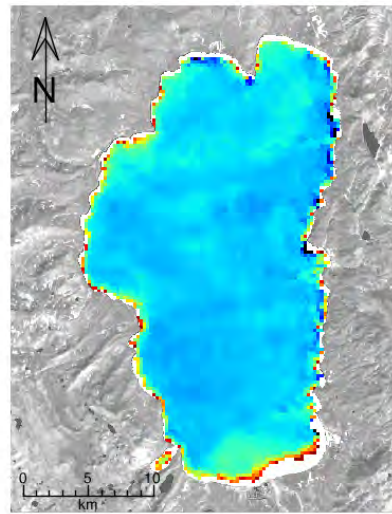


(c) Year: 2003, Day: 177

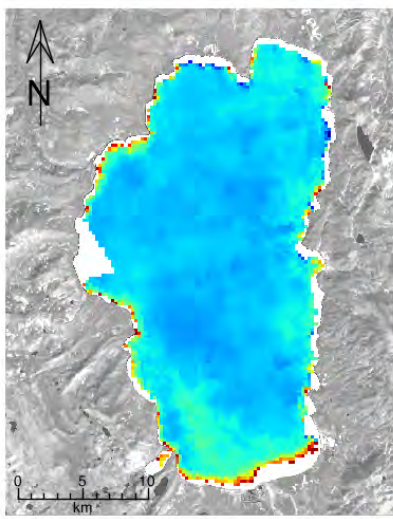
Figure 3.35: Maps showing growth and transport of chlorophyll *a* in 2003, Julian Days 159 – 177.



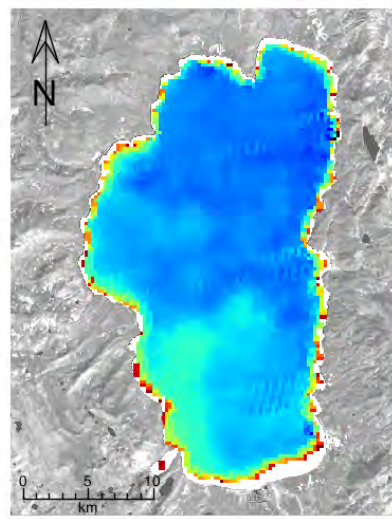
(a) Year: 2004, Day: 083



(b) Year: 2004, Day: 100

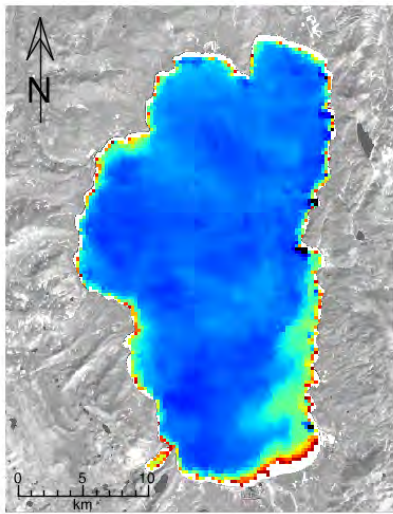


(c) Year: 2004, Day: 102

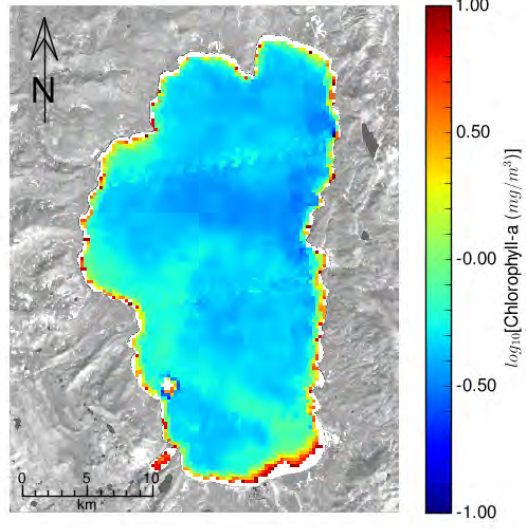


(d) Year: 2004, Day: 130

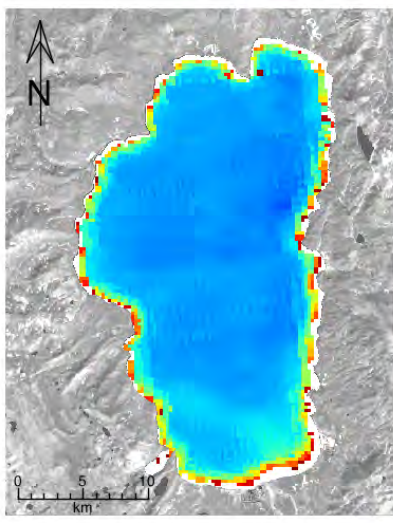
Figure 3.36: Maps showing cross-shore transport of chlorophyll *a* by jets and other currents.



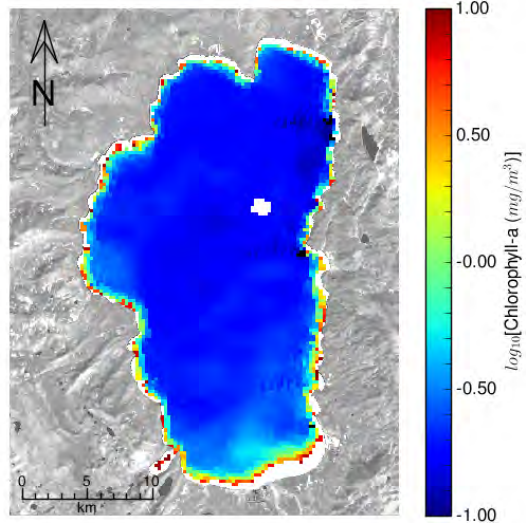
(a) Year: 2006, Day: 121



(b) Year: 2006, Day: 160

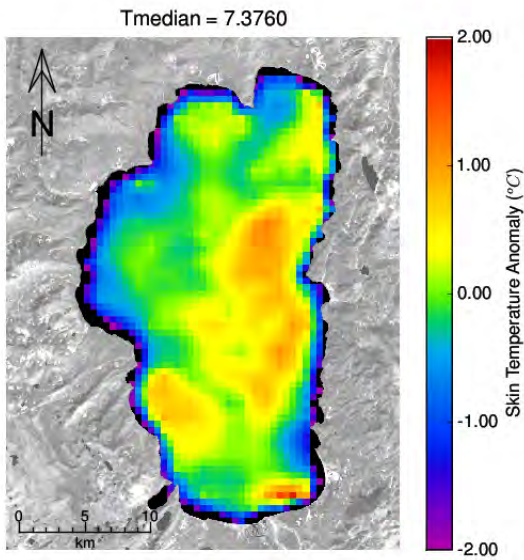


(c) Year: 2006, Day: 167

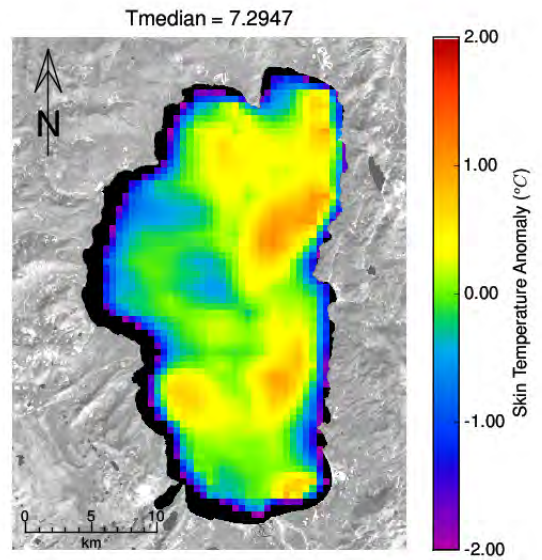


(d) Year: 2010, Day: 178

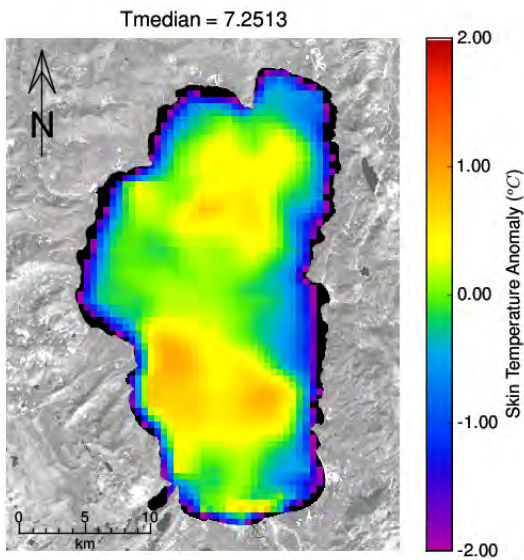
Figure 3.37: Maps showing cross-shore transport of chlorophyll *a* by jets and other currents.



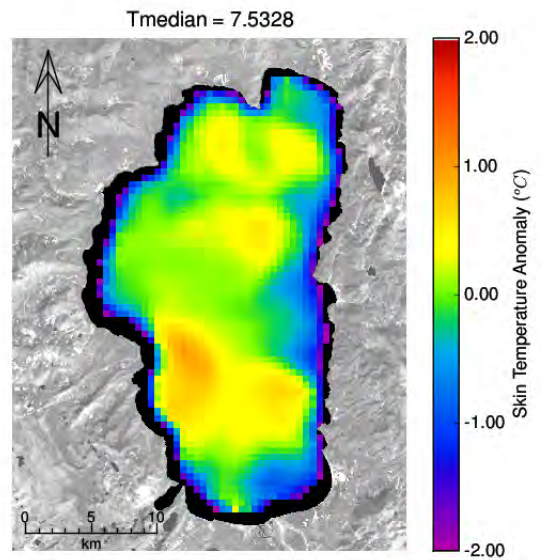
(a) MODIS-Terra WST, Year: 2004, Day: 100, 06:00 GMT



(b) MODIS-Aqua WST, Year: 2004, Day: 100, 10:10 GMT

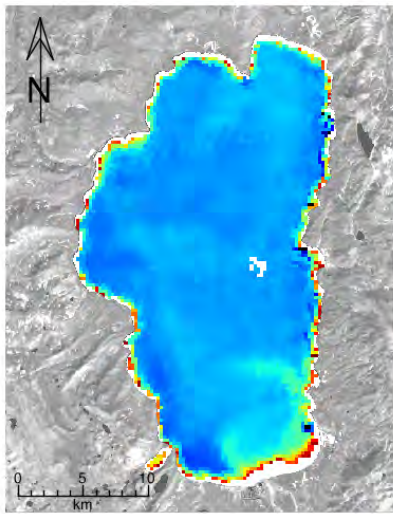


(c) MODIS-Terra WST, Year: 2004, Day: 102, 05:45 GMT

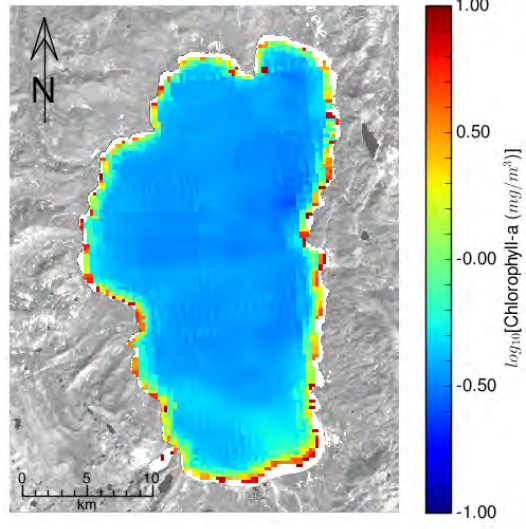


(d) MODIS-Aqua WST, Year: 2004, Day: 102, 09:55 GMT

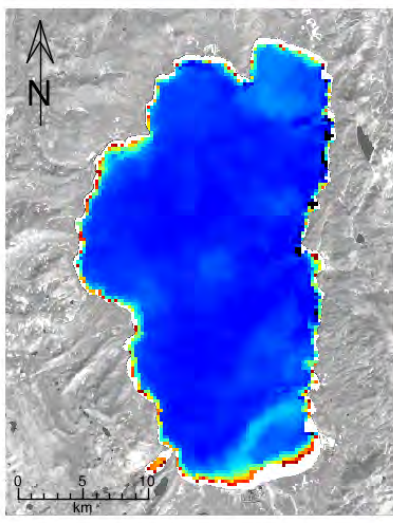
Figure 3.38: Water skin temperature (WST) of Lake Tahoe showing large-scale circulation and cross-shore transport of chlorophyll *a* by currents.



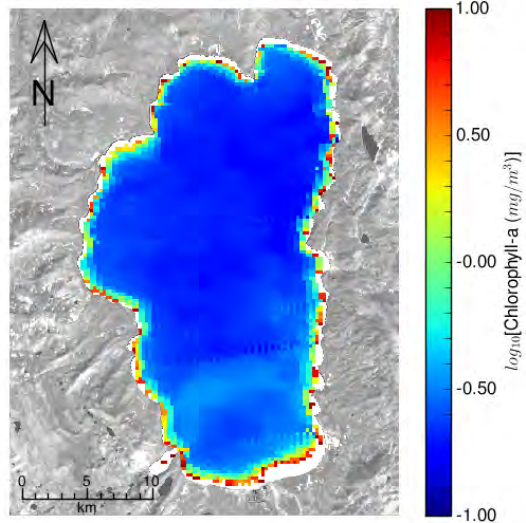
(a) Year: 2005, Day: 141



(b) Year: 2006, Day: 167



(c) Year: 2010, Day: 164



(d) Year: 2010, Day: 185

Figure 3.39: Maps showing cross-shore and along-shore transport of chlorophyll *a* by spiral eddies.

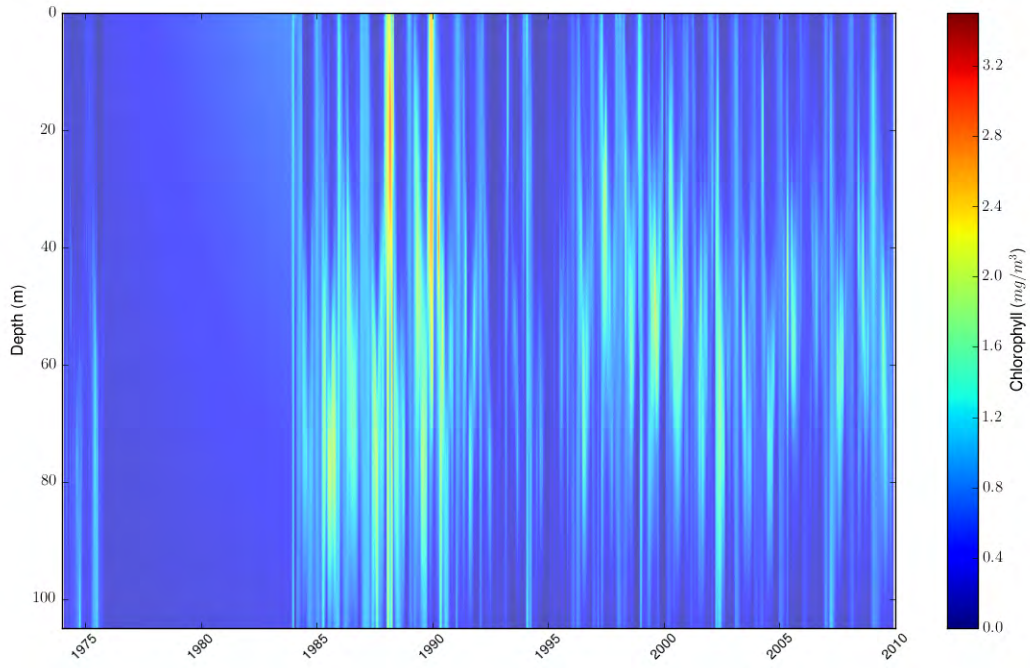
### 3.5.3 *In situ* Chlorophyll *a* Profiles: Characterization of Chlorophyll *a* Variability

To further clarify the spatial and temporal distribution and variability in chlorophyll *a*, as well as its vertical distribution and variability, pseudocolor (contour) plots of *in situ* chlorophyll *a* were created. The data set consisted of chlorophyll *a* samples acquired at multiple depths at the LTP and MLTP stations since 1974. The sampling depths and other details are outlined in Section 2.2.2. The individual samples were used to compute the depth-averaged concentration of chlorophyll *a* using the Trapezoidal Rule. Since the MLTP station is located at mid-lake, and the LTP station is located within 1 km of the shoreline (Figure 1.1), these can be used as proxies for offshore and nearshore variability, respectively.

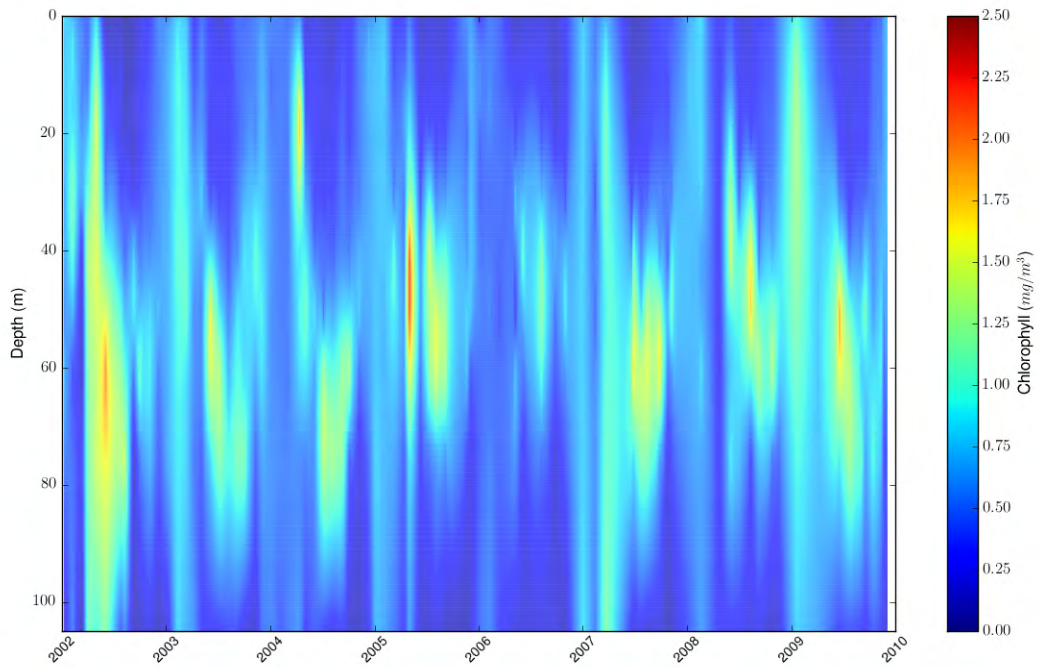
Figure 3.40(a) shows the chlorophyll *a* profile data for the entire 1974 – 2010 period of record at the LTP station, down to a depth of 105 m. To provide better detail of the data collected during the 2002 – 2010 study period, this figure was scaled to the smaller date range and is shown as Figure 3.40(b). Figures 3.41(a) and 3.41(b) show the analogous *in situ* chlorophyll *a* profiles collected at the MLTP station during the 1974 – 2010 and 2002 – 2010 periods, respectively.

Both the long-term and recent records show considerable seasonal and year-to-year variability in the Deep Chlorophyll Maximum (DCM). The width of this layer varies, as does the location of its peak, which can vary by as much as 50 m. Chlorophyll is periodically distributed throughout the surface layer through deep winter mixing, and this is evident in both the LTP and MLTP chlorophyll *a* profile data. The MLTP *in situ* chlorophyll *a* data show variation in the thickness of the DCM, but there is little variation in the location of the peak.

The vast majority of mixing occurs near lake boundaries [MacIntyre *et al.*, 1999; MacIntyre and Romero, 2000; MacIntyre and Jellison, 2001], and upwelling has been observed to occur frequently at Lake Tahoe [Steissberg *et al.*, 2005a]. This can transport the DCM upward or downward as internal waves increase in magnitude, affecting the depth of the DCM on the date of sampling. It can also control the depth of optimum nutrient availability [MacIntyre, 1998]. Since upwelling affects nearshore waters more than offshore waters [Steissberg *et al.*, 2005a], it is expected that the depth of the DCM will vary across the lake, as has been observed by Abbott *et al.* [1984]. Furthermore, the concentration of nutrients is larger in the shallow nearshore zone due to the smaller volume of water, and this shallow water can be significantly warmer than offshore water in the spring and summer, facilitating chlorophyll *a* growth in the nearshore zone. Therefore, the larger temporal and vertical variation of chlorophyll *a* observed at the LTP station is expected and confirms the greater temporal and horizontal variability observed in the MODIS-derived surface chlorophyll *a* data.

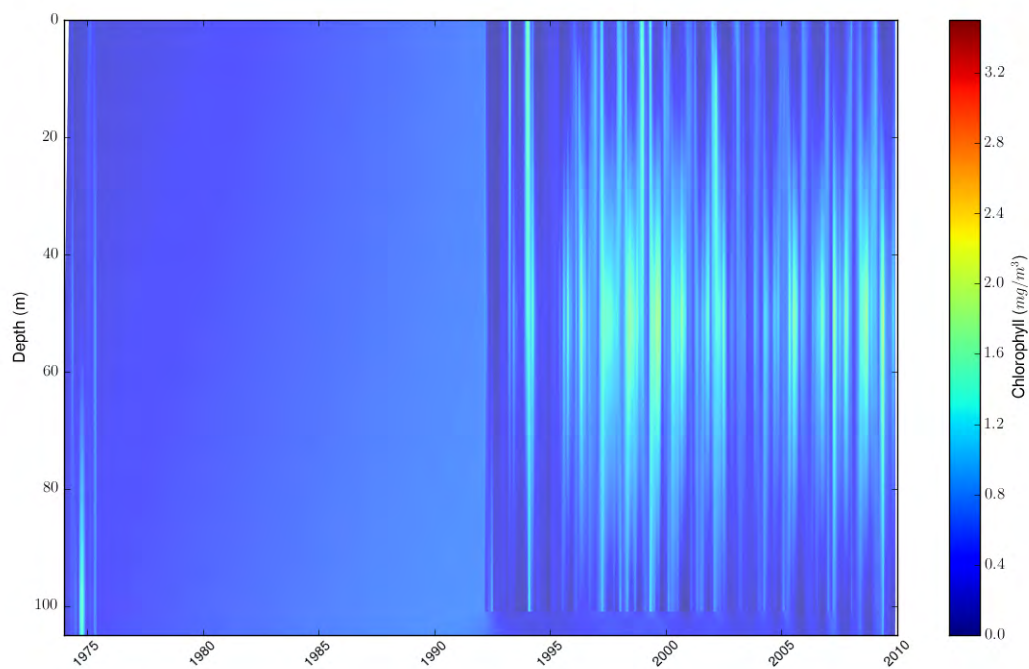


(a) *In situ* chlorophyll *a*, 1974 – 2010

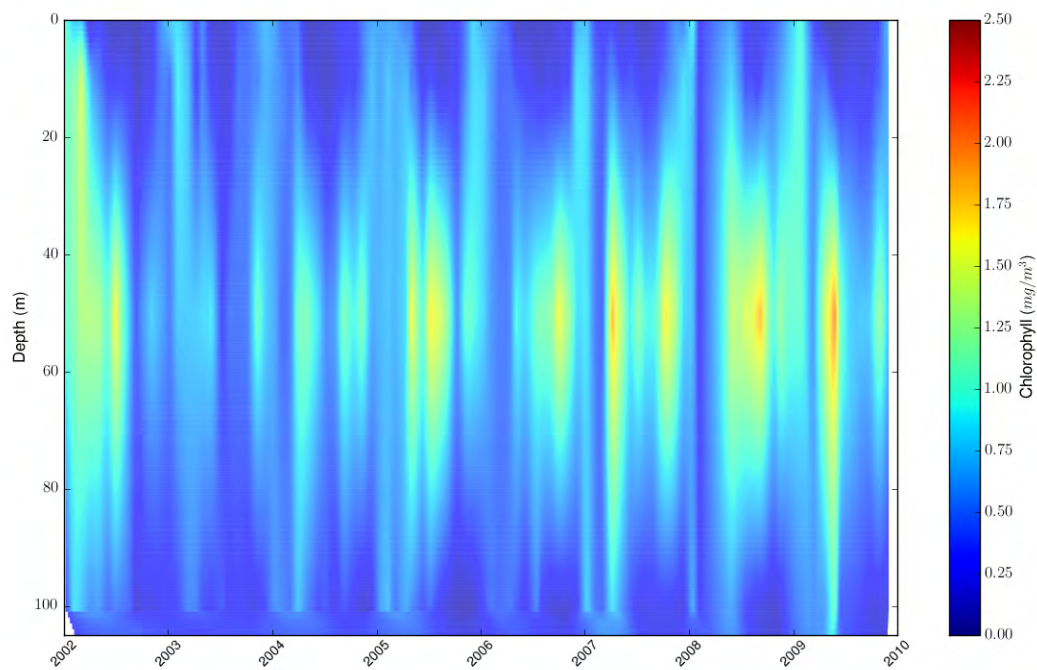


(b) *In situ* chlorophyll *a*, 2002 – 2010

Figure 3.40: *In situ* chlorophyll *a* measured at the LTP station. Both the period of record (1974 – 2010) and the MODIS-Aqua period (2002 – 2010) are shown.



(a) *In situ* chlorophyll *a*, 1974 – 2010



(b) *In situ* chlorophyll *a*, 2002 – 2010

Figure 3.41: *In situ* chlorophyll *a* measured at the MLTP station. Both the period of record (1974 – 2010) and the MODIS-Aqua period (2002 – 2010) are shown.

### 3.6 RS Water Quality Reporting System

**Goal:** *Develop a reporting system where RS-derived measures of water quality are made available on a near-real-time basis*

A reporting system has been developed to provide near-real-time RS-derived measurements of water quality. MODIS images can be easily ordered and downloaded at no cost. Then the scripts developed for this project can be applied in automated fashion to product chlorophyll *a* and Secchi Depth maps from the satellite images. The processed satellite data may be sampled at points of interest to generate time series and monthly averages of chlorophyll *a* and Secchi Depth. Sets of multiple images can be processed as simply as individual images. Prior to generation of water quality maps and time series, manual inspection of the high resolution true color MODIS images should be performed for QA/QC using the Qview program.

### 3.7 Methodology to Study Future Clarity Changes

**Goal:** *Develop a methodology that can be used to study future changes in nearshore and offshore water clarity for any region of concern around Lake Tahoe, which can be used in water quality management decision-making and design*

A methodology was developed during this study for use with MODIS-Aqua that can directly applied to MODIS-Terra to augment the data set. This methodology can continue to be applied to MODIS until both sensors cease operations. This method can then be applied to data collected by future ocean color sensors.

### 3.8 Methodology to Study Historical Clarity Changes

**Goal:** *Develop a methodology that can either be directly applied or easily adapted to current and previous measurements acquired by other sensors, including Landsat-5 Thematic Mapper (TM), to create a long-term record of clarity to help understand the historical patterns of clarity change, of importance to present and future basin management*

A methodology was developed during this study for use with MODIS-Aqua that can directly applied to MODIS-Terra to augment the data set and extend it back by 1.5 years. This methodology can be easily adapted to current and previous measurements acquired by other ocean color sensors. These sensors include SeaWiFS (1997 – present), MERIS (2002 – present), OCTS (1996 – present), and CZCS (1978 – 1986). This methodology employs SeaDAS for atmospheric correction and processing. SeaDAS was specifically designed for use with these sensors. These sensors do not possess high resolution bands, so they would be better suited to studying offshore water quality. It may be possible to develop a methodology to predict average weekly or monthly nearshore water quality using offshore water quality measurements acquired by these sensors.

### 3.9 Publication of Findings

**Goal:** *Publish findings in peer-reviewed journals*

A draft of a paper describing this research has been written. This is being reviewed by the co-authors in preparation for submission to *Limnology and Oceanography*.

## Chapter 4

# Conclusions

MODIS-derived maps of water quality (Secchi Depth and chlorophyll *a*) and nearshore/offshore time series extracted from these maps were analyzed to identify spatial and temporal patterns of Secchi Depth and chlorophyll *a* and their variability over the 2002 – 2010 study period. *In situ* streamflow, nutrient, Secchi Depth, and chlorophyll *a* data were paired with the satellite data to determine the effects of streamflow, upwelling, currents, circulation (gyres and smaller-scale eddies), and other factors on the seasonal and spatial changes in lake clarity and chlorophyll *a*.

The time series of stream inflows, sediment and nutrient loadings, and MODIS-derived Secchi Depths and chlorophyll *a* indicate that streamflow, and therefore sediment input, is the major contributor to short-term decreases in clarity. The lowest mean Secchi Depths were obtained nearest the streamflow locations around the lake coincident with peak spring inflows. However, autochthonous inputs due to sediment resuspension and vertical transport of nutrients appear to play a significant role in water quality distribution and variability.

Comparison of the nearshore, coastal, and offshore time series indicated that water clarity was significantly lower and chlorophyll *a* was significantly higher in the nearshore regions than the offshore regions, on average. The variability of these parameters was also much higher nearshore than offshore. In fact nearshore water quality was periodically better than offshore water quality, typically following upwelling.

The MODIS-derived water quality maps show that Secchi Depth and chlorophyll *a* often covary spatially and temporally, even though Secchi Depth itself is much more dependent on light scattering due to fine particles. The time series extracted from these maps show that chlorophyll *a* and particles generally covary during peak spring runoff, as suspended sediment and nutrients flow into the lake. While there is an immediate reduction in Secchi Depths, there is a delay of days or weeks between peak inflows and peaks in chlorophyll *a*, since chlorophyll *a* levels are dependent on phytoplankton growth. Since other environmental factors influence phytoplankton growth, chlorophyll *a* levels are not as closely linked to inflows as are Secchi Depths. Nevertheless, chlorophyll *a* and opacity (low Secchi Depth) levels are significantly increased during high flow years. Similar effects could be seen in moderate flow years that followed low flow years, releasing sediment that had accumulated over the previous two years.

Surface chlorophyll *a* and particle levels are typically inversely correlated during the fall, as upwelling transports clear, nutrient-rich water to the surface. During the winter periods of years 2004, 2005, 2007, and 2009, peaks in clarity (high Secchi Depths) and chlorophyll *a* occurred at several stations, following wind-driven upwelling induced by strong winds between 10 and 30 m/s. Strong upwelling can transport high clarity water to the surface, which contains low levels of particles but high levels of nutrients. If this water is transported from around the depth of the deep chlorophyll *a* maximum (DCM), chlorophyll *a* concentrations in the surface layer can increase immediately. Otherwise, chlorophyll *a* concentrations will increase over time, following upwelling-induced transport of nutrients to the surface layer. Both of these scenarios were observed in the satellite and field data.

The chlorophyll *a* maps and the nearshore/offshore chlorophyll *a* cycle derived from them reveal a significant seasonal pattern. Coincident with spring runoff, chlorophyll *a* begins to increase along the southern shore, concentrated near Stateline, and along the eastern shore, extending just north of Glenbrook Bay. The elevated chlorophyll *a* concentrations observed in the satellite-derived maps were found along the southern

and eastern shores in all but two years of this study, 2002 and 2008, which were low flow years. Patches of elevated chlorophyll *a* concentrations appeared during spring runoff and appear to be concentrated along the southern shore adjacent to the Upper Truckee River, Trout Creek, and Edgewood Creek inflows. Elevated concentrations were also observed near Incline Village and Glenbrook. The elevated concentrations appear to spread around the lake via large-scale circulation (gyres), with flow reversals and shore-to-shore (south-to-south or south-to-west) transport via smaller-scale (“spiral”) eddies 3 – 5 km in diameter. Chlorophyll *a* was observed to spread offshore in plumes or jets following upwelling events. The plumes and eddies may contribute to offshore diffusion.

Around the shoreline, the region adjacent to the Trout Creek and Upper Truckee River inflows showed the greatest variability, and highest peaks of opacity (low Secchi Depths) and chlorophyll *a* concentrations. Surprisingly, the lowest typical water quality measurements were recorded to the east of this point, adjacent to the Edgewood Creek inflow, despite significantly lower flows in Edgewood Creek. Higher temperatures and nutrient concentrations have been found in Edgewood Creek, possibly associated with the Edgewood-Tahoe Golf Course, as well as due to urban pollution affects. However, Edgewood Creek’s flows are low enough that computed loadings indicate a significantly lower impact than the Upper Truckee River. The lower water quality observed at this location may be due to currents transporting the Upper Truckee River and Trout Creek inputs eastward. In addition, there may be significant sediment resuspension from the shoals, which are only approximately 2 m deep between the Trout Creek and Edgewood Creek inflows, which may be transported eastward. Surface current analysis from satellite images and drogue data indicate that a spiral eddy is often found in the southeast corner of the lake. This eddy may concentrate and retain nutrients in this area.

The satellite data showed that a chlorophyll *a* plume often emanated from the southern shore, near the Upper Truckee River inflow, increasing chlorophyll *a* levels along the western and eastern shores. For the western shore, this chlorophyll *a* plume increased chlorophyll *a* levels along the western shore, just as chlorophyll *a* levels from spring runoff were decreasing. The difference in chlorophyll *a* between the western and southern shores prior to transport was larger than expected, given the relative magnitude of streamflows. Partial upwelling occurs during the spring storms, which bring strong winds in addition to rainfall. The upwelling may induce significant sediment resuspension over the South Lake Tahoe shoals, increasing chlorophyll *a* levels through autochthonous inputs.

The South Lake Tahoe / Stateline region has a number of factors that could contribute to lower water quality in addition to the significantly larger watershed and streamflow of the Upper Truckee River. First, the population in South Lake Tahoe is significantly larger than other areas of the lake, with ~24,000 permanent residents. By comparison, Incline Village has ~10,000 permanent residents, and Tahoe City has ~1,800. The significantly greater urbanization generates greater pollution, more runoff, and less infiltration, due to the greater quantity of impervious surfaces. South Lake Tahoe is adjacent to extensive shoals, which can generate warmer water during the daytime and the summer months, potentially assisting algal growth. This region is also subject to regular upwelling. Paired with the shallow bathymetry, significant resuspension of sediment could occur.

Along the eastern shore, the flows of Glenbrook and Logan House Creeks are significantly lower than the flows of the other basin streams. Based on streamflow and population distribution, in the absence of currents, the water quality along the eastern shore would be expected to be significantly better than other areas of the lake. However, currents transported inputs from South Lake Tahoe along the shoreline, commonly along the eastern shore. Therefore, the eastern shore typically exhibits higher chlorophyll *a* levels and lower Secchi Depth than the western shore.

Offshore water quality is linked to nearshore water quality via upwelling and spiral eddies, while along-shore transport occurs via large-scale circulation (gyres) and meso-scale eddies (“spiral eddies”). Analysis of high resolution images of Lake Tahoe, paired with MODIS data, indicates that the number of eddies, their direction of rotation, and their locations can change over time, with the eddies shifting between the southwest and southeast shore. They may also disappear altogether, leaving a simple large scale double-gyre system. These eddies themselves might even be transported by the larger-scale clockwise gyre. This would suggest typical large-scale clockwise transport in the southern basin, modified by counter-clockwise eddies, forming counter currents, leading to offshore transport and transport between shores at the corners of the lake. The latter transport mechanism “short-circuits” the along-shore transport, which may help explain the patchiness of the spread of invasive species.

The satellite data indicated that clarity improves quickly as flow decreases. It has been previously observed that lake clarity improved during El Niño years. The MODIS-derived nearshore data confirm that the El Niño signal needs to be removed to estimate the true impact of improved management practices on lake clarity. Furthermore, sediment can accumulate in the watershed during low flow years. During higher flow years, a larger quantity of sediment is available for transport. The MODIS Secchi Depth time series indicate that when a wet year follows a dry year, water quality can deteriorate rapidly, leading to significant inter-decadal variability of lake clarity.

Several regions in the lake merit further study. Water quality in Carnelian Bay was lower than expected at times, while the area adjacent to Blackwood Creek showed minimal impacts near its inflow points, despite its much greater inflows. Similarly disproportionate effects were observed along the eastern shore adjacent to the Glenbrook and Logan House Creek inflows, which were the lowest of the streamflows recorded during this study period. The inflows along the southern shore appear to have a very large impact on lake-wide water quality. Therefore, this region needs further study to quantify the point- and non-point sources of pollution into the lake and the contribution of sediment resuspension to water clarity.

# Bibliography

- Abbott, M. R., K. L. Denman, T. M. Powell, P. J. Richerson, R. C. Richards, and C. R. Goldman (1984), Mixing and the dynamics of the deep chlorophyll maximum in Lake Tahoe, *Limnology and Oceanography*, *29*(4), 862–878.
- Brezonik, P., K. D. Menken, and M. Bauer (2005), Landsat-based remote sensing of lake water quality characteristics, including chlorophyll and colored dissolved organic matter (CDOM), *Lake and Reservoir Management*, *21*(4), 373–382.
- Chavula, G., P. Brezonik, P. Thenkabail, T. Johnson, and M. Bauer (2009), Estimating chlorophyll concentration in Lake Malawi from MODIS satellite imagery, *Physics and Chemistry of the Earth*, *34*, 755–760.
- Chipman, J. W., T. M. Lillesand, J. E. Schmaltz, J. E. Leale, and M. J. Nordheim (2004), Mapping lake water clarity with Landsat images in Wisconsin, USA, *Canadian Journal of Remote Sensing*, *30*(1), 1–7.
- Dall’Olmo, G., A. A. Gitelson, D. C. Rundquist, B. Leavitt, T. Barrow, and J. C. Holz (2005), Assessing the potential of SeaWiFS and MODIS for estimating chlorophyll concentration in turbid productive waters using red and near-infrared bands, *Remote Sensing of Environment*, *96*(2), 176–187, doi:10.1016/j.rse.2005.02.007.
- Franz, B. A., P. J. Werdell, G. Meister, E. J. Kwiatkowska, S. W. Bailey, Z. Ahmad, and C. R. McClain (2006), MODIS land bands for ocean remote sensing applications, in *Proc. Ocean Optics XVIII*, pp. 9–13, Montreal, Canada.
- Fu, G., K. S. Baith, and C. R. McClain (1998), SeaDAS: The SeaWiFS data analysis system, in *Proceedings of the 4th Pacific Ocean Remote Sensing Conference, Qingdao, China, 28–31 July*, edited by M.-X. He and G. Chen, pp. 73–77, Beijing Fortune Quick Printing Corporation.
- Gohin, F., J. N. Druon, and L. Lampert (2002), A five channel chlorophyll concentration algorithm applied to SeaWiFS data processed by SeaDAS in coastal waters, *International Journal of Remote Sensing*, *23*(8), 1639–1661, doi:10.1080/01431160110071879.
- Gordon, H. R. (1978), Removal of atmospheric effects from satellite imagery of oceans, *Applied Optics*, *17*(10), 1631–1636.
- Hackley, S. H., B. C. Allen, D. A. Hunter, and J. E. Reuter (2005), Lake Tahoe Water Quality Investigations, Annual Report: July 1, 2004–June 30, 2005, *Tech. rep.*, University of California, Davis.
- Hatch, L. K., J. E. Reuter, and C. R. Goldman (2001), Stream phosphorus transport in the Lake Tahoe basin, 1989–1996, *Environmental Monitoring and Assessment*, *69*(1), 63–83.
- Heim, B., H. Oberhaensli, S. Fietz, and H. Kaufmann (2005), Variation in Lake Baikal’s phytoplankton distribution and fluvial input assessed by SeaWiFS satellite data, *Global and Planetary Change*, *46*(1–4), 9–27, doi:10.1016/j.gloplacha.2004.11.011.
- Heyvaert, A., and A. Parra (2005), Performance assessment of the coon street detention basin, Kings Beach, CA. Final report prepared for the Placer County Department of Public Works and the California Tahoe Conservancy, *Tech. rep.*, University of California, Davis.

- Hook, S. J., and G. Vaughan (2007), Absolute radiometric in-flight validation of mid infrared and thermal infrared data from ASTER and MODIS on the Terra spacecraft using the Lake Tahoe, CA/NV, USA, automated validation site, *IEEE Transactions on Geoscience and Remote Sensing*, 45(6), 1798–1807.
- Hook, S. J., F. J. Prata, R. E. Alley, A. Abtahi, R. C. Richards, S. G. Schladow, and S. Ó. Pálmarsson (2003), Retrieval of lake bulk and skin temperatures using Along-Track Scanning Radiometer (ATSR-2) data: A case study using Lake Tahoe, California, *Journal of Atmospheric and Oceanic Technology*, 20(4), 534–548.
- Hook, S. J., G. Chander, J. A. Barsi, R. E. Alley, A. Abtahi, and F. D. Palluconi (2004), In-flight validation and recovery of water surface temperature with Landsat-5 thermal infrared data using an automated high-altitude lake validation site at Lake Tahoe, *IEEE Transactions on Geoscience and Remote Sensing*, 42(12), 2767–2776.
- Horion, S., N. Bergamino, S. Stenuite, J. P. Descy, P. D. Plisnier, S. A. Loiselle, and Y. Cornet (2010), Optimized extraction of daily bio-optical time series derived from MODIS/Aqua imagery for Lake Tanganyika, Africa, *Remote Sensing of Environment*, 114(4), 781–791, doi:10.1016/j.rse.2009.11.012.
- Hu, C. M., Z. Q. Chen, T. D. Clayton, P. Swarzenski, J. C. Brock, and F. E. Muller-Karger (2004), Assessment of estuarine water-quality indicators using MODIS medium-resolution bands: Initial results from Tampa Bay, FL, *Remote Sensing of Environment*, 93(3), 423–441, doi:10.1016/j.rse.2004.08.007.
- Jassby, A. D., C. R. Goldman, J. E. Reuter, and R. C. Richards (1999), Origins and scale dependence of temporal variability in the transparency of Lake Tahoe, California-Nevada, *Limnology and Oceanography*, 44(2), 282–294.
- MacIntyre, S. (1998), Turbulent mixing and resource supply to phytoplankton, in *Physical Processes in Lakes and Oceans, Coastal and Estuarine Studies*, vol. 54, edited by J. Imberger, pp. 561–590, American Geophysical Union.
- MacIntyre, S., and R. Jellison (2001), Nutrient fluxes from upwelling and enhanced turbulence at the top of the pycnocline in Mono Lake, California, *Hydrobiologia*, 466(1-3), 13–29.
- MacIntyre, S., and J. R. Romero (2000), Predicting upwelling, boundary mixing, and nutrient fluxes in lakes, *Verhandlungen Internationale Vereinigung für Theoretische und Angewandte Limnologie*, 27, 246–250.
- MacIntyre, S., K. M. Flynn, R. Jellison, and J. R. Romero (1999), Boundary mixing and nutrient fluxes in Mono Lake, California, *Limnology and Oceanography*, 44(3), 512–529.
- Marti-Cardona, B., T. E. Steissberg, S. G. Schladow, and S. J. Hook (2008), Relating fish kills to upwellings and wind patterns in the Salton Sea, *Hydrobiologia*, 604, 85–95.
- Martinez, J.-M., L. Maurice Bourgoïn, P. Kosuth, F. Seyler, and J. Guyot (2003), Analysis of multitemporal MODIS and Landsat 7 images acquired over Amazonian floodplains lakes for suspended sediment concentrations retrieval, *International Geoscience and Remote Sensing Symposium (IGARSS)*, 3, 2122–2124.
- Pozdnyakov, D., R. Shuchman, A. Korosov, and C. Hatt (2005), Operational algorithm for the retrieval of water quality in the Great Lakes, *Remote Sensing of Environment*, 97(3), 352–370, doi:10.1016/j.rse.2005.04.018.
- Ruddick, K. G., F. Ovidio, and M. Rijkeboer (2000), Atmospheric correction of SeaWiFS imagery for turbid coastal and inland waters, *Applied Optics*, 39(6), 897–912.
- Sawaya, K., L. Olmanson, N. Heinert, P. Brezonik, and M. Bauer (2003), Extending satellite remote sensing to local scales: land and water resource monitoring using high-resolution imagery, *Remote Sensing of Environment*, 88(1-2), 144–156.
- Schladow, S. G., S. Ó. Pálmarsson, T. E. Steissberg, S. J. Hook, and F. J. Prata (2004), An extraordinary upwelling event in a deep thermally stratified lake, *Geophysical Research Letters*, 31(15), L15504, doi:10.1029/2004GL020392.

- Steissberg, T. E. (2008), Remote sensing of the surface layer dynamics of a stratified lake, Ph.D. Dissertation, University of California, Davis.
- Steissberg, T. E., S. J. Hook, and S. G. Schladow (2005a), Characterizing partial upwellings and surface circulation at Lake Tahoe, California-Nevada, USA with thermal infrared images, *Remote Sensing of Environment*, *99*(1–2), 2–15.
- Steissberg, T. E., S. J. Hook, and S. G. Schladow (2005b), Measuring surface currents in lakes with high spatial resolution thermal infrared imagery, *Geophysical Research Letters*, *32*(11), L11402, doi:10.1029/2005GL022912.
- Strickland, J. D. H., and T. R. Parsons (1972), *A Practical Handbook of Sea-water Analysis*, vol. 167, Fisheries Research Board of Canada.
- Swift, T. J., J. Perez-Losada, S. G. Schladow, J. E. Reuter, A. D. Jassby, and C. R. Goldman (2006), Water quality modeling in Lake Tahoe: linking suspended matter characteristics to secchi depth, *Aquatic Sciences*, *68*(1), 1–15.
- Vos, R. J., J. H. M. Hakvoort, R. W. J. Jordans, and B. W. Ibelings (2003), Multiplatform optical monitoring of eutrophication in temporally and spatially variable lakes, *Science of the Total Environment*, *312*(1–3), 221–243, doi:10.1016/S0048-9697(03)00225-0.
- Wang, M., and W. Shi (2007), The NIR-SWIR combined atmospheric correction approach for MODIS ocean color data processing, *Optics Express*, *15*(24), 15,722–15,733.
- Wilson, C., and X. Qiu (2008), Global distribution of summer chlorophyll blooms in the oligotrophic gyres, *Progress in Oceanography*, *78*(2), 107–134, doi:10.1016/j.pocean.2008.05.002.
- Wu, G., J. De Leeuw, A. K. Skidmore, H. H. T. Prins, and Y. Liu (2008), Comparison of MODIS and landsat TM5 images for mapping tempo-spatial dynamics of Secchi disk depths in Poyang Lake National Nature Reserve, China, *International Journal of Remote Sensing*, *29*(8), 2183–2198, doi:10.1080/01431160701422254.
- Wu, M., W. Zhang, X. Wang, and D. Luo (2009), Application of MODIS satellite data in monitoring water quality parameters of Chaohu Lake in China, *Environmental Monitoring And Assessment*, *148*(1–4), 255–264, doi:10.1007/s10661-008-0156-2.
- Xingwei, J., T. Junwu, Z. Minwei, M. Ronghua, and D. Jing (2009), Application of MODIS data in monitoring suspended sediment of Taihu Lake, China, *Chinese Journal Of Oceanology And Limnology*, *27*(3), 614–620, doi:10.1007/s00343-009-9160-9.

# Appendix A

## A.1 MODIS Time Series Coordinates

Table A.1: Coordinates of the locations where time series are extracted from each MODIS water quality map. The “nearshore” stations (NS) are located 750 m from either the shoreline or shoals that are shallow enough for bottom reflectance to contaminate the MODIS reflectance data. Similarly, the “coastal” (CS) and “offshore” (OS) stations are sited 1000 m and 1500 m, respectively, from the shoreline or visible shoals.

Station #	NS (750 m Offshore)		CS (1000 m Offshore)		OS (1500 m Offshore)	
	Lon	Lat	Lon	Lat	Lon	Lat
1	-120.005981	39.204810	-120.004597	39.202648	-120.001831	39.198865
2	-119.994568	39.215619	-119.992493	39.213998	-119.988689	39.210755
3	-119.982464	39.238049	-119.982810	39.235617	-119.983156	39.231293
4	-119.962752	39.231563	-119.964135	39.229402	-119.966902	39.225618
5	-119.944769	39.221024	-119.947190	39.220213	-119.952723	39.218592
6	-119.943731	39.201837	-119.946844	39.201837	-119.952723	39.202108
7	-119.939927	39.186434	-119.942694	39.186434	-119.948573	39.186704
8	-119.944077	39.171841	-119.946844	39.172111	-119.952723	39.172922
9	-119.945460	39.154276	-119.948227	39.155086	-119.953760	39.156438
10	-119.955835	39.139953	-119.958602	39.140494	-119.964481	39.141304
11	-119.964827	39.124279	-119.967594	39.124820	-119.973127	39.125901
12	-119.970360	39.105092	-119.973127	39.105092	-119.978660	39.104822
13	-119.956873	39.091581	-119.959639	39.091310	-119.965519	39.091040
14	-119.959985	39.076718	-119.963098	39.076718	-119.968631	39.076447
15	-119.956181	39.059422	-119.959294	39.059693	-119.964827	39.060503
16	-119.962406	39.043478	-119.965173	39.043749	-119.971052	39.044289
17	-119.964827	39.026994	-119.967939	39.026994	-119.973819	39.027264
18	-119.967248	39.008077	-119.969669	39.008888	-119.975202	39.010780
19	-119.969669	38.993214	-119.972435	38.992674	-119.977968	38.991593
20	-119.966902	38.969163	-119.968631	38.971055	-119.971744	38.975108
21	-119.986614	38.962948	-119.987652	38.965110	-119.989727	38.969163
22	-120.003214	38.957273	-120.003560	38.959705	-120.004943	38.964029
23	-120.021889	38.950517	-120.021889	38.952949	-120.022235	38.957273
24	-120.044368	38.953760	-120.043676	38.955922	-120.042639	38.960245
25	-120.063043	38.954300	-120.061659	38.956462	-120.059584	38.960516
26	-120.074109	38.971325	-120.071688	38.972946	-120.067193	38.975919
27	-120.081026	38.984567	-120.078605	38.985377	-120.073763	38.986999
28	-120.081026	38.998889	-120.078259	38.999970	-120.073072	39.002132
29	-120.094167	39.007267	-120.092438	39.008888	-120.087942	39.011861
30	-120.102467	39.019697	-120.100392	39.021049	-120.095551	39.023751
31	-120.105234	39.038344	-120.102122	39.038344	-120.096588	39.038074
32	-120.100047	39.056720	-120.097280	39.057260	-120.091401	39.057801
33	-120.103505	39.072934	-120.102122	39.074826	-120.098663	39.078609
34	-120.128405	39.078339	-120.127367	39.080501	-120.125984	39.084825
35	-120.148463	39.087797	-120.146042	39.088878	-120.140855	39.090770
36	-120.148117	39.105092	-120.145350	39.105092	-120.139471	39.105092
37	-120.144313	39.126982	-120.141892	39.125901	-120.137050	39.123469
38	-120.127367	39.148060	-120.126330	39.145898	-120.124600	39.141574
39	-120.093130	39.143466	-120.091747	39.141845	-120.088288	39.137791
40	-120.082755	39.161302	-120.080334	39.161302	-120.074109	39.161032
41	-120.083447	39.184272	-120.081026	39.183191	-120.075838	39.181029
42	-120.079297	39.203189	-120.076876	39.201837	-120.071688	39.199675
43	-120.065809	39.221294	-120.064426	39.219943	-120.060968	39.215619
44	-120.042985	39.222375	-120.043676	39.219673	-120.045060	39.215619
45	-120.028460	39.208864	-120.029843	39.206161	-120.031918	39.202378

# Appendix B

## B.1 Spiral Eddies at Tahoe

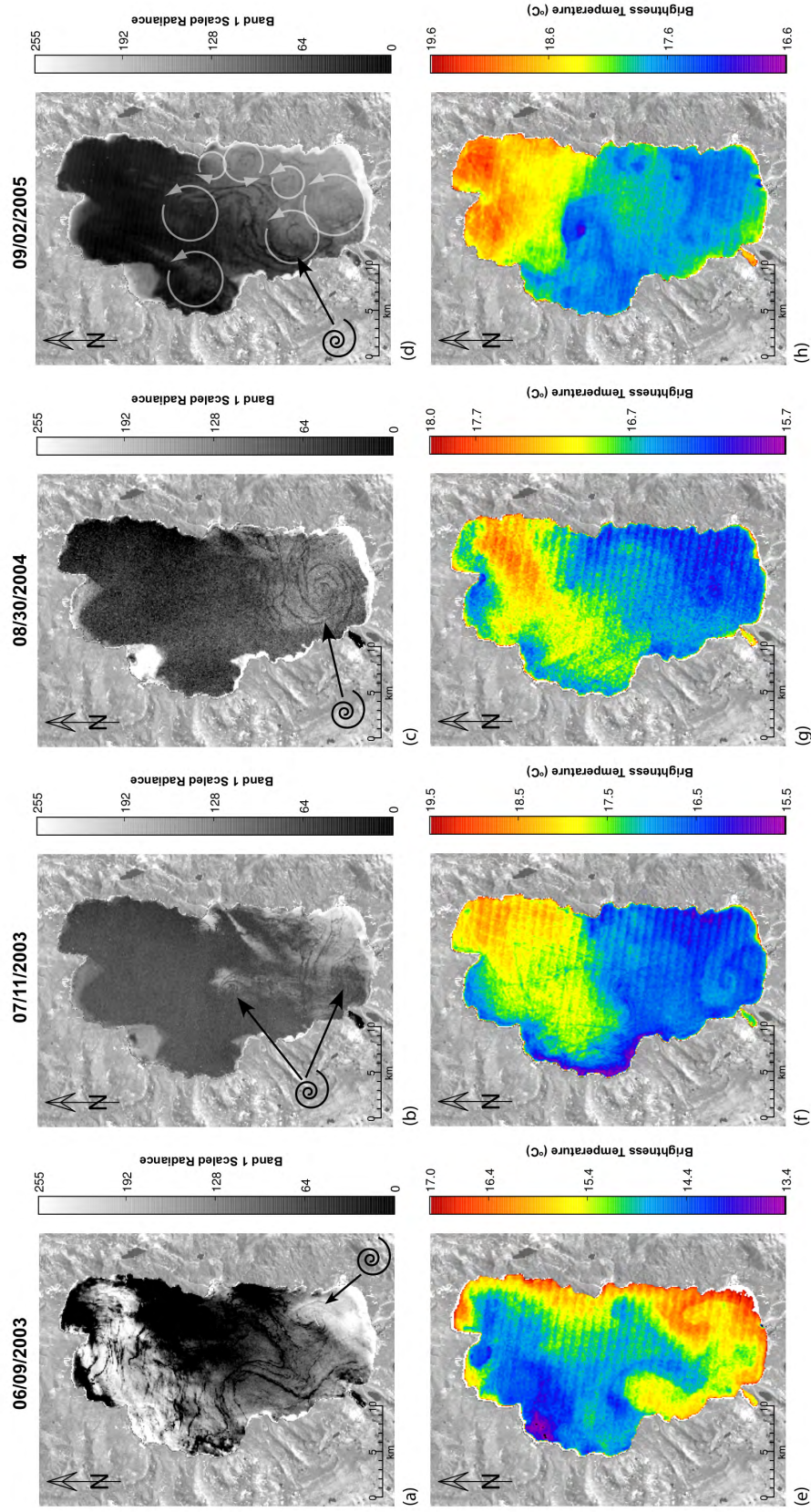


Figure B.1: Sun glitter maps and temperature maps showing spiral eddies at Lake Tahoe.

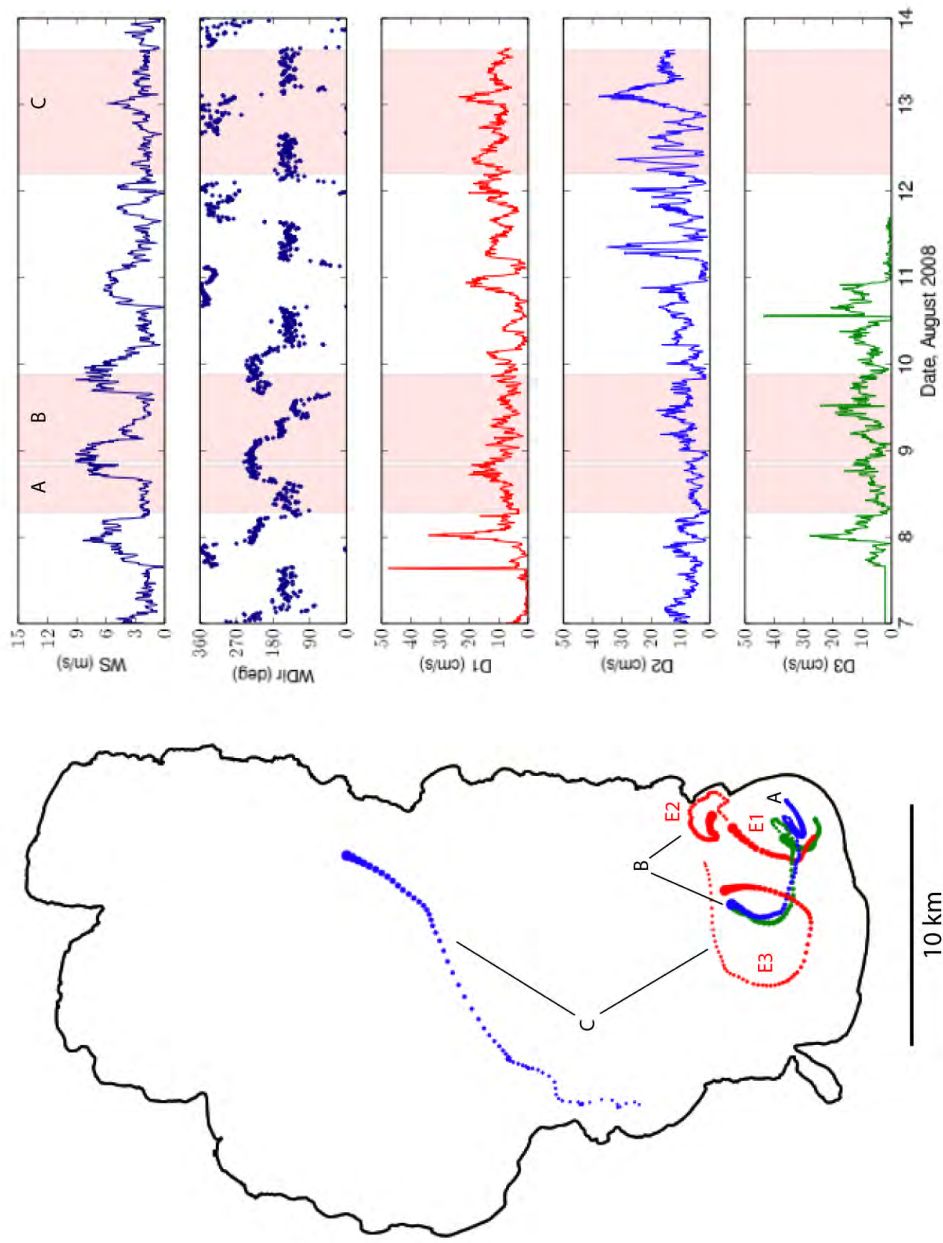


Figure B.2: Drogue tracks from August 2008. Direction of transport is indicated by dot size, larger dots indicating data recorded more recently.

## B.2 Current Patterns at Tahoe

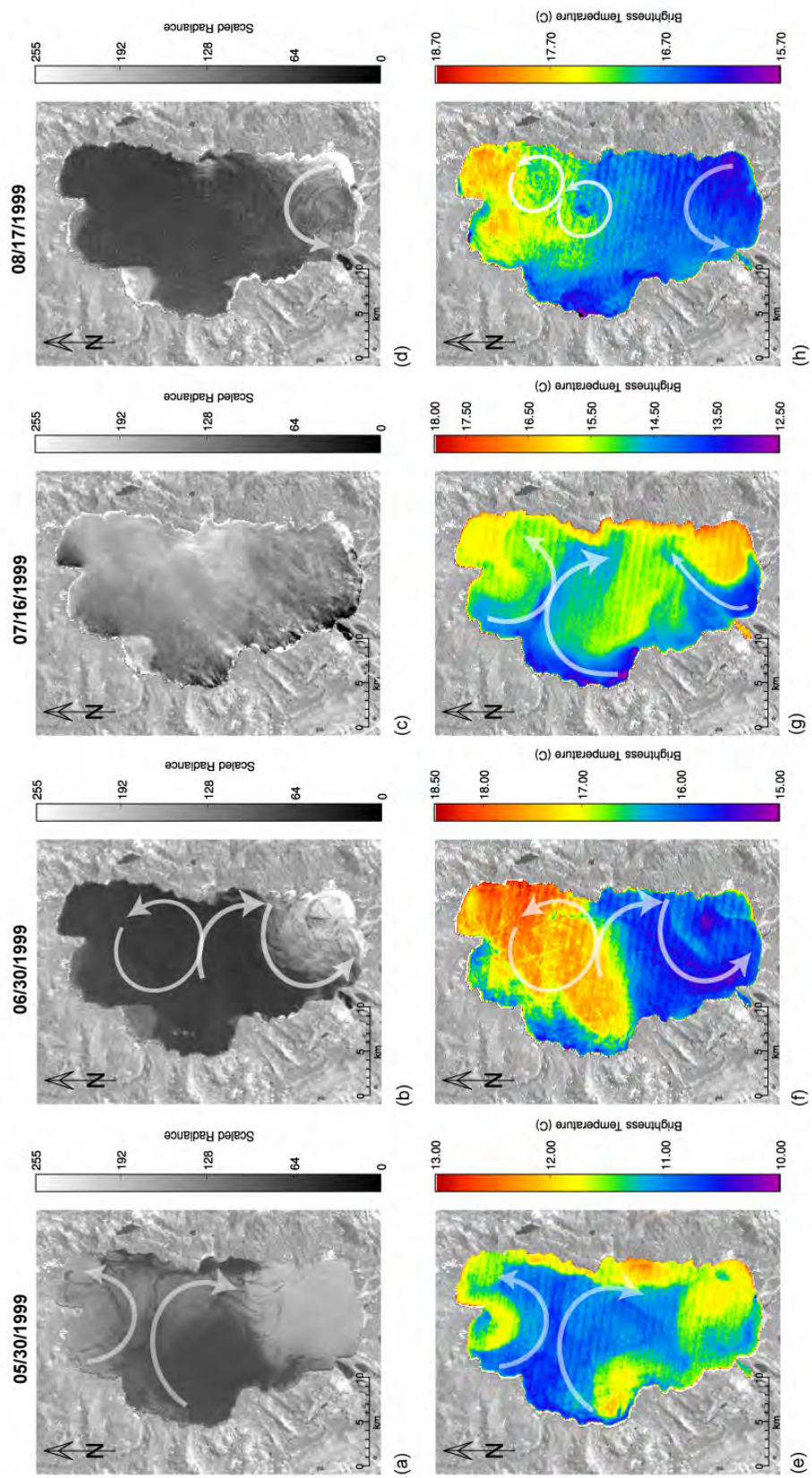


Figure B.3: Sun glitter maps and temperature maps showing large- and small-scale circulation patterns at Lake Tahoe, May 1999 – August 1999.

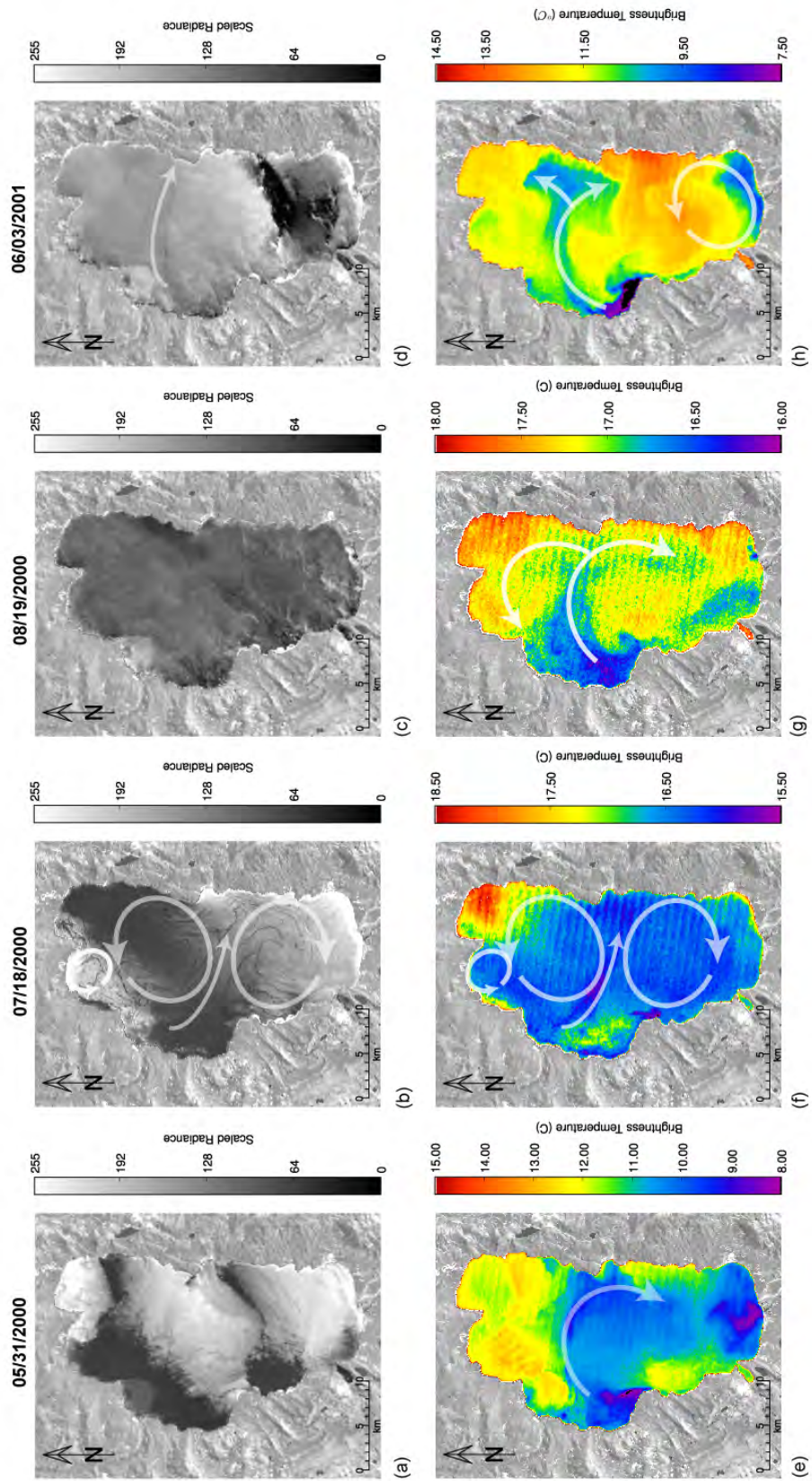


Figure B.4: Sun glitter maps and temperature maps showing large- and small-scale circulation patterns at Lake Tahoe, May 2000 – June 2001.

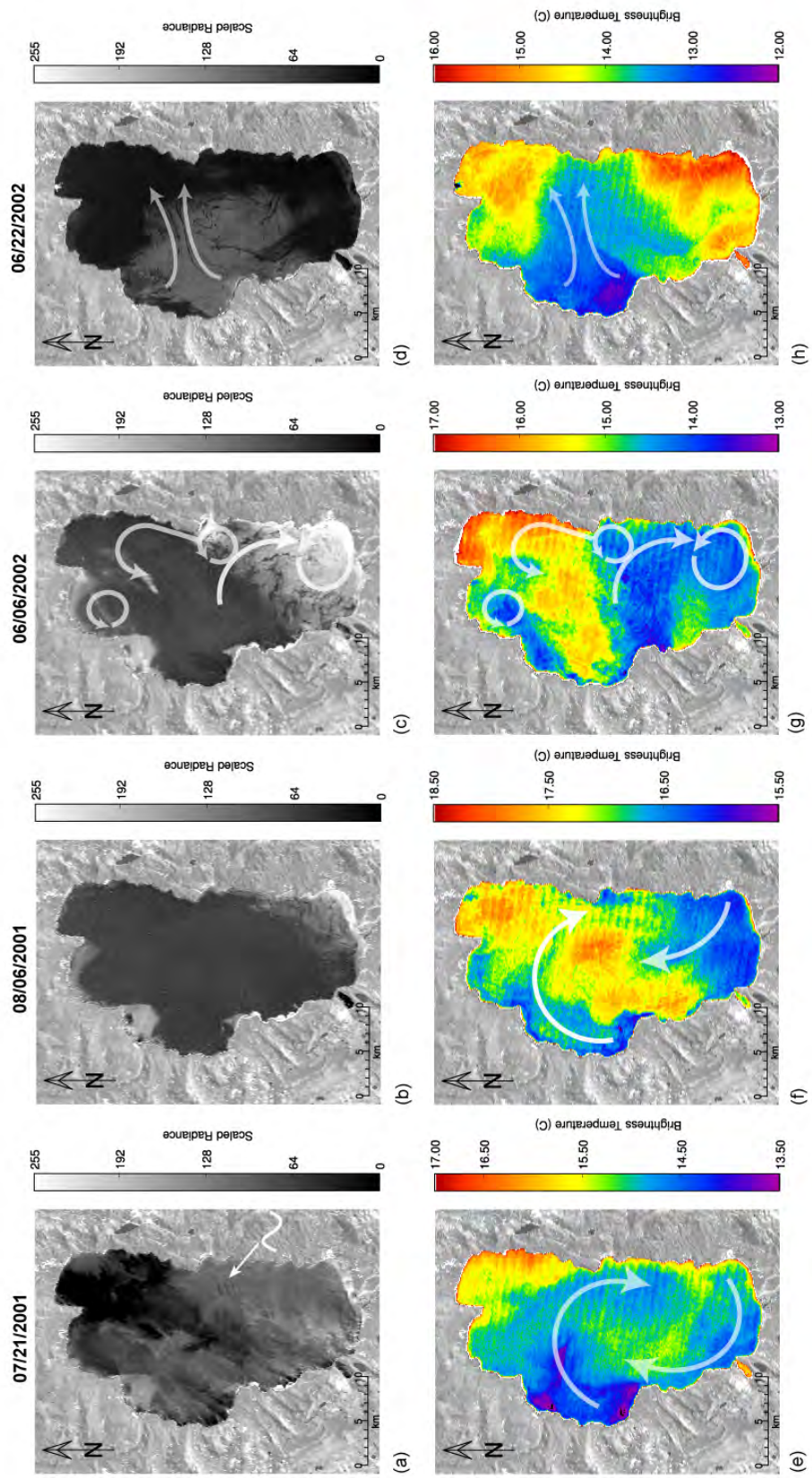


Figure B.5: Sun glitter maps and temperature maps showing large- and small-scale circulation patterns at Lake Tahoe, July 2001 – June 2002.

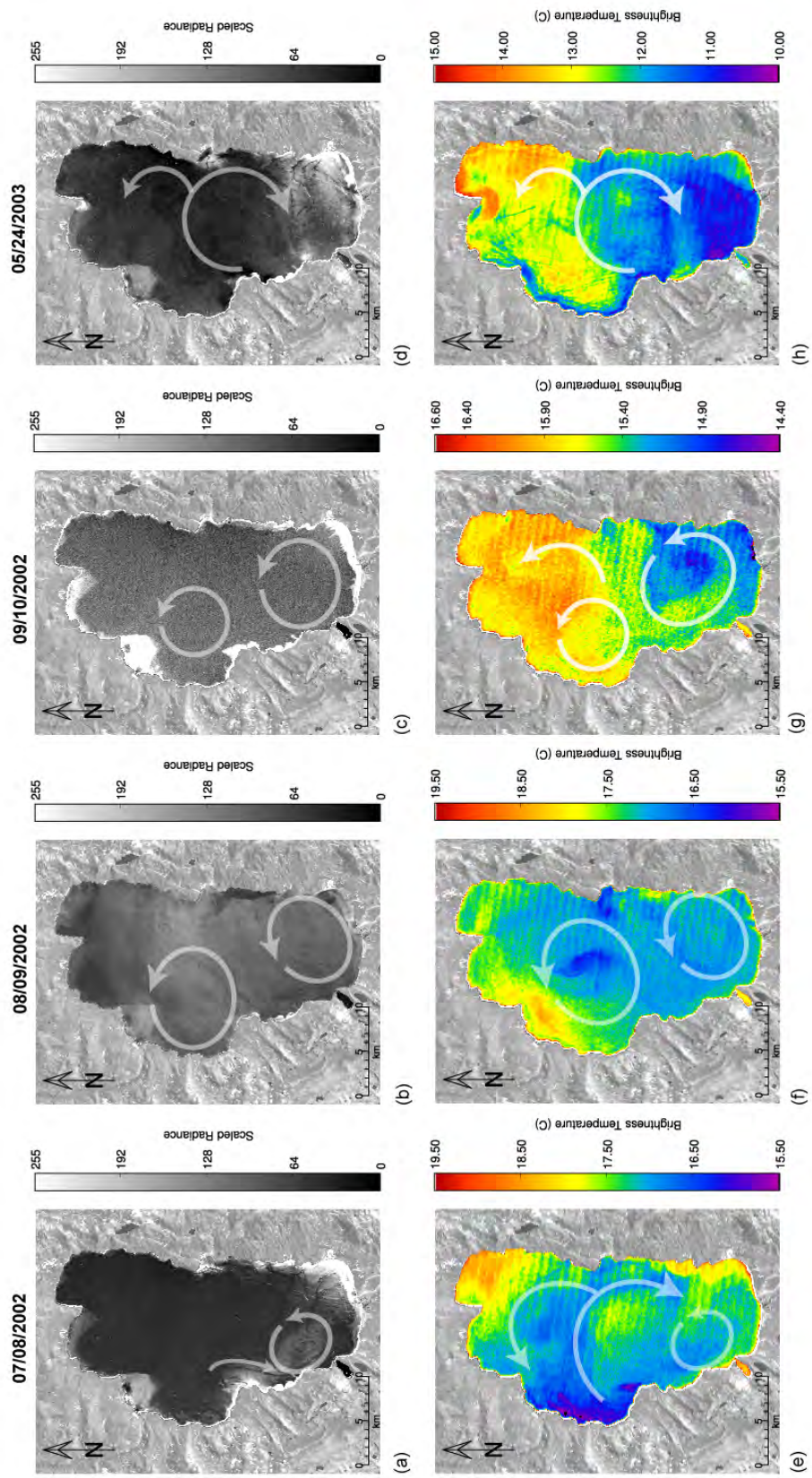


Figure B.6: Sun glitter maps and temperature maps showing large- and small-scale circulation patterns at Lake Tahoe, July 2002 – May 2003.

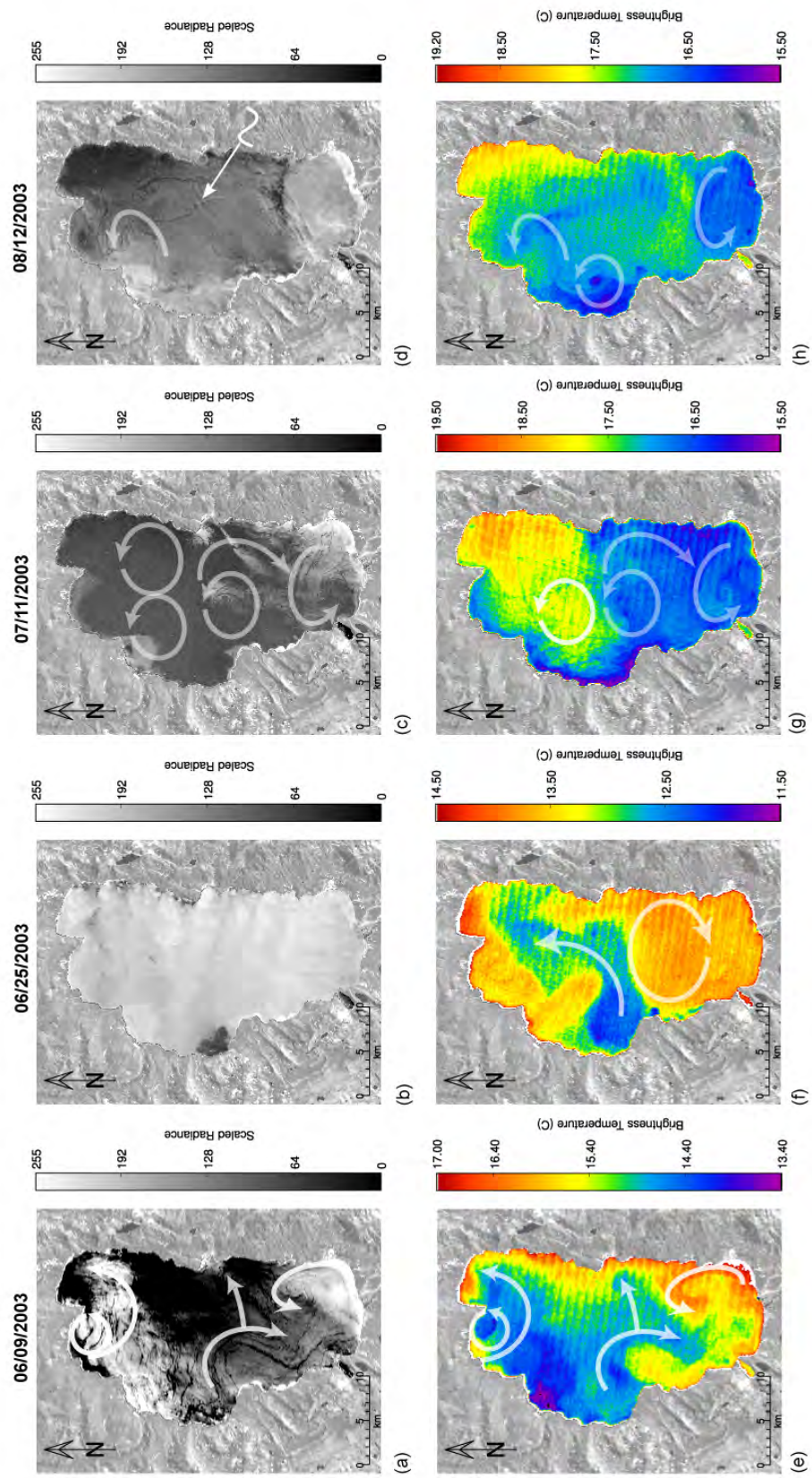


Figure B.7: Sun glitter maps and temperature maps showing large- and small-scale circulation patterns at Lake Tahoe, June 2003 – August 2003.

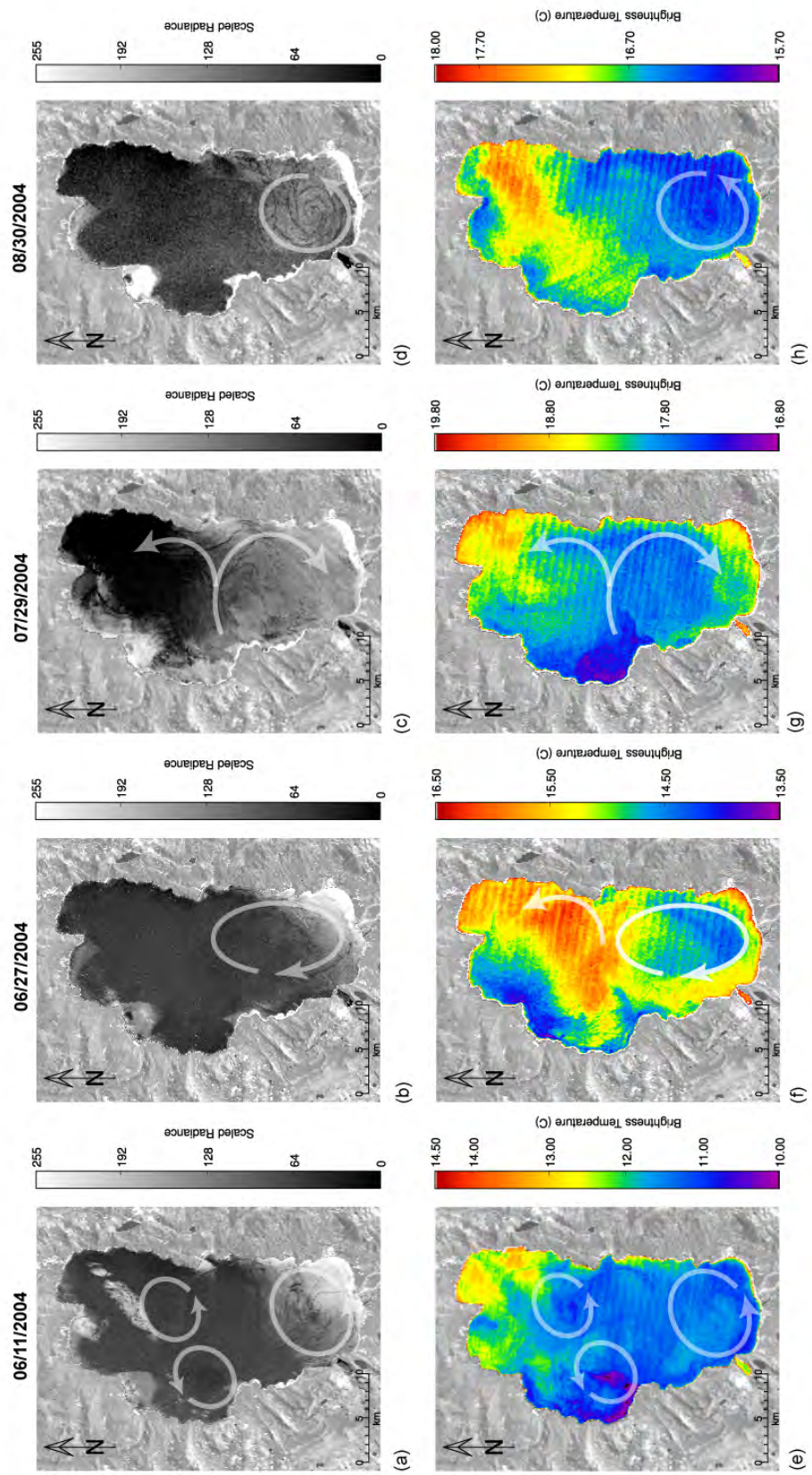


Figure B.8: Sun glitter maps and temperature maps showing large- and small-scale circulation patterns at Lake Tahoe, June 2004 – August 2004.

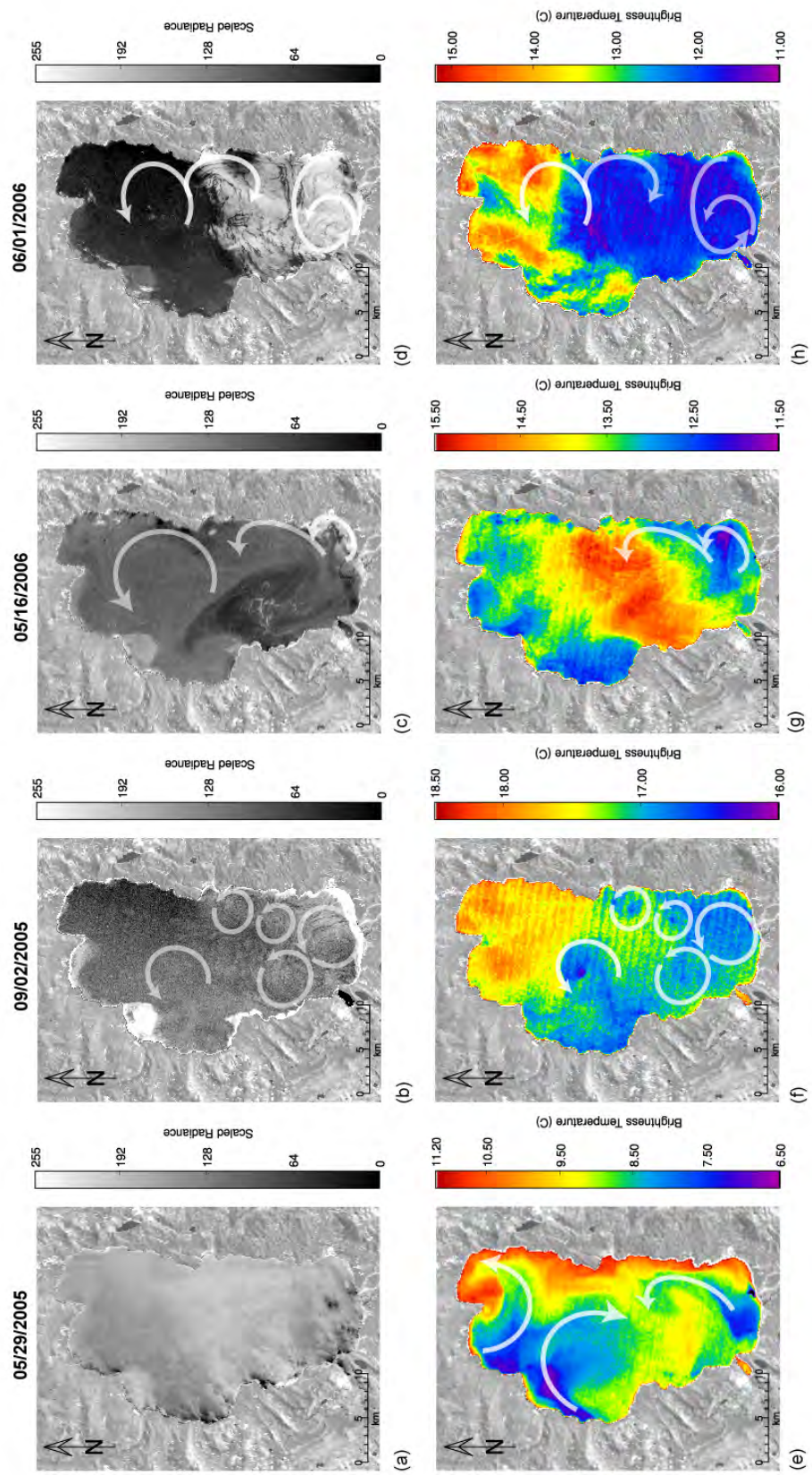


Figure B.9: Sun glitter maps and temperature maps showing large- and small-scale circulation patterns at Lake Tahoe, May 2005 – June 2006.

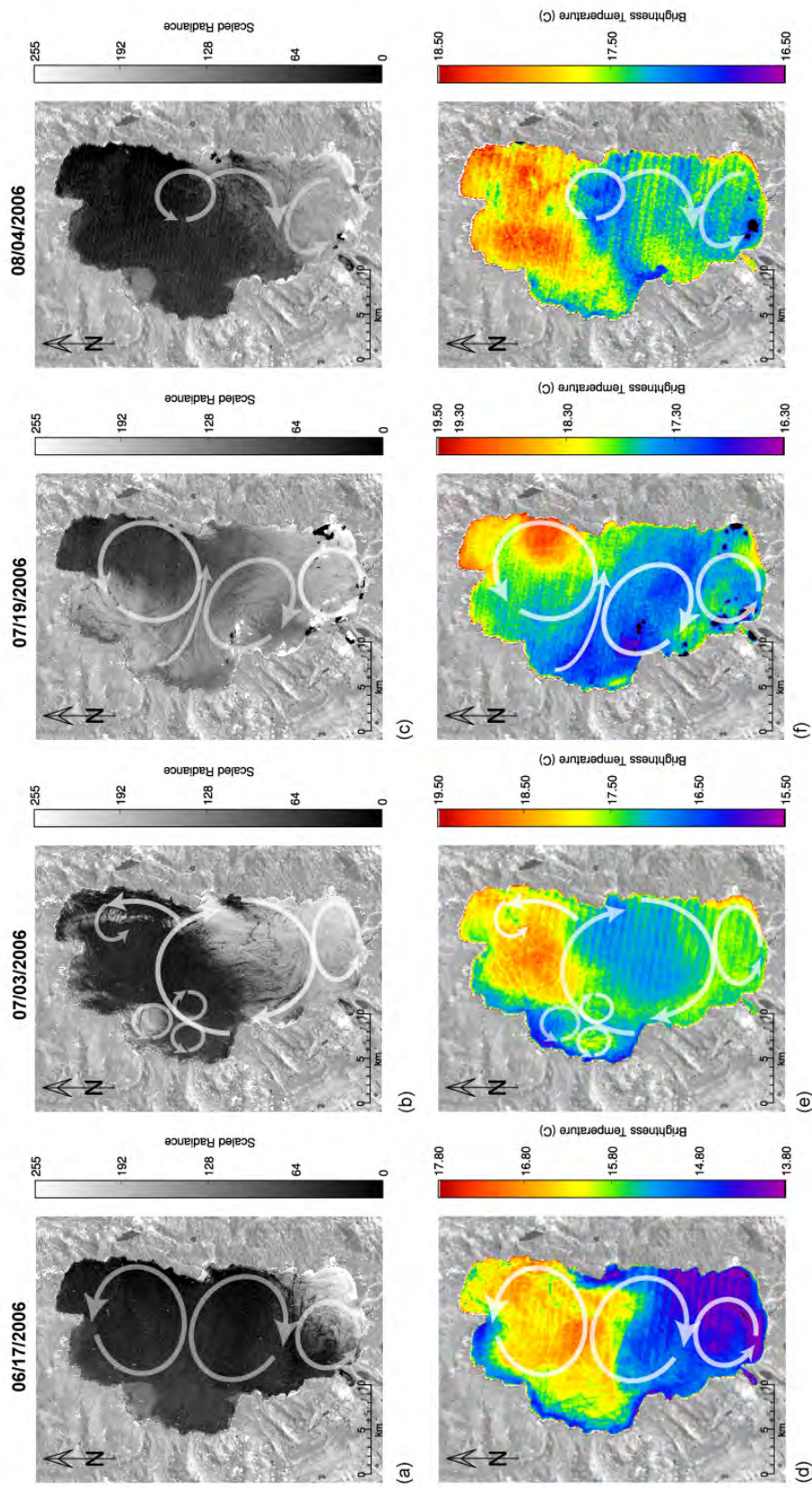


Figure B.10: Sun glitter maps and temperature maps showing large- and small-scale circulation patterns at Lake Tahoe, June 2006 – August 2006.

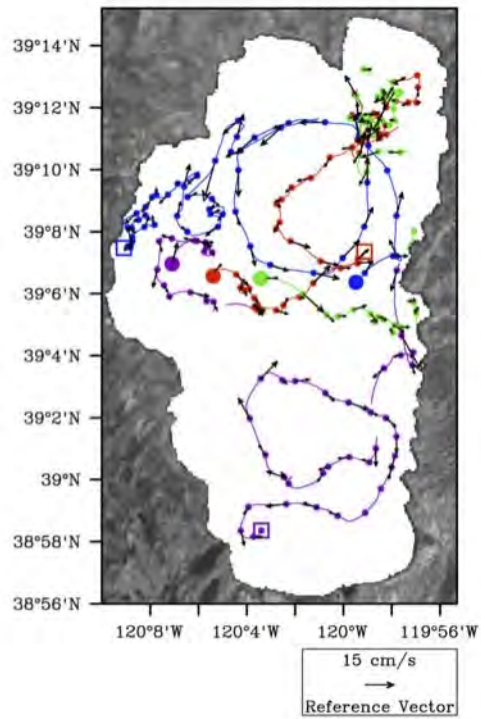


Figure B.11: Drogue tracks from September 2001. Direction of transport is indicated by vector arrows. A, B, and C show the corresponding meteorological data for each drogue track. E1, E2, and E3 denote the three spiral eddies delineated by the drogues.